

X820223x

488

1269383

RELATIONSHIP BETWEEN CAVITY FROM, RESTORATIVE TECHNOLOGY AND STRENGTH OF RESTORED TEETH

by D. L. Morin

Sponsoring Establishment

School of Mathematics, Statistics and Computing  
Thames Polytechnic

Collaborating Establishment

Biomaterials Program  
School of Dentistry  
University of Minnesota

Theses  
THAMES POLYTECHNIC LIBRARY  
617.  
6700  
151  
Mor

June 1985



Thesis submitted to the Council for National Academic Award in partial fulfillment of the requirements for the degree of Master of Philosophy

#### ABSTRACT

A number of very special people have made this work possible for me to accomplish. First I would like to thank Dr. Mark Cross who had the enthusiasm to take me on as one of his students, who provided constant optimism and the guidance necessary for me to attain my goals, and who always had a listening ear whether it be for research or for friendship. I am eternally grateful to Dr. William Douglas for providing me with this unique opportunity, for teaching and expounding on the philosophical aspects of this type of work, and for the persistence of faith he displayed which help me realize that we should live one day at a time. I would like to thank Dr. Ralph DeLong who provide invaluable insight into my experimental methodology, and Dr. Vaughn Voller who spent countless hours teaching me the finer aspects of IF ECS and modelling methodology. And special thanks is extended to the 3M Company who provide the necessary financial backing to this work. Finally, I would like to dedicate this work to my wife Keely who had to endure all the hours I spent participating in this work.

Model to simulate the strain generation and distribution in a tooth under a variety of cavity and restorative conditions. The model used the plane strain assumption and was based on the finite element method. Results demonstrated that when the restorative material is bonded to both the enamel and the dentin the strain distribution approximates that of a sound tooth. When bonding to just enamel is utilized in the restoration, the overall strain distribution approximates the sound tooth but localized areas of strain concentration still exist in the region bounded by the pulpal floor of the cavity and the pulp chamber. The modelling of a non-bonding restoration demonstrated no reduction in the strain magnitude or concentration.

CONTENTS

1. INTRODUCTION

1.1 Stress Analysis of Cavity Design

1.2 Numerical Stress Analysis

ABSTRACT

The results of an experimental and theoretical stress analysis of an in vitro human tooth are presented. The experimental work involved developing a technique utilizing strain gauge technology to evaluate the surface strains of a tooth which are produced under a variety of cavity and restorative conditions. The results indicated that a tooth with a cavity preparation is significantly less stiff than a intact, sound tooth. When the tooth was restored with a traditional, non-bonding, restorative material the overall stiffness showed no difference from that of the tooth with the cavity preparation. Bonding the restorative material to enamel and dentin resulted in a significant recovery of stiffness approaching that of the sound tooth. Also, the bonded restorations displayed much less hysteresis as compared to the non-bonded restorations.

The theoretical work consisted of formulating and validating a mathematical model to simulate the strain generation and distribution in a tooth under a variety of cavity and restorative conditions. The model used the plane strain assumption and was based on the finite element method. Results demonstrated that when the restorative material is bonded to both the enamel and the dentin the strain distribution approximates that of a sound tooth. When bonding to just enamel is utilized in the restoration ,the overall strain distribution approximates the sound tooth but localized areas of strain concentration still exist in the region bounded by the pulpal floor of the cavity and the pulp chamber. The modelling of a non-bonding restoration demonstrated no reduction in the strain magnitude or concentration.

6. FINITE ELEMENT METHOD RESULTS . . . . . 112

7. DISCUSSION OF FEM RESULTS . . . . . 134

8. CONCLUSION . . . . . 136

9. REFERENCES . . . . . 139

9.1 GLOSSARY . . . . . 143

## CONTENTS

1.	INTRODUCTION . . . . .	1
1.1	Stress Analysis of Cavity Design . . . . .	3
1.2	Numerical Stress Analysis . . . . .	8
1.3	Strength of Prepared Teeth . . . . .	15
1.4	Traditional Evaluation Methodology . . . . .	17
1.5	Introduction of New Evaluation Methodology . . . . .	23
2.	EXPERIMENTAL METHODS AND MATERIALS . . . . .	25
2.1	Theory of Strain Gauges . . . . .	25
2.2	Materials and Methods . . . . .	37
3.	RESULTS OF EXPERIMENTS . . . . .	58
4.	DISCUSSION OF EXPERIMENTAL RESULTS . . . . .	73
5.	THEORETICAL METHODS AND SOFTWARE . . . . .	77
5.1	Finite Element Method Theory . . . . .	77
5.2	IFECS . . . . .	94
5.3	Approaches to Modelling . . . . .	95
6.	FINITE ELEMENT METHOD RESULTS . . . . .	112
7.	DISCUSSION OF FEM RESULTS . . . . .	134
8.	CONCLUSION . . . . .	136
9.	REFERENCES . . . . .	138
9.1	GLOSSARY . . . . .	143

## 1. INTRODUCTION

The performance of any dental restoration is related to its ability to withstand the forces associated with the oral environment. Thus, in order to optimize the performance of any dental restoration it is necessary to minimize the stresses or strains that the existing tooth structure or the restorative material may experience. To accomplish this it is apparent that a thorough knowledge of the biomechanical behavior of the intact sound tooth is required. From this, it should be possible to formulate design criteria for a restored tooth such that the stresses and strains in both the existing tooth structure

Refer to glossary for definition of underlined words.

their respective strength properties. Using experimental stress analysis in conjunction with theoretical stress analysis, i.e. the finite element method, design proposals for dental restorations can be evaluated with respect to their potential for optimizing the stress-strain performance of the restorative material and the remaining tooth structure.

In order for design investigations to be meaningful it is necessary to have an indepth understanding of the basic philosophy of restorative dentistry. Traditionally, the dental restoration is required to restore the morphology or anatomical form lost through disease and/or injury processes. However, it is also necessary that the dental restoration provide strength and rigidity to the remaining tooth structure such that the tooth-restorative complex displays mechanical characteristics similar to the intact sound tooth. If strength and rigidity is achieved

## 1. INTRODUCTION

The performance of any dental restoration is related to its ability to withstand the forces associated with the oral environment. Thus, in order to optimize the performance of any dental restoration it is necessary to minimize the stresses or strains that the existing tooth structure or the restorative material may experience. To accomplish this it is apparent that a thorough knowledge of the biomechanical behavior of the intact sound tooth is required. From this, it should be possible to formulate design criteria for a restored tooth such that the stresses and strains in both the existing tooth structure and the restorative material do not exceed their respective strength properties. Using experimental stress analysis in conjunction with theoretical stress analysis, i.e. the finite element method, design proposals for dental restorations can be evaluated with respect to their potential for optimizing the stress-strain performance of the restorative material and the remaining tooth structure.

In order for design investigations to be meaningful it is necessary to have an indepth understanding of the basic philosophy of restorative dentistry. Traditionally, the dental restoration is required to restore the morphology or anatomical form lost through disease and/or injury processes. However, it is also necessary that the dental restoration provide strength and rigidity to the remaining tooth structure such that the tooth-restorative complex displays mechanical characteristics similar to the intact sound tooth. If strength and rigidity is achieved

in the tooth-restorative complex along with the incorporation of minimal stresses and strains then the operator can be assured that both the existing tooth structure and the restorative material will function at an optimum level with a minimal chance of any further mechanical deterioration.

Previously, the only dental restoration that provided any strength of rigidity to the existing tooth structure was the extracoronal cast metal restoration. However, with the advent of new bonding agents and techniques it is possible for the intracoronal restorations to reinforce the existing tooth structure and thus provide strength and rigidity to the tooth-restorative complex. Through the use of experimental stress analysis and finite element modelling an indepth evaluation can be obtained on the performance of the bonding agents and techniques. From this, design criteria can be formulated which optimize the tooth-restorative interaction while minimizing stresses and strains. *Inducing geometry and stress bearing caps*

The objective of this investigation is three-fold. First, using experimental stress analysis techniques, extracted human teeth will be characterized with regards to their ability to withstand a given force. This will include the examination of surface strains in the sound tooth, the prepared tooth, and the restored tooth. Second, finite element models of the sound tooth, the prepared tooth and the restored tooth will be formulated. These models will be validated using the results obtained from the experimental stress analysis. Finally, the

finite element models will be employed to provide an overall representation of the resulting strains and to determine the effect that various restorative techniques have on the magnitude and distribution of the resulting strains.

### 1.1 STRESS ANALYSIS OF CAVITY DESIGN

With the advent of experimental stress analysis it was possible to study more effectively the behavior of a tooth experiencing a given stress. Also, with the application of engineering principles an attempt was made to design cavity preparations and dental restorations that resulted in minimal stress concentration in the remaining tooth structure and restorative material.

One of the earliest applications of engineering principles to cavity design was done by Bronner<sup>1</sup>. He evaluated the traditional Class II cavity design in terms of stress inducing geometry and stress bearing capabilities. Resistive and retentive forms of cavity design were analyzed with regards to wall thickness and form. It was recognized that there was a need to minimize any stresses induced by the setting of the restorative material to prevent possible restorative-tooth failure.

Gabel<sup>2</sup> categorized the restorative-tooth failures into two groups, namely, fracture of the tooth at the buccogingival or linguogingival line angle and failure of the restoration at the axiopulpal line angle. A Class II restoration was considered to be similar to a beam of

rectangular form and behavior when loaded. Because of the plastic nature of an amalgam restoration, the proximal portion of the restoration becomes locked into irregularities of the dentinal walls of the cavity preparation. Thus, the restoration behaves as a cantilever beam with the occlusal portion deflecting under a given load. Due to the configuration of the restoration, the maximum stresses are at the point of fixation of the restoration, the axiopulpal line angle. Therefore from an engineering perspective the stresses are effectively tolerated by increasing the strength of the beam at the point of fixation. This involves increasing the depth of the restoration yielding a greater bulk of material.

Further work into the performance of restorations relative to accepted engineering principles was carried out by Brown and Weiland.<sup>3 5</sup> It was specified that two conditions must be fulfilled in a cavity preparation:

1. The cavity preparations should enhance the properties of the restorative material such that the unfavorable properties of the material are properly compensated for in terms of stresses.
2. The cavity preparation has to allow the operator to work efficiently such that a mechanically sound preparation is obtained.

Because amalgams greatest strength is in compression the cavity design should be such that shear and tensile forces are minimized or eliminated.

Noonan<sup>4</sup> provided one of the first studies of cavity design utilizing two-dimensional photoelastic stress analysis. From this followed a great number of studies

using the photoelastic technique<sup>6-16</sup>. These studies investigated the effect of differing Class II cavity designs on the stress dissipation within the remaining tooth structure and the restorative material. The conclusion reached from these studies were

1. Rounded internal line angles and retention points provided minimal stress concentration.
2. Rounded pulpal floor provided minimal stress concentration as compared to a flat planar pulpal floor.
3. Occlusal convergence of the cavity walls should be of a minimal degree in order to provide maximal support to the restoration.
4. The restorative material should be of sufficient bulk to withstand any induced tensile stresses.
5. Carving of the restoration should be such that proper occlusion is restored but no deep grooves or deep anatomy should be introduced since this may cause deleterious stress concentration.

One of the first reported uses of three-dimensional photoelastic stress analysis was done by Davidson<sup>17</sup>. Johnson et al.<sup>18</sup> expanded on this method of stress analysis and used three-dimensional models to study the resulting stress distributions in operatively prepared teeth. They concluded that there are significant stress concentrations in areas within the remaining tooth structure that experienced no loading. Also, the rounding of internal line angle significantly reduced the stress concentration in the tooth structure. Slight undercutting of the axial walls combined with rounded internal line angles did not result in any stress concentration. A continuously rounded pulpal floor was satisfactory in

terms of stress dissipation.

An investigation into the effect of the buccolingual shape of the Class II cavity on the edge strength of amalgam was carried out by Granath et al.<sup>19</sup> using strain gauges. They concluded that the optimal cavity design with respect to restorative performance was not the same as the optimal cavity design for minimal stress concentration in the remaining tooth structure. By increasing the occlusal convergence of the axial walls there was a decrease in the avulsive tensile stresses in the restorative material.

In order to provide validity and accuracy to photoelastic modelling techniques, Tanner<sup>20</sup> investigated factors affecting the design of these models. Points of load application, external morphology, pulp chamber morphology, variation in elastic moduli and mode of support of the restoration were examined. It was concluded that variation in external morphology did not significantly affect the stress distribution when the loading was strictly on the restorative material or the tooth structure. On the other hand, pulp chamber morphology had significant influence on the stress distribution in the restoration when the load was applied to the restoration. When a load was applied to the tooth-restoration interface there was large variation in the stress distribution depending on the ratio of the elastic moduli between the restorative material and the tooth structure. The manner in which the restoration was supported by tooth structure appeared to be the most

important factor affecting the compatibility between the experimental model and the actual physical structure. This support was dependent on the ratio of the elastic constants between the tooth structure and the restorative material.

21  
Fisher et al. using two-dimensional photoelasticity investigated the intracoronal and extracoronal preparation. It was concluded that under a given load, excessive stress was generated in a tooth restored with an intracoronal restoration. These damaging stresses associated with the intracoronal restorations were effectively minimized by incorporating occlusal coverage into the restoration in the form of an onlay.

Considering the limitation of the photoelastic modelling scheme and the need to provide cavity designs that are realistically obtainable by the operator the following recommendations were made by Craig et al.<sup>22</sup> to minimize stresses and fractures in Class II amalgam restorations:

1. A rounded pulpal floor.
2. The axial walls should converge slightly towards the occlusal surface.
3. Rounded internal line angles with no sharp developmental grooves in the amalgam carving.
4. Reasonable thickness of amalgam to provide the necessary bulk required to minimize stresses.
5. The isthmus should be located as near the pulpal wall as possible.
6. Contact points should be away from the pulpal, axial and gingival walls.

Experimental stress analysis has provided methodology

by which cavity design can be evaluated. The resulting stress distribution in both the restorative material and existing tooth structure can be effectively modelled using photoelastic techniques. However, it must be emphasized that photoelastic models only account for differences in the elastic moduli and ignores any orthotropic or inelastic behavior. The models are generally formulated in two dimensions due to the difficulty of analyzing three dimensional models. This leads to the assumption that the stress perpendicular to the plane of interest is a constant. Finally, the overall limiting factor in the photoelastic modelling is the lack of experimental verification of results or validation of the model's behavior. This is of utmost importance in developing a model that can be applied to a variety of restorative conditions.

## 1.2. NUMERICAL STRESS ANALYSIS

The finite element method (FEM) was first introduced into the area of stress analysis of biological structures in 1972 by Brekelmans et al.<sup>37</sup> . Since then there has been a growth in the use of FEM in orthopedic biomechanics and the stress analysis of teeth and associated restorative prostheses and materials. The FEM is extremely well suited for the analysis of biological structures because of its ability to model complex geometries composed of multiple material types. With the application of nonlinear continuum theory and the incorporation of

inhomogenous material theory the FEM is capable of providing indepth information on the biomechanical behavior of many complex biological structures.

<sup>24</sup>  
Thresher et al. were the first to apply the FEM to analyze the stress distribution in a sound human tooth. Using a plane strain model of a maxillary central incisor they demonstrated the importance of using a non-homogenous tooth model to determine the internal stress distribution. As was expected, the model predicted that a major proportion of the given load was supported by the enamel portion of the model.

A combination of photoelastic and FEM stress analysis of a restored molar was made by Farah et al. <sup>25</sup> Making the assumption of axisymmetry of the first molar the FEM model was formulated to represent the first molar restored with a full coverage crown. They concluded that the FEM, even with the simplifying assumptions, provided sound and reliable information concerning the stress distribution in the tooth. When compared to the photoelastic technique, the FEM provided a more detailed evaluation of the complete stress distribution in the model.

<sup>26,27</sup>  
Further work by Farah et al. included the application of the FEM to determine the stresses and displacement of the pulpal floor of a cavity as a function of condensor size. Also, the effect of the cement base on the stresses in amalgam restorations was studied using the same model.

A comparison of axisymmetric and plane stress idealizations of the maxillary second premolar was made by

Selna et al. . . . The plane stress model consisted of a midsagittal section of the maxillary premolar expanded in the third (depth) dimension. The root section was not rigidly fixed but rather connected to an elastic foundation composed of springs in both the horizontal and vertical direction. The axisymmetric representation consisted of taking the lingual half of the midsagittal section and rotating it about an axis corresponding to the central axis of the tooth. By definition the axisymmetric model loads were distributed as annular line loads as compared to the plane stress point loads. Results demonstrated the maximum stress gradient to be near the point of load application. In the roots of the teeth, the stress distribution was of low magnitude and very uniform. Also, an eccentric load application caused the magnitude and direction of the principal stresses to exceed the strength of the materials composing the model.

A more in depth FEM analysis of the crowns of normal teeth was performed by Yettram et al. . . . The model consisted of a plane strain, two-dimensional representation of a mandibular second premolar. Load application consisted of both eccentric and centric type positioning. Also, the enamel was assumed to be isotropic for the first analysis and in the second the enamel was ascribed orthotropic mechanical properties; the long axis of the enamel prisms being taken as the primary or stiffer direction. The results of both analyses indicated that enamel with its greater stiffness over dentin was able to react to a larger proportion of the applied load. This

too was observed by Lehman et al. using three dimensional photoelasticity. The forces due to the masticatory type loads tended to flow around the enamel cap with relatively high compressive forces in the cervical region of enamel while the dentin remained lightly stressed. As the modular ratio between the enamel and dentin decreased, there was a tendency for the stress distribution to be more equal between the two materials and for stress concentration at the amelocemental junction to be reduced. Also, results indicated that there are relatively high tensile forces in the region of the fissure of the central groove under normal masticatory loads. It was thought that this force on the enamel prisms may assist the attack of caries in this region of the tooth.

Using an axisymmetric representation of mandibular second premolar a FEM analysis was made on Class I amalgam restorations subjected to setting and thermal expansion by Wright et al.<sup>31</sup> The analysis considered both the unlined and lined cavity preparations. It was found that the "free" amalgam setting expansion of 10 um/cm length was equivalent to an unrestrained thermal expansion resulting from a uniform temperature increase of 40 degrees C. Thus, by lowering the temperature of the mouth from 37 degrees C to 0 degrees C by the ingestion of very cold foods, the prestresses initially present are almost completely removed. Also, the results demonstrated that enamel with its greater stiffness over dentin deformed to a lesser extent than did the dentin. Thus the compressive

stresses induced in the amalgam at the enamel-amalgam interface were of a greater magnitude than those induced in the restoration near the dentin.

Further work into the behavior of teeth under various loading conditions utilizing the FEM was performed by Takahashi et al.<sup>32</sup> Using the plane strain assumption an analysis of tooth deflection, rotational centre, stresses in the periodontal membrane, turning moments of the tooth and supporting forces of the periodontal membrane was made. The results obtained indicated that as the loading angulation deviated away from vertical the deflection of the tooth increased. Also, the supporting function of the periodontal membrane was maximum near the cervical region and minimum in the apical third. The effect of loading angulation on tooth behavior was greatest in the mandibular first molar and least in the maxillary central incisor.

In an attempt to estimate the physiological stresses associated with a natural tooth with a fibrous PDL structure, Atmaram et al.<sup>33</sup> used the FEM. Comparisons were made of both a the continuous and the fibrous PDL structure with regards to the manner in which the stresses were distributed to the surrounding alveolar bone. The model consisted of a plane strain representation of a molar tooth. When the PDL was modelled as fibrous, beam type elements were used while the traditional triangular elements were used for the continuous PDL structure. The beam elements supported only compressive and tensile stresses along their axes and did not support any bending

stresses. This is true of the fibrous bundles of the PDL in the actual tooth. Results indicated that while the continuous PDL model yielded reasonable stresses in the enamel and dentin, the associated alveolar stresses did not correspond with the natural tooth having a fibrous PDL. The fibrous PDL modelling scheme yielded stresses that more accurately represented the natural situation.

Because of the frequency of cuspal failure following the placement of an MOD restoration the FEM was employed by Bell et al.<sup>34</sup> in an attempt to gain insight into the possible mechanism causing the failure. Using an idealized plane strain model of a molar, an analysis of an unrestored cavity, conventional non-bonded MOD restoration, perfectly bonded MOD restoration and an extracoronal onlay restoration were examined. They concluded that when a force is applied to the cusp of a tooth restored with the conventional non-bonded MOD restoration, the restoration plays no role in sustaining the applied force. However, when the restoration is bonded to the existing cusps the restoration plays an intimate role in distributing the stresses internally. Because of this, the propagation of cracks along maximal stress gradients in the tooth structure would be minimized and the resulting cuspal failures reduced.

A biomechanical stress analysis of the amalgam-tooth interface utilizing the FEM was carried out by Peters et al.<sup>35</sup> A series of interface parameters regarding the amalgam-tooth boundary were compared. For an axisymmetric mandibular first molar with loading conditions on the

tooth only and on the restoration only, there were significant changes in the stress distribution depending on the interface design. The assumption of perfect bonding between the tooth structure and the restorative material yield the greatest stress reduction. The study demonstrated that the selection of boundary conditions for the tooth-restorative interface has a definite effect on the magnitude and distribution of the resulting stresses.

A three-dimensional FEM formulation of a human tooth was made by Rubin et al.<sup>36</sup> The three dimensional model took into account the non-symmetric geometry and loading of a mandibular first molar and also accounted for the material inhomogeneities of the tooth. The results indicated that the more sophisticated three-dimensional model was an improvement over existing two-dimensional FEM modelling schemes, especially the plane stress/strain assumption. The overall principal stress distribution was significantly lower than that predicted by two-dimensional modelling. This indicates a more even distribution of applied loads in the tooth structure.

There have been numerous other studies utilizing the FEM to investigate stresses associated with the oral structures. Craig et al.<sup>22</sup> have done extensive work on stresses associated with full coronal coverage as a function of marginal design and on the stresses associated with fixed partial bridges. Both Davy et al.<sup>37</sup> and Rheinhardt et al.<sup>38</sup> have used the FEM to investigate dowel design and the of diminishing bone support in post-reconstructed teeth. Other applications of three-

dimensional FEM includes the analysis of porous root Co-Cr-Mo alloy dental implants by Cook et al.<sup>39</sup> and the development of a three-dimensional model of the human mandible by Bach et al.<sup>40</sup>, Gupta et al.<sup>41</sup> and Knoell<sup>42</sup>.

The FEM is a well established stress analysis technique. It has been applied not only to purely mechanical and structural systems but also to biological systems involving both bone and hard tooth structure. Not only has the stress distribution in the sound tooth been examined but the resulting stress distributing associated with different restorative conditions has been extensively investigated. As was the case for the photoelastic models, the finite element models have lacked experimental verification and validation. This results in models that may present excellent geometric representations but fail to establish credibility in physical behavior. Models have been formulated using an enormous number of nodes in an attempt to provide quantitative results. This requires vast amounts of computer storage and computing time, and increases the computing expense. When dealing with models involving biologic systems it must be understood that due to the high degree of variability between specimens, and the complex nature of biologic materials, the models must be viewed as qualitative. This results in a more general representation of the actual physical behavior.

### 1.3 STRENGTH OF PREPARED TEETH

Cavity preparation of teeth includes the mechanical

removal of diseased, infected or damaged tooth structure along with any weakened remaining tissue. Traditionally the cavity design has to be such that the restorative material is retained in place. Because of this, significant removal of tooth structure usually occurs. This may in fact compromise the remaining tooth structure with regards to its ultimate strength and resistance to fracture.

One of the first studies into the effect of cavity preparation on the strength of teeth was by Vale<sup>43,44</sup>. Comparisons were made of sound teeth to teeth with mesio-occluso-distal (MOD) cavity preparations. The isthmus widths of the cavity preparation were  $1/4$  and  $1/3$  the intercuspal distance. It was found that there was no difference in the ultimate fracture strength of the sound teeth and the teeth with the  $1/4$  intercuspal cavity preparation. However, when the isthmus width was increased to  $1/3$  the intercuspal distance there was a significant weakening of the prepared tooth. Also, when the teeth were restored with either amalgam or gold inlays and then tested there was no increase or recovery of strength of the tooth over that of a tooth with the cavity preparation and no restoration.

The Work by Rasmussen et al.<sup>45</sup> was aimed at determining the mechanics by which the fracture of enamel and dentin occurred. They concluded that both dentin and enamel behaved as brittle materials and that forces generated through mastication and bruxism had the potential to initiate fractures when the tooth had been altered by

cavity preparation. Therefore, the importance of designing the cavity preparation to reduce any potential stress concentrations was recognized.

A comparison of the fracture strength of Class I and II cavity preparations was made by Mondelli et al.<sup>46</sup> Class I preparation with isthmus widths of  $1/4$ ,  $1/3$  and  $1/2$  the intercuspal distance all had ultimate fracture strengths less than that of the sound tooth. Comparable findings were obtained for the two surface and three surface Class II preparation with similar isthmus widths. However, the Class I preparation yield less strength reduction than a Class II preparation of similar isthmus width. This was possibly due to the marginal ridges remaining intact in the Class I preparation.

#### 1.4 TRADITIONAL EVALUATION METHODOLOGY

The traditional evaluation methodologies used in dentistry can be categorized as either clinical or laboratory based in nature. The clinical evaluation examines a new restorative material or technique in vivo and patients receiving the treatment are monitored over a given time frame with respect to the variable of interest. The laboratory evaluation often is aimed towards the determination of the physical properties or the stress-strain relationship associated with a restorative material or technique. Usually a laboratory evaluation and a clinical evaluation are necessary before a new restorative material or technique can be accepted as a viable

alternative in restorative dentistry. A laboratory evaluation is first performed and if results are comparable to those of materials/techniques accepted for clinical use then a clinical evaluation is warranted. From this it is ultimately determined if the material can be effectively utilized in the oral environment.

Even though this type of evaluation methodology is the basis for determining the acceptance of a new material/technique, there are severe inadequacies that can limit the amount of useful information obtained. Current laboratory methodology for the evaluation of a restorative material/technique generally consists of testing individual or isolated samples of material independent of environmental factors or biomechanical considerations associated with the dentition, also, the formulation of photoelastic and numerical models tend to oversimplify the stated problem. The results of this type of traditional testing scheme is the determination of material properties and stress-strain relationships. However, the meaning of these results are difficult to interpret with respect to what is required for a material/technique to perform successfully in the oral environment. Thus, a laboratory methodology that more closely simulates the biomechanical and environmental factors of the dental structures could yield more meaningful information.

To obtain this information it is important to consider the manner in which the force is applied to the test sample in the laboratory methodology. Traditionally this force application has been isotonic or under stroke

control. This means the testing apparatus senses a displacement of the test sample rather than monitoring the stress or applied force. This method of force application is intrinsically different from that of the associated dental structures. When considering the teeth, the supporting alveolar bone of the mandible, and the facial and cranial bony network it is apparent that the force application to the dentition in centric occlusion is isometric or that the force is monitored as a load (load control) rather than as a displacement. This is due to the rigid nature of the dentition and its supporting bony network which essentially eliminates the possibility of displacement. Thus, in the laboratory methodology the test sample should be examined under a load control situation in order to more closely simulate conditions of force application in the dentition.

The use of isolated sample testing has gained wide acceptance in the laboratory methodology due as a consequence of its use in traditional engineering material testing. However, due to the complex geometry and physical nature of dentin and enamel and the complex geometry of cavity design it is difficult to interpret the meaning of an ultimate compressive/tensile strength, dimetral strength or crushing strength of a material with respect to its applicability in being a successful restorative material. Current laboratory methodology ignores the true biomechanics of the tooth when evaluating a restorative material. It is common practice to evaluate the material either in pure compression or tension.

However, the forces that the restorative material will experience in the oral environment are a complex function of compression, tension, and shear forces. Thus, if a new material could be evaluated such that the biomechanics of the tooth are incorporated into the test procedure more insight could be obtained as to the ability of the material to function successfully in the restorative state.

The assumptions used to formulate the photoelastic and numerical models also have to be closely examined with regard to the relevance of the modelling exercise to the actual dentition. For the photoelastic technique it is important to realize that the model only accounts for differences in the modulus of elasticity between materials assuming isotropic and elastic behavior. Thus, any effect due to the orthotropic or inelastic nature of a material are neglected. Because of the difficulties in formulating and analyzing three dimensional photoelastic models two dimensional models are generally used, requiring the plane strain assumption. The numerical model, on the other hand, can account for three dimensional orthotropic and inelastic behavior. However, formulating the model, carrying out the analysis and finally interpreting the results is very time consuming, difficult, and costly to perform. Therefore, two dimensional or axisymmetric models assuming isotropic/elastic behavior are generally employed. Thus, the plane strain assumption is again made. Even though the numerical modelling technique is well suited for analyzing complex geometries made up of

multiple material types, the assumption of continuity between adjacent materials often makes the modelling scheme difficult to employ and interpret. This is due to traditional restorative materials not forming chemical or mechanical bonds of significant strength to the prepared tooth. Finally, when the photoelastic or numerical modelling techniques are employed in the laboratory evaluation there is usually an absence of an experimental verification of the formulated model. This results in a lack of understanding of the model's validity and ultimately the limitations of the model are not known or fully understood.

Another important factor that is often overlooked or neglected in the current laboratory methodology is the effect of environmental conditions on the performance of a restorative material/technique. The oral environment is an extremely hostile environment. The restorative material must withstand the effects of high humidity, corrosion, the presence of micro-organisms and the products they produce, and the dynamic loading and temperature fluctuations that the oral environment can produce. This too should be included in the design of the laboratory evaluation to provide a much more comprehensive evaluation such that the data base of the evaluation will be an indicator of a material or technique's performance as a restorative.

Even though the clinical evaluation is the final step in determining a new restorative materials feasibility it does present certain limitations which make the

methodology extremely difficult and costly to perform. Because of the large variability associated with a clinical evaluation an extremely large sample population is necessary so that inferential statistics can be applied. This large sample population is both very costly and time consuming to manage due to the logistics associated with examining and treating so many individuals. Also, the time frame associated with a clinical evaluation is extremely long due to the rate at which the phenomena of interest occurs, whether it be wear, histological responses, marginal integrity, maintenance of anatomical form, etc. Another difficult problem to address in the clinical evaluation is the control of the variables or parameters of the study. Not only are the individuals of the study different but so too are the variables associated with each individual. This results in evaluations that are classified as non-parametric in design. Thus, only qualitative differences can be ascertained from the evaluation. Along with this, the clinical evaluation often is inconclusive with regards to the phenomena of interest, thus making it extremely difficult to obtain a strong justification for the methodology. Finally, the moral and ethical questions associated with human experimentation have to be addressed with respect to the social and scientific benefits obtained from such a clinical evaluation of new experimental materials and techniques.

## 1.5 INTRODUCTION OF NEW EVALUATION METHODOLOGY

Through the use of strain gauge technology and servohydraulics in conjunction with finite element modelling a new investigative methodology has been developed that overcomes several limitations of past methodologies. This methodology consists of an experimental phase and a theoretical or modelling phase. The experimental phase consists of evaluating different restorative materials and techniques with respect to their strain reducing capabilities. Using extracted teeth with no evidence of any carious lesions, strain gauges are mounted on the buccal and lingual surfaces and the stress-strain behavior of the sound tooth is evaluated when an axial force is applied using servohydraulics under programmed load control. Having established a base line or an ideal stress-strain behavior, the tooth is prepared using traditional cavity design and then restored with different materials and techniques. These materials or techniques can now be evaluated in a true biomechanical sense by determining the resulting stress-strain behavior of the restored tooth. Ideally, a restorative material/technique would return the restored tooth to the same stress-strain behavior displayed by the sound tooth under all conditions.

The theoretical or modelling phase of the methodology consists of formulating a mathematical or finite element model of a sound tooth, a tooth with a cavity preparation, and a tooth in the restorative condition. Using the finite element method (FEM) the principal strains

### 3. EXPERIMENTAL METHODS AND MATERIALS

throughout each model under a given axial force are calculated. By validating the theoretical or modelling results against experimental results, the formulated model can be used to investigate the behavior of the tooth under a wide variety of restorative conditions. Using this model the effect of materials with different moduli, cavity design, and the resulting strain distribution in critical areas can be easily examined. From this the relationship between cavity design, restorative material and restorative technique can be determined and used to optimize the performance of the tooth-restorative complex.

48.47.30  
recorded

Electrical Resistance strain gauges are based on the principle that the resistance of a conductor is a function of the normal strain induced on the conductor. Thus, if  $R$  is the resistance of a conductor and  $\epsilon$  is the normal strain, then the change in resistance is expressed as

$$\Delta R = S_A R \epsilon \quad (1)$$

where  $S_A$  is the strain sensitivity of the conductor material and where the conductor material displays a linear sensitivity over a wide range of strains for that material. Also, it is imperative that the conductor display a high degree of thermal stability so as to minimize apparent strains due to transient temperature fluctuations.

The fundamental characteristics that limit strain gauge responses and that must be determined in order to establish accuracy in strain measurement are

## 2. EXPERIMENTAL METHODS AND MATERIALS

### 2.1 THEORY OF STRAIN GAUGES

The use of electrical resistance strain gauges is one of the most common methods of measurement used in experimental stress analysis. These gauges overcome many of the shortcomings of the application of other methods of experimental stress measurement. The electrical resistance strain gauge is relatively simple to install and responds adequately to both rapidly fluctuating or static strains with an output signal which is easily recorded<sup>48,49,50</sup>.

Electrical resistance strain gauges are based on the principle that the resistance of a conductor is a function of the normal strain induced on the conductor. Thus, if  $R$  is the resistance of a conductor and  $\epsilon$  is the normal strain, then the change in resistance is expressed as

$$\Delta R = S_A R \epsilon \quad (1)$$

where  $S_A$  is the gauge factor, normally determined by the material and where the conductor material displays a linear sensitivity over a wide range of strains for that material. Also, it is imperative that the conductor display a high degree of thermal stability so as to minimize apparent strains due to transient temperature fluctuations.

The fundamental characteristics that limit strain gauge responses and that must be determined in order to establish accuracy in strain measurement are

1. Linearity of conductor material
2. Temperature effects
3. Cross-strain sensitivity of the gauge
4. Gauge current heating effects

Linearity of the conductor is a function of the material the conductor is fabricated from and whether or not the gauge is used for dynamic or static testing scheme. It is essential that linearity is displayed over the range of the strain being investigated.

With changes in ambient temperature a resulting differential thermal expansion between the gauge and the test specimen occurs. The gauge conductor changes length and induces an apparent strain of magnitude

$$\epsilon_{APP} = (\alpha_s - \alpha_g) \Delta T \quad (2)$$

where  $\alpha_s$  and  $\alpha_g$  are the coefficients of thermal expansion of the test specimen and the gauge respectively.

The change in resistance of the conductor is given by

$$\left( \frac{\Delta R}{R} \right)_1 = (\alpha_s - \alpha_g) S_g \Delta T \quad (3)$$

where  $S_g$  is the gauge factor, normally determined by the manufacturer. In addition to differential thermal expansion between the specimen and the gauge there are changes in resistance of the gauge due to temperature changes. This change in resistance is expressed as

$$\left( \frac{\Delta R}{R} \right)_2 = \gamma \Delta T \quad (4)$$

where  $\gamma$  is the temperature resistivity of the gauge conductor. The combined effect of thermal expansion and temperature changes yields an overall change in resistance

given by

$$\left(\frac{\Delta R}{R}\right)_{\Delta T} = (\alpha_s - \alpha_g) S_g \Delta T + \gamma \Delta T \quad (5)$$

There are two methods to compensate for temperature effects. One method involves the gauge conductor to be self compensating with respect to temperature. Thus

$$\left(\frac{\Delta R}{R}\right)_{\Delta T} \sim 0 \quad (6)$$

and

$$(\alpha_s - \alpha_g) S_g = -\gamma \quad (7)$$

The other method involves utilizing another strain gauge mounted on the same material as the test specimen and incorporating it into an adjacent arm of the wheatstone bridge circuit. Thus, any temperature effects in the test gauge are cancelled out by an equal and opposite effect in the compensating gauge.

Cross-strain or transverse strains arise because of the conformation of the gauge when stressed in an axial direction. Thus there is a contribution to the measured total strain from cross-strains. The presence of cross-strains in a axial loading scheme is due to Poisson's effect, which indicates for a deformation in the axial direction a corresponding deformation occurs in the cross-sectional area of the specimen.

The gauge factor can be expressed as

$$S_g = \frac{\frac{\Delta R}{R}}{\epsilon_x} \quad (8)$$

with

$$\epsilon_y = -\nu \epsilon_x \quad (9)$$

where  $\nu$  is Poisson's ratio for the gauge and is equal to 0.285. The x-axis is in the axial direction with the y-axis perpendicular to the x-axis. Under conditions of gauge use such that  $\epsilon_y = -\nu \epsilon_x$  then  $S_g = \frac{\Delta R/R}{\epsilon_x}$  yields an exact result. If  $\epsilon_y \neq -\nu \epsilon_x$  then a small error will be introduced with a magnitude proportional to the deviation of  $\epsilon_y/\epsilon_x$  from  $(-\nu)$ .

Because the gauge is a resistor  $R$ , with a gauge current  $I$ , there is heat generated according to the law  $I^2 R$ . The temperature rise in the gauge itself is dependent on the gauge current and on the heat dissipation properties of the test specimen and the gauge backing. The temperature rise will effect gauge output and cause a zero shift. Once the rate of change of temperature of the gauge equals zero, the rate of heat dissipation from the gauge will approach equilibrium and output from the gauge will be accurate and precise. Thus, a warm up period to accommodate gauge current heating effects is essential prior to any strain measurements.

Strain gauge instrumentation utilizes the wheatstone bridge as the primary circuit used in the stress-strain measurements. The bridge is extremely sensitive to small changes in resistance. The output voltage  $E$  of the bridge is proportional to the change in resistance in the bridge circuit. For a given change in output voltage

$$\Delta E \approx V_r \left( \frac{\Delta R_1}{R_1} - \frac{\Delta R_2}{R_2} + \frac{\Delta R_3}{R_3} - \frac{\Delta R_4}{R_4} \right) \quad (10)$$

where

$$r = \frac{R_1 R_2}{(R_1 + R_2)^2} = \frac{R_3 R_4}{(R_3 + R_4)^2} \quad (11)$$

If only one gauge of resistance  $R$  is used in the bridge then  $R_1 = R_2 = R_3 = R_4 = R$ ,  $\Delta R_1 = \Delta R_2 = \Delta R_3 = \Delta R_4 = \Delta R$  and  $\Delta R = \Delta R = \Delta R = \Delta R = 0$ . Thus, the resulting change in output voltage is given by

$$\Delta E = V_r \frac{\Delta R_g}{R_g} \quad (12)$$

and it is known from equation 8 that

$$\frac{\Delta R_g}{R_g} = S_g \epsilon \quad (13)$$

Thus it follows

$$\Delta E = V_r S_g \epsilon \quad (14)$$

From the above equation it is evident that the change in output voltage of the gauge is directly proportional to the strain on the gauge.

For truly accurate strain measurements, one of two criteria must be met, namely, the gauge itself must be self temperature compensating or a compensating gauge must be incorporated into the wheatstone bridge circuit to minimize the effects of transient changes in ambient temperature.

When using a compensating gauge it is necessary that it be of the same resistance and gauge factor as the active gauge. Also, it is essential that the compensating gauge be mounted on the same material that the active

gauge is mounted on. Within the bridge circuit the compensating gauge is designated as resistor  $R_2$  while the active gauge is resistor  $R_1$ . As the test specimen is loaded and a change in temperature occurs, the resulting change in resistance is given by

$$\frac{\Delta R_1}{R_1} = S_g \epsilon + \frac{(\Delta R_g)_{\Delta T}}{R_g} \quad (15)$$

and

$$\frac{\Delta R_2}{R_2} = \frac{(\Delta R_g)_{\Delta T}}{R_g} \quad (16)$$

where  $(\Delta R_g)_{\Delta T}$  is the resistance change of the gauge due to change of temperature  $\Delta T$ . Because there are only two gauges utilized in the bridge circuit  $\Delta R_3 = \Delta R_4 = 0$ . Substitution into equation 10 yields an output voltage

$$\Delta E = V_r \left( S_g \epsilon + \frac{(\Delta R_g)_{\Delta T}}{R_g} - \frac{(\Delta R_g)_{\Delta T}}{R_g} \right) \quad (17)$$

Thus

$$\Delta E = V_r S_g \epsilon \quad (18)$$

and temperature effects are eliminated from the measurement.

#### OPTIMIZING STRAIN GAUGE EXCITATION LEVELS

The voltage applied to the strain gauge bridge creates a power loss in each arm which is dissipated in the form of heat. Therefore the sensing portion of every strain gauge operates at a temperature higher than that of the substrate. The heat generated within the strain gauge is transferred to the substrate via conduction and is a function of the thermal conductivity of the substrate

and mounting adhesive along with the gauge power level.

When an excessive bridge excitation causes a temperature rise which is excessive for optimal gauge performance the following occurs:

- 1) a loss of self-temperature compensation occurs at grid temperatures considerably above specimen temperatures
- 2) hysteresis and creep effect are magnified
- 3) zero (no load) stability is affected

Power-dissipation capability of a strain gauge varies approximately with the area of the grid. The amount of water proofing or encapsulation generally does not affect the value. Also high thermal conducting adhesives generally do not improve the power dissipation due to the adhesives increased viscosity resulting in a greater glue thickness (ideal glue thickness = 0.0024 mm - 0.0076 mm).

Factors essential for optimum strain gauge excitation include:

- 1) strain gauge grid use
- 2) gauge resistance - higher resistances permit higher voltage for a given power level
- 3) heat sink properties of the mounting surface
- 4) environmental operating temperature range of the gauge installation
- 5) required operational specifications  
-- can drive a gauge under dynamic loading conditions at a higher level and achieve a higher signal-to-noise ratio
- 6) installation and wiring technique  
-- partially unbounded soldering tabs or non-uniformity in glue line will create problems where the gauge is operated under higher excitation levels.

Stacked rosette gauges present a problem because the thermal path length is much greater from the upper grid to the substrate and also because the temperature rise of the lower grid adds directly to the grids above it. For a three-element stacked rosette a reduction factor of 2.5 should be used on the bridge excitation. On a two-element stack rosette a reduction factor of 1.7 should be used on the bridge excitation.

Experimental determination of maximum gauge excitation level under no-load conditions is performed by increasing the excitation voltage until a definite zero stability is observed. At this point the excitation should be reduced until zero reading becomes stable without any significant offset from the low-excitation zero reading.

The power-density levels for the strain gauge can be calculated from

$$\text{Power Dissipation in Grid (watts) } (P_G)$$

where

$$P_G = \frac{E_B^2}{4 R_g} \quad (19)$$

$$\text{Power Density of Grid (watts/in) } (P'_G)$$

where

$$P'_G = \frac{P_G}{A_G} \quad (20)$$

and

R = gauge resistance in ohms

G

A = grid area (gauge length x grid width)

G

$E_B$  = bridge excitation in volts

$$E_B = 2 \sqrt{\frac{R P A}{G G G}}$$

By understanding the behavior of the bridge excitation voltage as a function of grid area at a constant power-density level and the heat sink capacity of the test specimen the optimal conditions for utilizing the strain gauge can be determined.

#### TEMPERATURE-INDUCED APPARENT STRAIN AND GAUGE FACTOR VARIATION IN STRAIN GAUGES

Resistance strain gauges vary not only with strain but also with temperature. In addition the relationship between strain and resistance, the gauge factor, varies with temperature. These deviations from ideal behavior can result in significant errors if not properly accounted for.

Once a gauge is installed, subsequent changes in temperature of the gauge installation will generally produce a resistance change in the gauge. This purely temperature induced strain is referred to as an apparent strain.

During static strain measurements temperature changes are potentially the most serious error source. The apparent strain is caused by two concurrent and algebraic additive effects in the strain gauge installation. The electrical resistivity of the grid conductor is temperature dependent, and any resistance change with temperature due to this effect appears as a strain on the instrumentation. Also, differential thermal expansion

between the grid conductor and the substrate material to which the gauge is bonded results in an apparent strain. With a change of temperature, the substrate expands or contracts and since the strain gauge is firmly bonded to the substrate it undergoes the same expansion or contraction. With differences in thermal expansion coefficients between the strain gauge grid and the substrate material, the grid is mechanically strained in conforming to the free expansion or contraction of the substrate material. The resultant resistance change appears as a strain on the instrumentation.

The net temperature induced apparent strain can be expressed as

$$\epsilon_{APP(G/S)} = \left[ \frac{\beta_G}{F} + (a_s - a_G) \right] \Delta T \quad (21)$$

where

$\epsilon_{APP(G/S)}$  = apparent strain of grid G on substrate material S

$\beta_G$  = thermal coefficient of resistance of grid conductor

$(a_s - a_G)$  = difference in thermal expansion coefficient between substrate and grid

$\Delta T$  = temperature change from an arbitrary initial reference temperature.

F = gauge factor

The above equation is non-linear with temperature since all of the coefficients are themselves temperature dependent. The equation does demonstrate that apparent strain exhibited with temperature change depends not only on the nature of the gauge itself but also on the material

to which the gauge is bonded.

If a test part with a strain gauge mounted on it is brought to the test temperature in the test environment maintaining the test part completely free of mechanically or thermally induced stresses, the strain indicator should be balanced to yield zero strain under these conditions and no apparent strain will exist when subsequent strain measurements are made at that specific temperature. Thus, when during a strain measurement no temperature changes are encountered there will be no apparent strain induced into the testing system. However, in practice this is rarely achievable and it becomes necessary to account for apparent strains. In purely dynamic testing there is no need to maintain a stable zero-strain reference because of the higher frequency of the dynamic strain signal compared to the temperature change frequency.

Theoretically the error due to apparent strain can be eliminated by employing a dummy gauge in the adjacent arm of the wheatstone bridge mounted on an unstrained specimen made of the identical material as the test specimen and subject to the same temperature conditions as the active gauge. Therefore both gauges should exhibit the same apparent strain and since identical strains in adjacent arms of the wheatstone bridge cancel exactly, only the stress induced strain will be measured. For the above to be precisely true the lead wires to the dummy and active gauge must be exactly the same length to prevent difference in resistance and they must travel together to ensure that temperature changes in both leads will be

identical. Certain metallurgical properties of gauge alloys are such that they can be processed to minimize the apparent strain over wide range of temperature values when bonded to materials with coefficients of thermal expansion for which the gauge alloy matches. This is referred to as self-temperature-compensated alloys (STC).

With the use of STC strain gauges the requirements for matching as unstrain dummy gauge is greatly relaxed. In the practice of making a strain measurement at or near room temperature is sufficient to utilize a STC strain gauge in a quarter bridge arrangement completing the bridge circuit with a stable fixed resistor in the adjacent arm of the wheatstone bridge. Such a bridge completion resistor should have temperature coefficients of resistance not exceeding  $1 \times 10^{-6}$  per degree C.

When STC strain gauges are used with conventional temperature compensating techniques (active and dummy gauges on identical material) incorporating the STC strain gauges into adjacent arms of the wheatstone bridge yields excellent temperature compensation over a wide range of temperature.

The alloys used in resistance strain gauges typically exhibit a change in gauge factor with temperature. Depending on the circumstances of use, the alloy involved, and the requirements of accuracy the effect of the gauge factor variation may be small and insignificant or it may introduce significant errors into the strain measurement.

The gauge factor is determined for a given type of

strain gauge at room temperature. This is the value of the gauge factor that is normally supplied by the manufacturer. Thus when the gauges are used at a temperature other than room temperature, the resulting gauge factor will be different and may require correction depending on the circumstances.

By knowing the gauge factor variation as a function of temperature any strain measurement can be easily corrected from one gauge factor to another. If a strain was measured assuming a gauge factor of  $F_1$  and it is necessary to correct the strain to the actual gauge factor then the corrected strain  $F_2$  is calculated from

$$\epsilon_2 = \epsilon_1 \frac{F_1}{F_2} \quad (22)$$

## 2.2 MATERIALS AND METHODS

The experimental stress analysis was conducted in two separate phases. Phase I investigated the effect of cuspal reinforcement by a restoration placed using the acid-etch technique. Phase II expanded on this by examining the effect of dentinal bonding in conjunction with the acid-etch technique on cuspal reinforcement by an intracoronal restoration.

Twenty freshly extracted, non-carious maxillary premolars were selected for the study. The teeth were stored in deionized water at 4 degrees centigrade until they were prepared for testing. A general characterization of each tooth was obtained by measuring the intercuspal distance.

The strain gauges used in the study consisted of a constantan grid fully encapsulated in a polyimide, Fig. 1. The grid specifications are as follows: #CEA-06-032UW-120, resistance = 120.0 ohms +/- 0.3%, gauge factor = 2.13 +/- 1% at 24 degrees centigrade, length = 0.81 mm, width = 1.52 mm, thickness = 0.056 mm (Micro-Measurements Division, Measurements Group, Raleigh, N.C.). The polyimide gauge backing was trimmed to optimize grid conformation to the contours of the tooth surface.

In phase I of the study the strain gauges were bonded to the buccal surface of twelve teeth using the acid-etch technique. The buccal surface was etched with a 37% by volume solution of orthophosphoric acid for 60 seconds. The tooth was then rinsed in water and dried with a stream of air. The gauge backing was cleaned with chloroform to ensure an oil free surface. Enamel Bond Resin (3M Company, St. Paul, MN) was coated onto the prepared tooth and gauge backing. The two surfaces were brought into contact such that the grid of the strain gauge was positioned over the crest of convexity of the buccal surface of the tooth.

Two teeth with strain gauges bonded were mounted in close proximity to each other in a nylon ring using improved dental stone, Fig. 2. The lead wires for the strain gauges were partially embedded in the stone to immobilize them. With this arrangement, one of the teeth acted as a compensator for any strains due to temperature fluctuations and was not subjected to any force. The remaining tooth was the test sample. The two strain

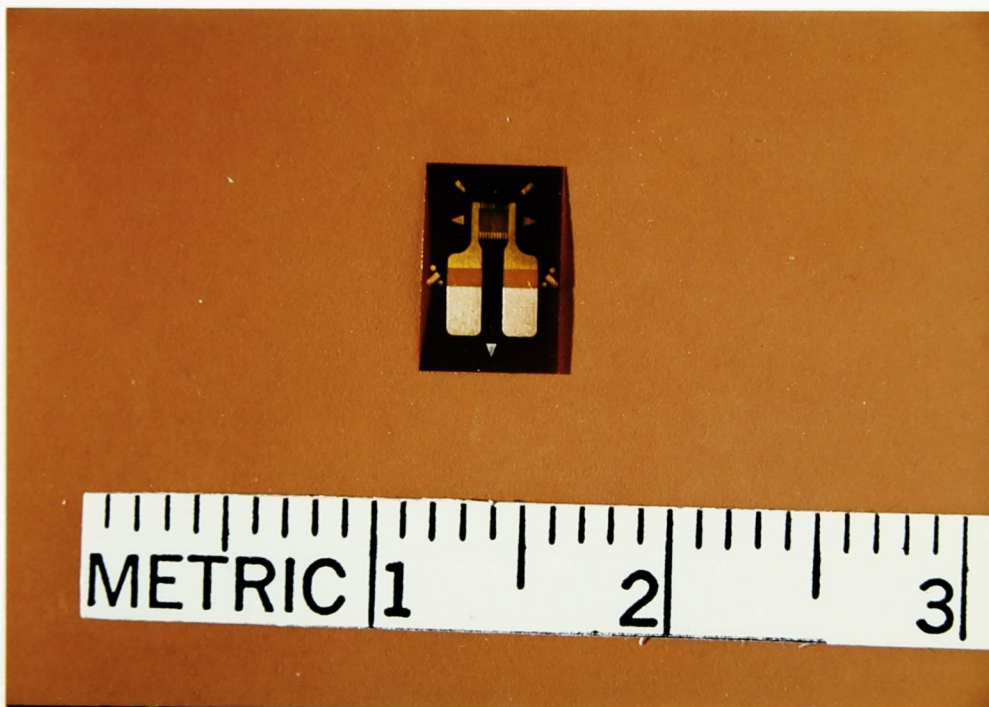


Figure 2. Teeth with bonded strain gauges mounted in Figure 1. Polyimide encapsulated strain gauge.

gauges were connected such that they supplied one-half of a wheatstone bridge, the other half being internal to a 2100 Strain Measurement System (Instruments Division, Measurements Group, Raleigh, N.C.). This setup of instrumentation allows for any changes in resistance due to ambient temperature fluctuations experienced by the strain gauge on the test sample to be compensated for by an equal and opposite change in resistance by the non-test sample strain gauge. Thus, the bridge circuit detects unbalanced conditions resulting from only a stress-induced



to the buccal and lingual surfaces of the tooth. The points of contact of the steel sphere on the tooth were also far enough up the buccal incline such that when the tooth was subsequently prepared and restored, the steel sphere did not contact the cavosurface margin of the cavity or restoration.

The M.T.S. machine was configured to monitor the force applied to the sample (load control). It was

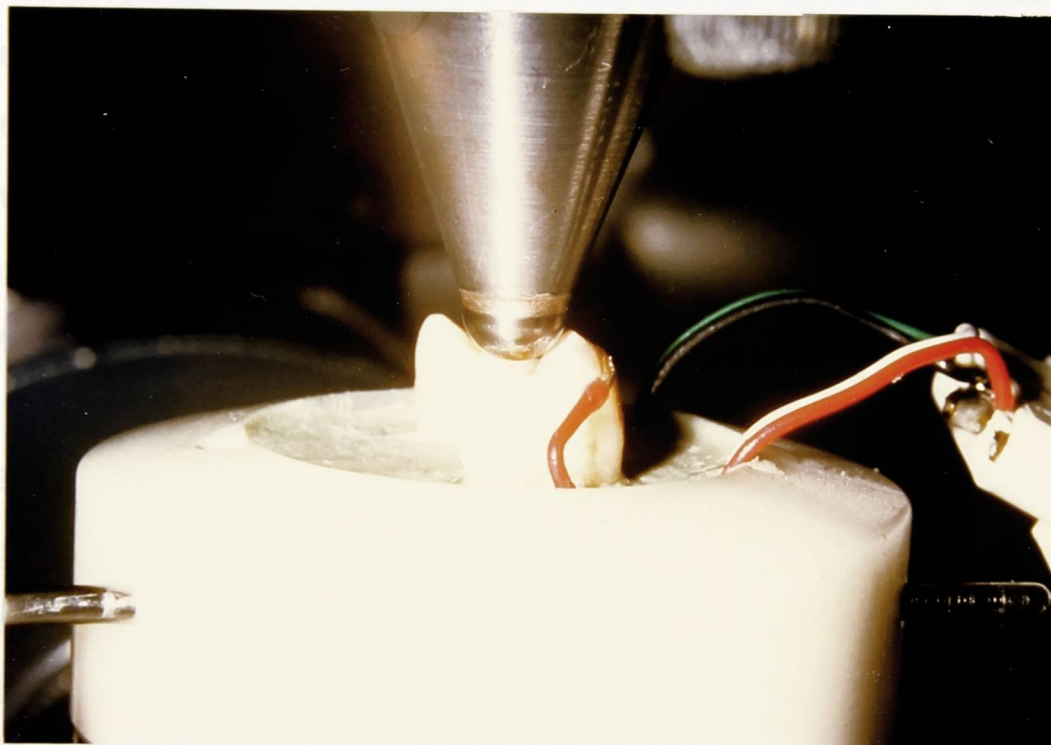
Figure 2. Teeth with bonded strain gauges mounted in dental stone.

gauges were connected such that they comprised one-half of a wheatstone bridge, the other half being internal to a 2100 Strain Measurement System (Instruments Division, Measurements Group, Raleigh, N.C.). This set-up of instrumentation allows for any changes in resistance due to ambient temperature fluctuations experienced by the strain gauge on the test sample to be compensated for by an equal and opposite change in resistance by the non-test sample strain gauge. Thus, the bridge circuit detects unbalanced conditions resulting from only a stress-induced strain on the test sample.

The mounted teeth were positioned on the lower platen of an M.T.S. 812 Servohydraulic Testing Machine (M.T.S. Systems, Eden Prairie, MN). A steel sphere 6.35 mm in diameter was rigidly attached to the upper crossmember of the machine. The steel sphere was brought into simultaneous contact with both the buccal and lingual cusps of the tooth, Fig. 3. The points of contact on the tooth were modified with a flame-shaped equilibrating bur to ensure that the normal force was directed perpendicular to the buccal and lingual surfaces of the tooth. The points of contact of the steel sphere on the tooth were also far enough up the cuspal inclines such that when the tooth was subsequently prepared and restored, the steel sphere did not contact the cavosurface margin of the cavity or restoration.

The M.T.S. machine was configured to monitor the force applied to the sample (load control). It was programmed to deliver an axial force to the occlusal of the MTS machine.

surface of the tooth at a constant rate of 74.1 N/second up to a maximum force of 271.4 N. The tooth was unloaded at the same rate. These forces are within the range expected in the oral cavity. By applying the force under load control, the apparatus compensates for any relaxation within the tooth or the mounting. Under these conditions, the force applied to the tooth results in the deformation of both the lingual and buccal cusps. The strain gauges bonded to the buccal surface of the tooth will measure the strain.



design for use with a single tooth. The bar was used for each cavity preparation. The bucco-lingual width of the cavity isthmus was approximately one-fourth the intercusp distance. The proximal boxes were dimensioned and positioned to represent an idealized clinical situation. The modified MOD preparation included a 1-mm-wide, 45 degree bevel of all cavosurface margins.

In all restorative conditions there was a smooth and

Figure 3. Positioning of the mounted teeth on the platen of the MTS machine.

surface of the tooth at a constant rate of 74.1 N/second up to a maximum force of 222.4 N. The tooth was unloaded at the same rate. These forces are within the range expected in the oral cavity<sup>51</sup>. By applying the force under load control, the servohydraulics compensate for any relaxation within the tooth or the mounting. Under these conditions, the force applied to the tooth results in the deformation of both the lingual and buccal cusps. The strain gauge bonded to the buccal surface of the tooth will produce a change in resistance which is measured by the wheatstone bridge circuit and is directly proportional to the magnitude of deformation of the buccal cusp of the test sample. The simultaneous read-out of the strain gauge and the applied force were used to generate a force-strain curve for the buccal cusp of the tooth.

The study design for phase I is shown in Table 1. Each sample tooth was subjected to an occlusal preparation, a mesial-occlusal-distal (MOD) preparation, and a number of restorations in a carefully sequenced order. The cavity preparation followed the traditional design for use with amalgam. A new bur was used for each cavity preparation. The bucco-lingual width of the cavity isthmus was approximately one-fourth the intercuspal distance. The proximal boxes were dimensioned and positioned to represent an idealized clinical situation. The modified MOD preparation included a 1-mm-wide, 45 degree bevel of all cavosurface margins.

In all restorative conditions there was a smooth and continuous transition from the restorative material to

TABLE 1  
STUDY DESIGN FOR PHASE I

Sequence of Procedures for each Tooth	Condition No.
Sound Tooth	1
Occlusal Preparation	2
MOD Preparation	3
Composite A* Restoration	4
Restoration Removed	5
Composite B# Restoration	6
Restoration Removed	7
Amalgam\$ Restoration	8
Restoration Removed	9
Composite B@, Acid Etch, Overcontoured	10
Restoration Removed, MOD with Beveled Cavosurface Margins	11
Composite B@, Acid Etch, Beveled Margins	12

\*Concise, 3M Company, St. Paul, MN 55101

#P-10, 3M Company, St. Paul, MN 55101

\$Dispersalloy, Johnson & Johnson, East Windsor, NJ 08520

@P-10 and Enamel Bond, 3M Company, St. Paul, MN 55101

tooth structure except for the bonded restoration involving composite B in the unmodified MOD cavity preparation (Table 1, condition 10). In this instance, composite B was over contoured on all cavosurface margins to maximize the interaction between the restorative material and the etched enamel. The overcontouring was such that it did not interfere or contact with the steel sphere when the force was applied to the tooth.

The procedure for acid-etching the cavosurface of the unmodified and modified MOD cavity preparations (Table 1, conditions 9 and 11) was the same as the procedure for acid-etching the buccal surface of the tooth for the bonding of the strain gauge. Care was taken to limit the etching to a 1-mm-wide strip around the cavosurface of the MOD cavity preparation. An intermediate layer of resin was placed on the etched enamel prior to placement of the composite.

A force-strain curve was generated for the sound tooth, the occlusal cavity preparation, the MOD cavity preparation and each restorative condition. This testing regime was repeated for each of the twelve teeth in phase I of the study. The composite restorations were allowed to set for 30 minutes before a force-strain curve was generated. Amalgam restorations were allowed to set for one hour at which time 50% of its ultimate compressive strength had developed.

Phase II of the study utilized eight teeth which were subjected to a different sample preparation and testing regime. Two strain gauges, similar to those used in phase

I, were bonded to each tooth with the grid of the gauge being centered over the buccal and lingual crest of convexity, Fig. 4, 5. The acid-etching of the buccal and lingual surfaces of the teeth was the same as in phase one of the study. A special cyanoacrylate adhesive, M-Bond 200 (Micro-Measurements Division, Measurements Group, Raleigh, N.C.), specifically designed to provide minimal adhesive thickness with maximum bond strength to the strain gauge, was used to bond the strain gauge to the tooth surface. The strain gauges were then coated with Enamel Bond Resin to ensure waterproofing of the strain gauge and the exposed ends of the leads.

The mounting of the teeth in preparation for force application in phase II of the study consisted of actually bonding the tooth to the mounting material, Fig. 6. The root of the tooth was cleaned of any residual soft tissue and then prepared by removing the thin cemental layer with a rotary green stone. The root was then coated with a intermediate layer of Scotch Bond Dentinal Adhesive (3M Company, St. Paul, MN). The mounting material was bisphenol A - glycidyl methacrylate (BIS-GMA) resin with a 60% by weight filler of silane treated quartz. The use of this mounting scheme resulted in a chemical bonding of the root of the tooth to the BIS-GMA mounting resin. This provided greater stability and enhanced reproducibility since the BIS-GMA resin does not deteriorate in the presence of water as does the improved dental stone. The lead wires to the strain gauges were also partially embedded in the mounting to immobilize them. The strain

A



B

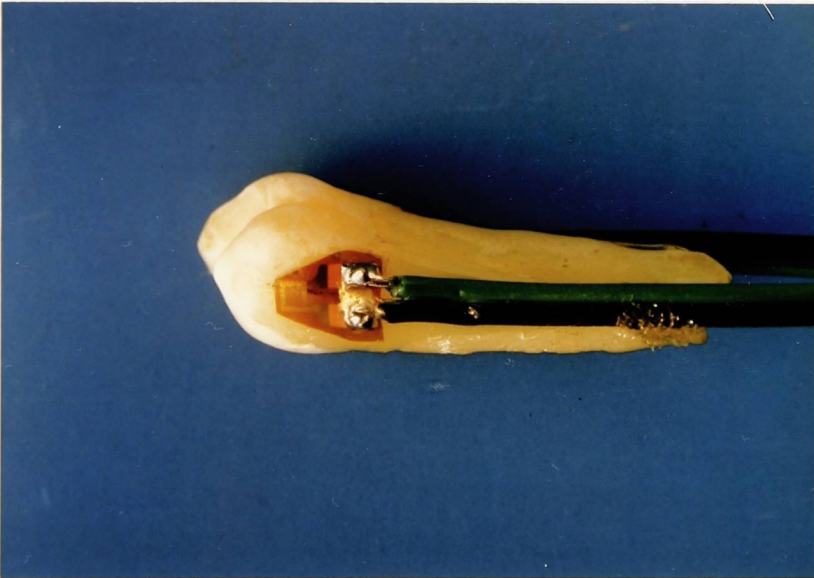


Figure 4. Positioning of strain gauges on the buccal, A, and lingual, B, cusps.



Figure 5. Proximal view of the tooth with strain gauges on the buccal and lingual cusps.

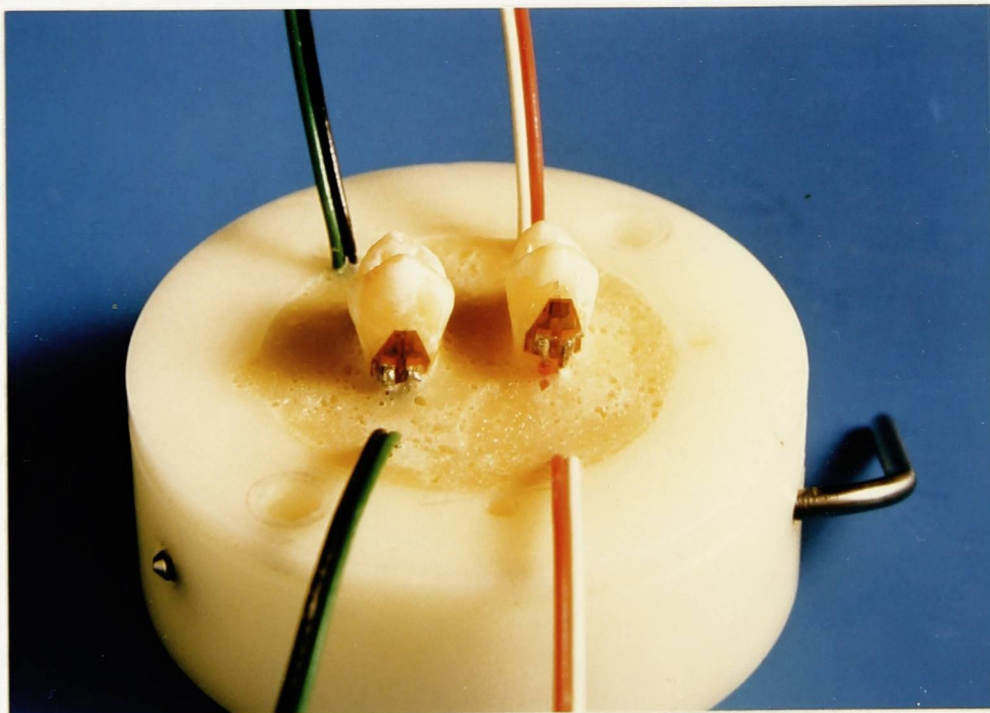
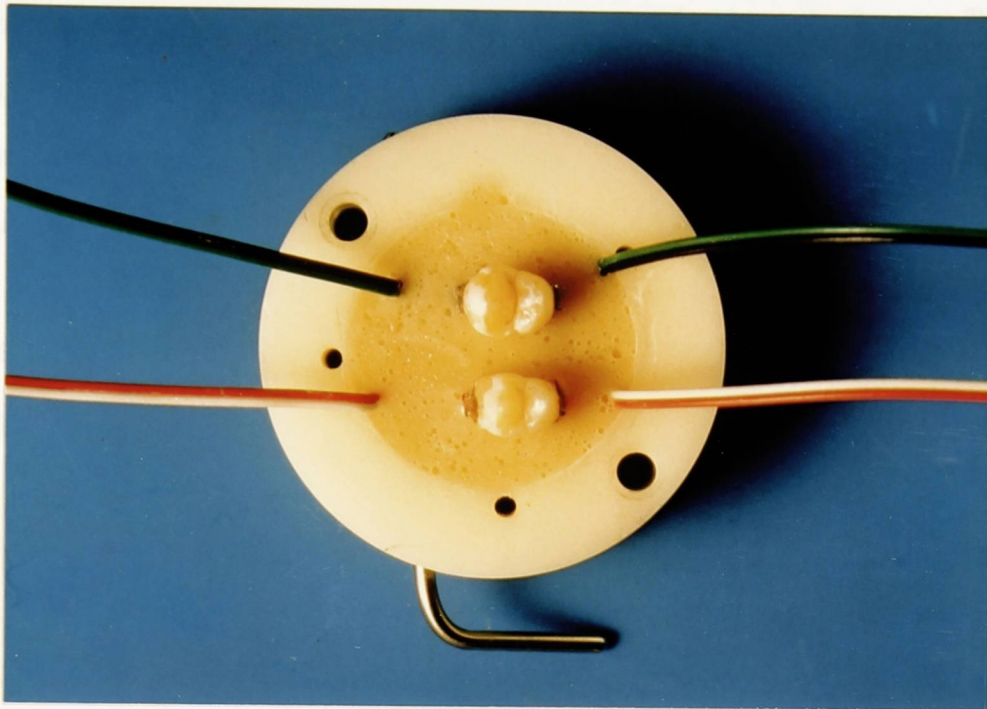


Figure 6. The teeth with bonded strain gauges mounted in composite.

gauge instrumentation was the same as in phase I.

The mounted teeth were positioned in the M.T.S. machine the same as in phase one of the study. The axial force applied to the occlusal surface of the tooth was at a constant rate of 37.1 N/second up to a maximum force of 111.2 N. The tooth was unloaded at the same rate.

The study design for phase II is shown in Table 2. Each sample tooth was subjected to four MOD cavity preparations of increasing dimension and a number of restorations in a sequenced order. The dimension of the preparations were determined by dividing the cavity isthmus dimension by the intercuspal distance of that tooth. This resulted in a fraction which indicated the relative size of the cavity preparation. These values of relative size are listed next to the corresponding MOD cavity preparation in Table 3. The cavity preparations followed the traditional design for use with amalgam but included a 1-mm-wide, 45 degree bevel of all cavosurface margins.

In all restorative conditions there was a smooth and continuous transition from the restorative material to tooth structure. The procedure for acid-etching the cavosurface of the modified MOD cavity preparation was the same as in phase one of the study. However, the intermediate resin was applied not only to the etched enamel but also to any exposed dentinal surface.

A force-strain curve was generated for the sound tooth, the MOD cavity preparations and each restorative condition recording both the buccal and lingual strain

TABLE 2  
 CAVITY STUDY DESIGN FOR PHASE II

Sequence of Procedures for each Tooth	Condition No.
Sound Tooth	1
MOD Preparation (1)	2
Composite B*	3
MOD Preparation (2)	4
Composite B*	5
MOD Preparation (3)	6
Composite B*	7
MOD Preparation (4)	8
Composite C#	9

\*P-10 and Scotch Bond, 3M Company, St. Paul, MN 55101  
 #P-30 and Scotch Bond, 3M Company, St. Paul, MN 55101

Gauge output. The composite restorations were allowed to set 45 minutes prior to any testing.

To determine the experimental values of Young's modulus of the different restorative technology was

**TABLE 3**

**CAVITY SIZE AND CAVITY RATIO FOR THE MOD CAVITY PREPARATIONS IN PHASE II**

Condition	Cavity Size (mm)	Std. Dev. Cavity Size	Cavity Ratio (CR)	Std. Dev. (CR)
2 (MOD 1)	1.32	0.21	0.21	0.03
4 (MOD 2)	2.17	0.25	0.35	0.03
6 (MOD 3)	2.97	0.28	0.47	0.04
8 (MOD 4)	3.48	0.28	0.56	0.02

amalgam. Sample preparation for the P-30 composite consisted of filling a glass vial with the material and the allowing the material to polymerize while under a load of 178 N. A dental syringe was modified so that it could be positioned on the plates of the M.S.S. machine and maintain the vial containing the material in position to receive the load, Fig. 7. After being under load for fifteen minutes the material samples were placed in a 40 degree C oven for one hour to ensure complete polymerization.

P-30 composite and Dispersalloy amalgam were prepared in a slightly different manner. Due to the high viscosity of the P-30 composite it was necessary to warm the composite to a temperature of 40 degrees C to help facilitate its placement into the vial. Because the P-30 composite has a light activated polymerization mechanism,

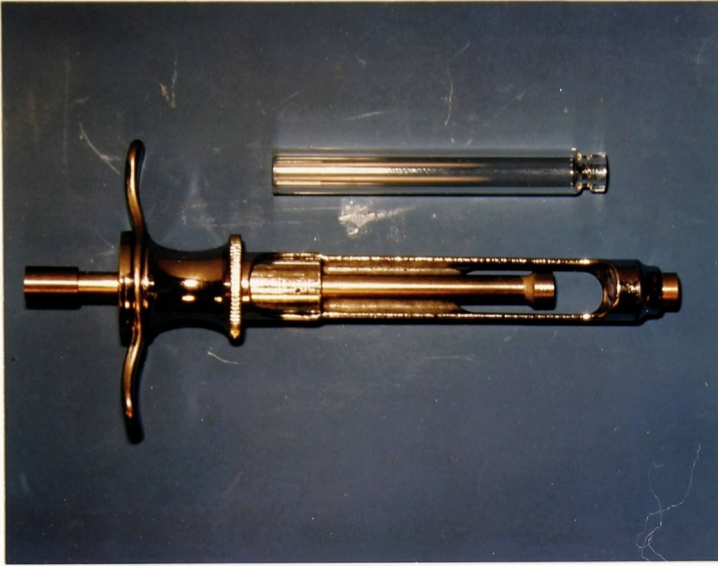
gauge output. The composite restorations were allowed to set 45 minutes prior to any testing.

To determine the experimental values of Young's modulus of elasticity and Poisson's ratio for different restorative materials, strain gauge technology was employed. Utilizing two-element rosette strain gauges with the elements orientated at right angles, cylindrical specimens of the restorative materials were stressed at low loads in compression recording the resulting strain output. From this the material properties were calculated.

Three different restorative materials were evaluated, namely P-10 composite, P-30 composite and Dispersalloy amalgam. Sample preparation for the P-10 composite consisted of filling a glass vial with the material and allowing the material to polymerize while under a load of 178 N. A dental syringe was modified so that it could be positioned on the platen of the M.T.S. machine and maintain the vial containing the material in position to receive the load, Fig. 7. After being under load for fifteen minutes the material samples were placed in a 40 degree C oven for one hour to ensure complete polymerization.

P-30 composite and Dispersalloy amalgam were prepared in a slightly different manner. Due to the high viscosity of the P-30 composite it was necessary to warm the composite to a temperature of 40 degrees C to help facilitate its placement into the vial. Because the P-30 composite has a light activated polymerization mechanism,

A



B



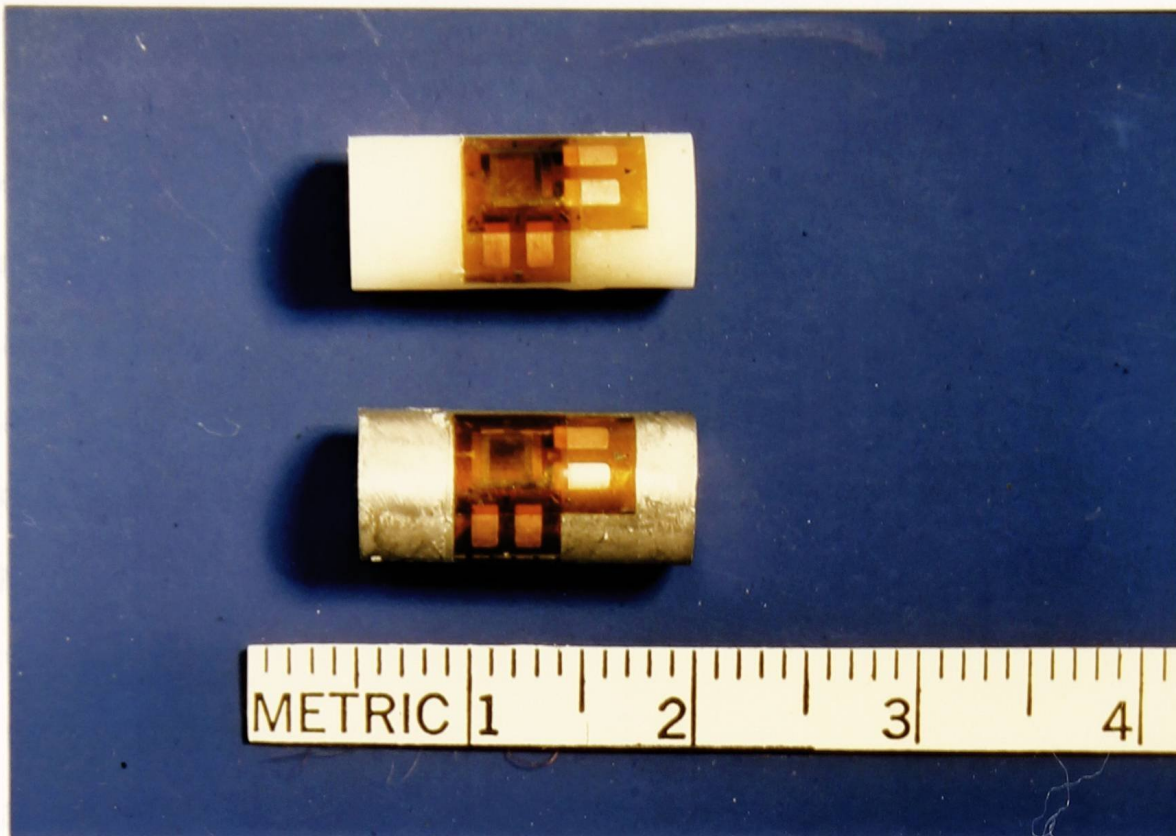
Figure 7. Modified dental syringe and vial, A. Positioning of the modified syringe and vial on the platens of the MTS machine, B.

the samples were illuminated with blue light via a Kulzer Translux light generator for fifteen minutes under a load of 178 N while positioned in the M.T.S. machine. The samples were then placed in a Berkey Ascor light generator for ten minutes and then in the 40 degree C oven for one hour. The Dispersalloy amalgam was first placed into the vial and then hand condensed with a 6.35 mm plunger until a sufficient amount of material had been placed into the vial. The vial was then positioned in the M.T.S. machine under a load of 133 N and cyclically loaded with a half sine wave to a maximum load of 178 N for five hundred cycles. The sample was then maintained at a load of 178 N for one hour, and then placed into the 40 degree C oven for a twentyfour hour period.

The material samples were dimensioned such that the length to diameter ratio was nearly 2:1. Thus, for an average diameter of 6.68 mm the length of the samples was prepared at 14.00 mm. The strain gauges were positioned at the midpoint along the length of the samples, Fig. 8. For the P-10 composite, Enamel Bond resin was used to attach the gauges to the samples. For the other restorative materials, M-Bond 200 strain gauge adhesive was used. The strain gauges were incorporated into a quarter Wheatstone Bridge arrangement with an internal dummy resistor contained with the 2100 Strain Measurement System. The excitation voltage across the bridge was 0.90 volts.

Prior to the actual testing of the samples, a thin layer of P-10 composite was applied to both ends of the

samples. The samples were prepared between the  
A atoms of the crystal lattice when a load of 22.5 N for



15.1 N per second under load control to a nominal load of  
111.2 N and 222.4 N. The corresponding stress from the

B  
two-element rosette was

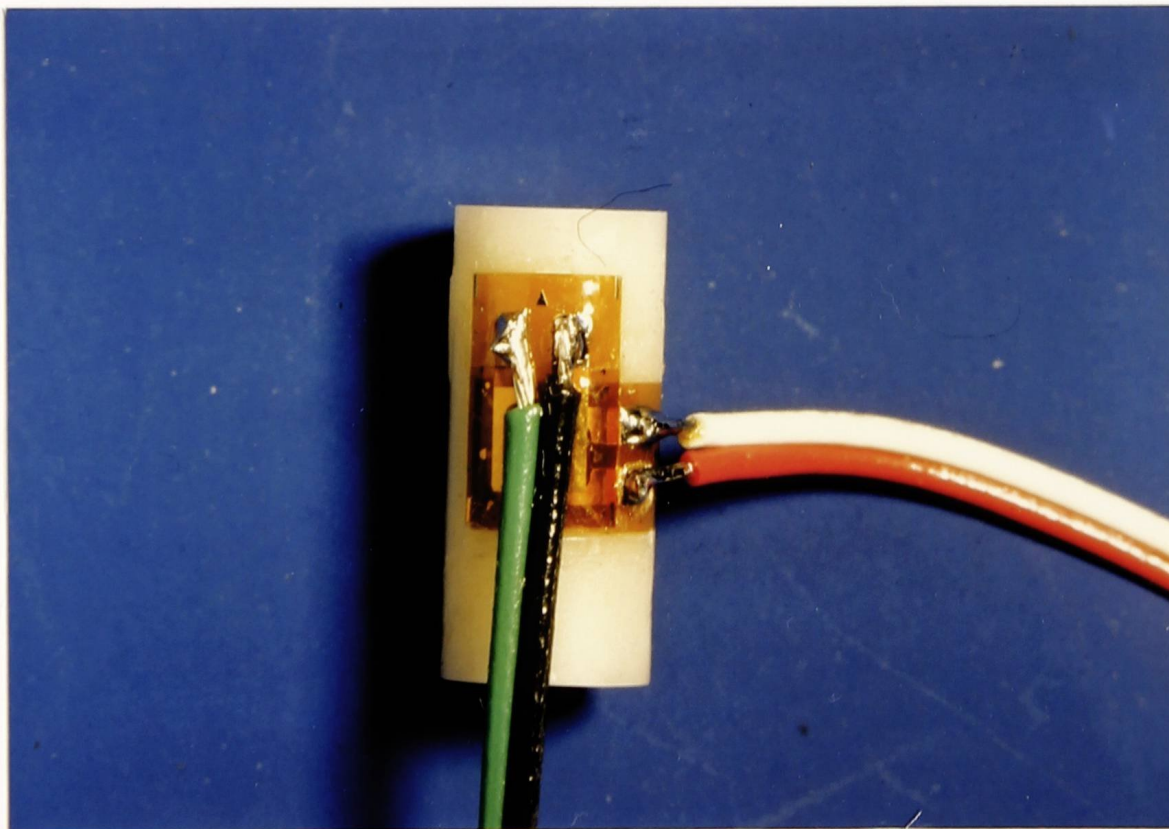


Figure 8. Material samples with bonded rosette strain gauges, A, and lead wire attachment, B.

samples. The samples were then positioned between the platens of the M.T.S. machine under a load of 22.5 N for five minutes at which time the thin layer of P-10 composite had cured. The thin layer ensured that the ends of the samples were square to the platens of the M.T.S. machine and that upon loading there would be a uniform application of force to the sample. This eliminated apparent strain effects due to non-symmetrical loading. Once the samples were in position on the platens of the M.T.S. machine and the thin layer of P-10 had fully cured the samples were not allowed to disengage either end from the platens. A baseline load of 4.4 N ensured this. Samples were loaded and unloaded at a constant rate of 35.1 N per second under load control to a maximum load of 111.2 N and 222.4 N. The corresponding strains from the two-element rosette were recorded.

-----  
 Maximum load applied to sound tooth  
 -----  
 Maximum strain recorded from the sound tooth  
 -----  
 Maximum strain recorded from sound tooth  
 -----  
 Maximum strain recorded in treatment condition

Because the maximum load applied to both the sound tooth and the treatment conditions are the same, these two terms in the above equation cancel. Therefore, the relative stiffness (RS) reduces to a simple ratio of strain values. A relative stiffness equal to one,  $RS = 1.0$ , represents the normalized value of the sound tooth and is considered to be an ideal value. If during any treatment condition the relative stiffness of the cusp is less than one,

### 3. RESULTS OF EXPERIMENTS

The strain data for both phase I and II of the experimental stress analysis are presented in Tables 4 and 5 respectively. The strain data for the different conditions was normalized to that of the sound tooth and are presented in Tables 6 and 7. This normalization compares between the different treatment conditions and minimizes the experimental and morphologic differences among the various teeth. These normalized values are termed the relative stiffness (RS) of the cusp and are defined as:

$$\begin{aligned}
 \text{RS} &= \frac{\text{stiffness of the cusp during treatment condition}}{\text{stiffness of the cusp in the sound tooth}} \\
 &= \frac{\frac{\text{Maximum load applied in treatment condition}}{\text{Maximum strain recorded in treatment condition}}}{\frac{\text{Maximum load applied to sound tooth}}{\text{Maximum strain recorded from the sound tooth}}} \\
 &= \frac{\text{Maximum strain recorded from sound tooth}}{\text{Maximum strain recorded in treatment condition}}
 \end{aligned}$$

Because the maximum load applied to both the sound tooth and the treatment conditions are the same, these two terms in the above equation cancel. Therefore, the relative stiffness (RS) reduces to a simple ratio of strain values. A relative stiffness equal to one,  $RS = 1.0$ , represents the normalized value of the sound tooth and is considered to be an ideal value. If during any treatment condition the relative stiffness of the cusp is less than one,

TABLE 4

THE STRAIN VALUES FOR THE BUCCAL CUSP OF  
MAXILLARY PREMOLARS UNDER DIFFERENT TREATMENT  
CONDITIONS IN PHASE I

Condition	Mean Strain	Std. Dev. of Mean Strain
1	116.4	54.5
2	138.6	54.3
3	207.9	80.2
4	200.7	75.7
5	223.8	84.5
6	187.7	87.8
7	223.8	94.0
8	237.6	93.3
9	242.5	88.2
10	140.2	70.6
11	277.1	90.0
12	132.3	72.7

TABLE 5  
 STRAIN VALUES FOR THE BUCCAL AND LINGUAL CUSPS OF  
 MAXILLARY PREMOLARS UNDER DIFFERENT TREATMENT  
 CONDITIONS IN PHASE II

Condition	Mean Strain	Std. Dev. of Mean Strain
BUCCAL		
1	51.7	32.5
2	135.0	103.3
3	53.9	34.2
4	141.3	70.1
5	53.2	41.5
6	178.2	114.1
7	71.0	42.6
8	245.0	174.8
9	64.7	45.9
-----		
LINGUAL		
1	146.9	28.6
2	262.6	62.0
3	174.2	69.9
4	266.3	100.5
5	207.7	102.5
6	291.4	68.7
7	223.1	88.9
8	372.8	135.7
9	262.4	142.8

TABLE 6

RELATIVE STIFFNESS AND DEFORMATION OF THE BUCCAL  
CUSP OF MAXILLARY PREMOLARS UNDER DIFFERENT TREATMENT  
CONDITIONS IN PHASE I

Condition	Mean Relative Stiffness	Std. Dev. of Relative Stiffness
BUCCAL		
1	1.0	---
2	0.84	0.12
3	0.56	0.09
4	0.58	0.10
5	0.52	0.09
6	0.62	0.13
7	0.52	0.12
8	0.49	0.09
9	0.48	0.12
10	0.83	0.18
LINGUAL		
11	0.42	0.10
12	0.88	0.32

RS < 1.0, then there was a loss of stiffness due to the treatment. Contrary to this, if the relative stiffness approaches one or is equal to or greater than one, then there was no significant change in stiffness. This parameter has the advantage that it is insensitive to variations in both tooth morphology and strain-gauge orientation/position on the tooth. This allows for direct comparisons between different teeth to be made. The mean C values are presented in Tables 2 and 3. Because of the magnitude of the standard deviation in the data, a log scale analysis of the strain data from phase II. The results are presented in Tables 11, 12 and 13. A comparison was considered significant (S) if the p value was less than 0.01 otherwise it was non-significant (NS).

TABLE 7

RELATIVE STIFFNESS AND DEFORMATION OF THE BUCCAL AND LINGUAL CUSPS OF MAXILLARY PREMOLARS UNDER DIFFERENT TREATMENT CONDITIONS IN PHASE II

Condition	Mean Relative Stiffness	Std. Dev. of Relative Stiffness
<b>BUCCAL</b>		
1 RS restored - RS NOs	1.00	---
2 RS sound tooth - RS	0.39	0.13
3	1.03	0.20
4	0.38	0.13
5	1.01	0.17
6	0.29	0.06
7	0.71	0.18
8	0.22	0.09
9	0.81	0.28
<b>LINGUAL</b>		
1	1.00	---
2	0.56	0.10
3	0.95	0.32
4	0.59	0.25
5	0.86	0.35
6	0.53	0.15
7	0.73	0.3
8	0.45	0.20
9	0.79	0.34

RS < 1.0, then there was a loss of stiffness due to the treatment. Contrary to this, if the relative stiffness approaches one or is equal to or greater than one, RS ≥ 1.0, then the treatment condition contributed significantly to the stiffness of the cusp.

To determine the percent recovery (loss) of sound tooth stiffness due to restorative treatment the parameter C is defined as

$$C = \frac{RS \text{ restored} - RS \text{ MOD}}{RS \text{ sound tooth} - RS \text{ MOD}} \times 100$$

This parameter has the advantage that it is insensitive to variations in both tooth morphology and strain-gauge orientation/position on the tooth. This allows for direct comparisons between different teeth to be made. The mean C values are presented in Tables 8 and 9.

Because of the magnitude of the standard deviation in the strain data in phase II a log scale analysis was performed. This helped to smooth the data such that the relative magnitude of change in the strain between different conditions could be compared. Results are listed in Table 10.

An analysis of variance was performed using both the stiffness ratios (RS), the percent recovery parameter C, and the log scale analysis of the strain data from phase II. The results are presented in Tables 11, 12, and 13. A comparison was considered significant (S) if the p value was less than 0.01, otherwise it was nonsignificant (NS).

TABLE 8

PERCENT RECOVERY OF STIFFNESS OF THE BUCCAL CUSP  
OF MAXILLARY PREMOLARS UNDER DIFFERENT RESTORATIVE  
CONDITIONS IN PHASE I

Condition	Percent Recovery of Stiffness (C)
BUCCAL	
4	(-1.0)
6	24.0
8	(-6.0)
10	68.0
12	88.0
LINGUAL	
3	48.0
5	45.0
7	48.0
9	48.0

TABLE 9

PERCENT RECOVERY OF STIFFNESS OF THE BUCCAL  
AND LINGUAL CUSPS OF MAXILLARY PREMOLARS UNDER  
DIFFERENT RESTORATIVE CONDITIONS IN PHASE II

Condition	Percent Recovery of Stiffness (C)	Std. Dev of (C)
BUCCAL		
3	107.0	33.0
5	102.0	29.0
7	65.0	23.0
9	78.0	33.0
-----		
LINGUAL		
3	94.0	68.0
5	60.0	49.0
7	50.0	60.0
9	66.0	53.0

TABLE 10

LOG SCALE ANALYSIS OF STRAIN DATA FROM THE BUCCAL  
AND LINGUAL CUSPS OF MAXILLARY PREMOLARS UNDER  
DIFFERENT TREATMENT CONDITIONS IN PHASE II

Condition	Log( 1 + Strain )	Std. Dev. of Log Value
BUCCAL		
1	1.65	0.35
2	2.07	0.30
3	1.64	0.34
4	2.07	0.27
5	1.52	0.58
6	2.18	0.32
7	1.80	0.29
8	2.29	0.32
9	1.73	0.30
-----		
LINGUAL		
1	2.16	0.09
2	2.41	0.10
3	2.20	0.17
4	2.41	0.16
5	2.26	0.20
6	2.45	0.10
7	2.33	0.17
8	2.54	0.18
9	2.37	0.23

TABLE 11  
 STATISTICAL COMPARISON OF STIFFNESS  
 FOR CAVITY PREPARATIONS IN PHASE I

SOUND TOOTH	OCC PREP	MOD PREP 3	MOD PREP 5	MOD PREP 7	MOD PREP 9	MOD PREP 11
	0.001	0.000	0.000	0.000	0.000	0.000
		0.513	0.000	0.012	0.000	0.000
OCC PREP S		0.000	0.000	0.000	0.000	0.000
	NS		0.004	0.001	0.000	0.002
MOD PREP 3 S	S		0.040	0.754	0.169	0.001
	S	NS		0.000	0.001	0.005
MOD PREP 5 S	S	NS		0.078	0.008	0.001
	NS	NS	S		0.000	0.000
MOD PREP 7 S	S	NS	NS		0.129	0.001
	S	S	S	S		0.131
MOD PREP 9 S	S	NS	S	NS		0.013
	S	S	S	S	NS	
MOD PREP 11 S	S	S	S	S	NS	
BEVEL						

TABLE 12

STATISTICAL COMPARISON OF DIFFERENT RESTORATIVE CONDITIONS IN PHASE I

	MOD PREP (3)	COMP A (4)	COMP B (6)	AMALGAM (8)	COMP B (10)	COMP B (12)
MOD PREP (3)		0.613	0.000	0.012	0.000	0.000
COMP A (4)	NS		0.024	0.471	0.000	0.002
COMP B (6)	S	NS		0.000	0.001	0.005
AMALGAM (8)	NS	NS	S		0.000	0.000
COMP B (10)	S	S	S	S		0.183
COMP B (12)	S	S	S	S	NS	

TABLE 13

STATISTICAL COMPARISON OF THE LOG SCALE  
ANALYSIS OF THE STRAIN DATA IN PHASE II

	SOUND TOOTH	MOD (1)	MOD (2)	MOD (3)	MOD (4)	REST (1)	REST (2)	REST (3)	REST (4)
SOUND TOOTH		0.00	0.00	0.00	0.00	0.76	0.18	0.00	0.09
MOD (1)	S		0.99	0.01	0.00	0.00	0.00	0.00	0.00
MOD (2)	S	NS		0.03	0.00	0.00	0.00	0.00	0.00
MOD (3)	S	NS	NS		0.01	0.00	0.00	0.00	0.00
MOD (4)	S	S	S	S		0.00	0.00	0.00	0.00
REST (1)	NS	S	S	S	S		0.23	0.00	0.12
REST (2)	NS	S	S	S	S	NS		0.04	0.14
REST (3)	S	S	S	S	S	S	NS		0.25
REST (4)	NS	S	S	S	S	NS	NS	NS	

Table 5 (conditions 1, 2, 3, 11) and Table 6 (conditions 1, 2, 4, 6, 8) demonstrate that as tooth structure is removed through cavity preparation the relative stiffness (RS) of the crown decreases while the relative deformation (RD) increases. Table 5 shows that the MOD preparations and the non-bonded restorative conditions can be grouped together with a relative stiffness (RS) in the range of 0.48 to 0.62 (conditions 3, 4, 5, 6, 7, 8). Further, the bonded restorations in both experiments, phase I and phase II, displayed a significant recovery of stiffness approaching that of the sound tooth.

Statistically, the bonded restorations were significantly different from all other conditions except for condition 7 in phase II. This restoration, however, still provided significant recovery of stiffness and was statistically different from all the MOD preparations. There was significant difference between the bonded restorations except again for condition 7 in phase II.

#### MATERIAL PROPERTY RESULTS

It has been demonstrated that when a strain gauge is installed on a sharply curved surface, the resulting apparent strain due to temperature fluctuations is different from that for a gauge mounted on a flat surface<sup>49</sup>. The curvature induced apparent strain is termed incremental apparent strain and is due to the thickness of the adhesive and gauge backing between the strain sensitive grid and the test sample. The incremental apparent strain can normally be considered a second-order effect and can be ignored. However, when the

radius of curvature becomes very small then the effect can become significant. Generally when the radius of curvature is less than 12.7 mm then the effect of the incremental strain should be corrected for in the strain measurement. An expression for estimating the incremental strain is written as

$$\Delta \epsilon_{APP} = \frac{1}{R} \left[ (1 + 2\nu_{A-B})(h_A \alpha_A - h_B \alpha_B) - 2\nu_{A-B} \alpha_s (h_A + h_B) \right] \Delta T \quad (23)$$

where

$\Delta \epsilon_{APP}$  = curvature-induced incremental apparent strain

$R$  = radius of curvature of test surface at gauge site

$\nu_{A-B}$  = average Poisson's ratio of adhesive and backing

$h_A, h_B$  = adhesive and backing thickness respectively

$\alpha_A, \alpha_B$  = thermal expansion coefficients of adhesive and backing respectively

$\alpha_s$  = thermal expansion of test sample

$\Delta T$  = temperature change from reference temperature

The radius of curvature is positive for a convex surface while negative for a concave surface. The estimated incremental apparent strain is added algebraically to the apparent strain value for a given temperature thus yielding a curvature corrected apparent strain. Thus for a 1 degree C change from ambient temperature (24 degrees C) the resulting curvature corrected apparent strain is on the order of one microstrain. Considering that the strain measurements were made under dynamic loading conditions, both the incremental apparent strain and the apparent strain were neglect from the calculations.

4. DISCUSSION OF DATA AND RESULTS

Results are as follows:

MATERIAL	YOUNG'S MODULUS ( $\times 10^{10}$ N/M <sup>2</sup> )	POISSON'S RATIO
P-10 composite	2.06 +/- 0.008	0.252 +/- 0.008
P-30 composite	4.88 +/- 0.117	0.29 +/- 0.05
Dispersalloy amalgam	4.83 +/- 0.042	0.32 +/- 0.02

less stiff than the sound tooth. In addition, the placement of bevels on the surface of the MOD preparation further decreases the stiffness of the crown. In phase II of the experiments each consecutive beveled MOD preparation displayed a decrease in the relative stiffness of the crown.

The placement of non-bonded restorative materials in two of the treatment conditions in phase I (conditions 4, 8) showed no statistical difference from the MOD preparation. However, the study did show that condition 4 did provide for a significant recovery of stiffness. This may have been due to the frictional effect between the fired walls of the proximal boxes and composite B which contains a very high percentage weight of quartz filler. The recovery of 24% of sound tooth stiffness for this treatment condition was still significantly less than that afforded by the bonded restorations (phase I conditions 10, 12 and phase II conditions 3, 5, 7, 9).

The use of a dentinal bonding agent in conjunction with the acid etch technique in phase II demonstrated significant recovery of stiffness. Conditions 3 and 5,

#### 4. DISCUSSION OF EXPERIMENTAL RESULTS

The decrease in the relative stiffness of the crown of a tooth that accompanies a traditional intracoronal cavity preparation is in agreement with studies on the effect of said cavity preparations on the ultimate fracture strength of the tooth<sup>46</sup>. In phase I of the experimental stress analysis both the conservative occlusal preparation and the MOD preparation rendered the tooth significantly less stiff than the sound tooth. In addition, the placement of bevels on the cavosurface of the MOD preparation further decreases the stiffness of the crown. In phase II of the experiments each consecutive beveled MOD preparation displayed a decrease in the relative stiffness of the crown.

The placement of non-bonded restorative materials in two of the treatment conditions in phase I (conditions 4, 8) showed no statistical difference from the MOD preparation. However, the study did show that condition 6 did provide for a significant recovery of stiffness. This may have been due to the frictional effect between the flared walls of the proximal boxes and composite B which contains a very high percentage weight of quartz filler. The recovery of 24% of sound tooth stiffness for this treatment condition was still significantly less than that afforded by the bonded restorations (phase I conditions 10, 12 and phase II conditions 3, 5, 7, 9).

The use of a dentinal bonding agent in conjunction with the acid etch technique in phase II demonstrated significant recovery of stiffness. Conditions 3 and 5,

where the isthmus width of the cavity equaled 21% and 35% of the bucco-lingual width of the occlusal table respectively, provided greater than 100% recovery of stiffness of the crown. When the isthmus width equaled 47% of the bucco-lingual width of the occlusal table (condition 7) the stiffness recovery measured 65%. This decrease in stiffness recovery can be attributed to the increased demand for performance of the restorative material due to the larger cavity size. Condition 9, where the isthmus width equaled 56% of the bucco-lingual width of the occlusal table, demonstrated a 78% recovery of stiffness. This increase in stiffness recovery over the previous condition can be attributed to the use of composite C which has a modulus of elasticity twice that of composite B.

An interesting phenomena arises from the force-strain curves shown in Figure 9. It can be noted from the shape of the loading and unloading curves in (A) that the development and the release of strain were almost coincidental for the sound tooth. However, this was not so for the non-bonded restoration, (B). There is a wide divergence (hysteresis) between the two force-strain curves. This indicates that the cusp recovers its original form at a much slower rate after removal of the force, resulting in a intermittent gap between the hard tissue and the restoration. (C) shows the force-strain curves closely resemble those of a sound tooth, displaying only slight hysteresis. Thus, an important point in favor of the acid-etch bonding technique is that not only does

the restored tooth resist deformation, but the cusps also display reduced hysteresis.

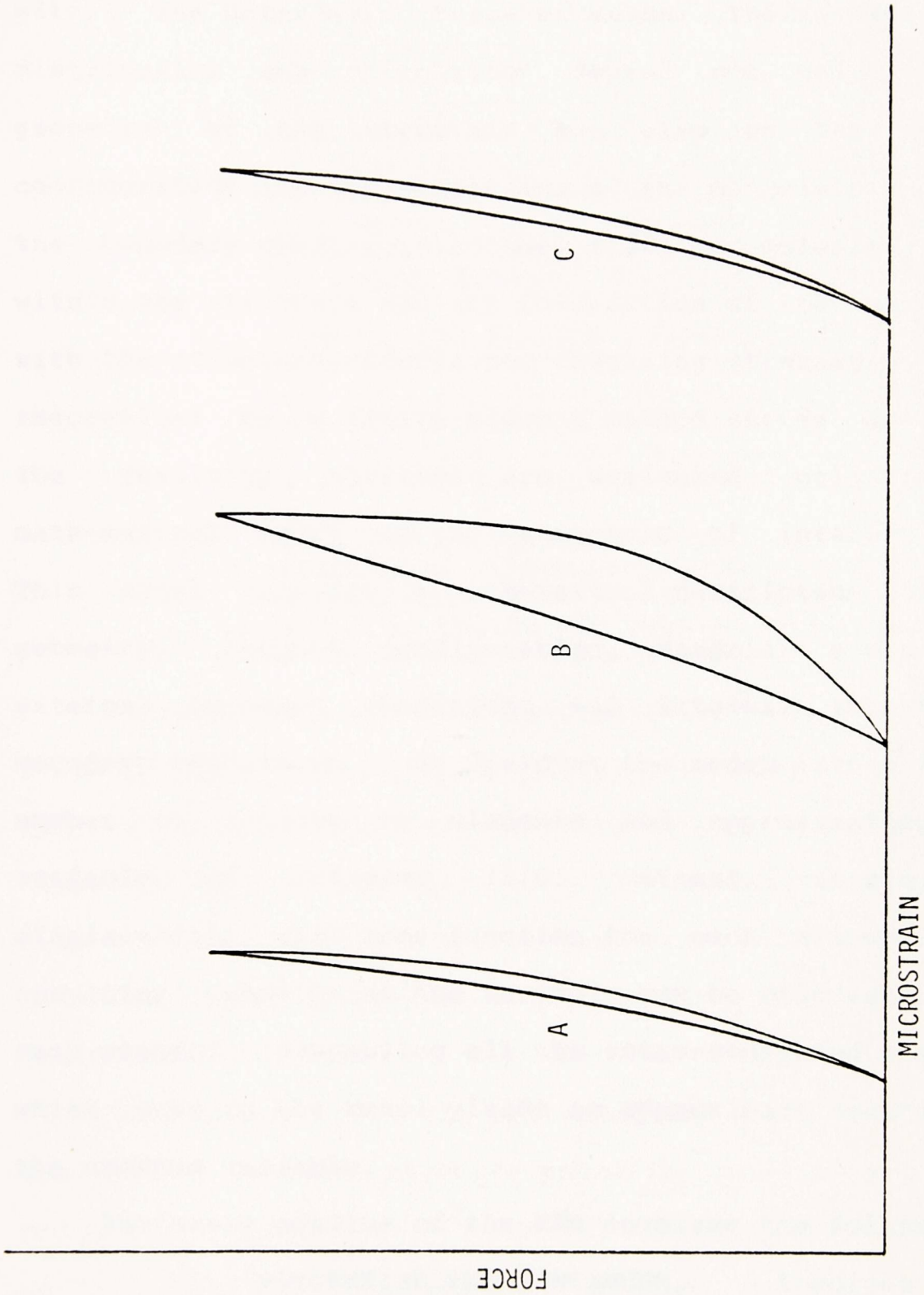


Figure 9. Force-strain curves where A = sound tooth; B = restored tooth with a non-bonded restoration; and C = restored tooth with a bonded restoration.

the restored tooth resist deformation, but the cusps also display reduced hysteresis.

### 5.1 FINITE ELEMENT METHOD THEORY

When a structure is loaded, stresses are generated within the material. These stresses, their magnitude, distribution and orientation depend not only on the geometry of the structure but also on the loading configuration and the properties of the materials. Also, the boundary conditions between different material types within the structure and the interaction of the structure with the structure affects the resulting stresses. With a theoretical or a finite element method stress analysis, the resulting stresses are evaluated utilizing a mathematical model of the structure of interest. This model provides a mathematical description of the geometry, loading configuration, material properties, external boundary conditions and internal interfacial boundary conditions. By dividing the model into a finite number of regions or elements and approximating the variable of interest (i.e. stress, strain, or displacement) with some function for each element, the resulting behavior of the variable can be calculated for each element. Assembling all the inter-connected elements which make up the model yields an approximate solution to the unknown variable.

The basic outline of the FEM involves the following:

1. DISCRETIZE THE CONTINUUM. Involves dividing the region of interest into discrete elements. Several different element types are possible along with combinations of different element types within the region.

## 5. THEORETICAL METHODS AND SOFTWARE

### 5.1 FINITE ELEMENT METHOD THEORY

When a structure is loaded, stresses are generated within the material. These stresses, their magnitude, distribution and orientation depend not only on the geometry of the structure but also on the loading configuration and the properties of the materials. Also, the boundary conditions between different material types within the structure and the interaction of the structure with the structure affects the resulting stresses. With a theoretical or a finite element method stress analysis, the resulting stresses are evaluated utilizing a mathematical model of the structure of interest. This model provides a mathematical description of the geometry, loading configuration, material properties, external boundary conditions and internal interfacial boundary conditions. By dividing the model into a finite number of regions or elements and approximating the variable of interest (i.e. stress, strain, or displacement) with some function for each element, the resulting behavior of the variable can be calculated for each element. Assembling all the inter-connected elements which make up the model yields an approximate solution to the unknown variable.

The basic outline of the FEM involves the following:

1. **DISCRETIZE THE CONTINUUM.** Involves dividing the region of interest into discrete elements. Several different element types are possible along with combinations of different element types within the region.

2. SELECTION OF INTERPOLATION FUNCTIONS.

For the given nodes assigned to an element an interpolation function is selected to predict the variation of the field variable over the element. This interpolation function can be of several forms but polynomials are generally used due to the ease of numerical integration and differentiation.

3. CALCULATE ELEMENT PROPERTIES. Matrix equations are determined that describe the properties of each element. This can be done by using one of four techniques: direct approach, variational approach, weighted residual approach, or the energy balance approach.

4. ASSEMBLE THE ELEMENT PROPERTIES TO OBTAIN THE SYSTEM EQUATIONS. The matrix equations expressing the behavior of individual elements are assembled to form matrix equations describing the behavior of the entire solution region.

5. SOLVE THE SYSTEM EQUATIONS. From the assembly of system equations a set of simultaneous equations emerges which are solved to obtain the unknown nodal values of the field variable.

There are a variety of methods within the FEM for the formulation of element properties. Because of this the FEM offers certain advantages over other techniques of numerical stress analysis, i.e. finite differences. The following describes the use of the variational approach in the formulation of element properties in the FEM.

VARIATIONAL APPROACH

The concept that all processes are characterized by quantities defined at every point in space is known as continuum mechanics. Continuum problems can be characterized by partial differential equations with appropriate boundary conditions. Continuum problems with a solution being sought over some region defined by a

boundary on which certain conditions are specified are classified as boundary value problems.

There are several techniques to find solutions to boundary value problems in continuum mechanics. These methods range from purely analytical to completely numerical in nature. However, there are very few problems that yield exact solutions. Thus, the analytical technique is of little practical use in solving boundary value problems. The numerical method does not yield exact solutions to the problems but rather forms an approximation to the solution. However, through the use of digital computers it is possible to attain a high degree of accuracy in the approximation with the solution converging on the exact solution.

The Ritz method is a numerical method that offers approximations of high accuracy to boundary value problems. The method depends on the variational approach of continuum problems which attempts to find the unknown function or functions that extremize or make stationary a functional or system of functionals subjected to the same boundary conditions. The Ritz method consists of assuming the form of the unknown solution in terms of trial functions with unknown adjustable parameters. The trial function that renders the functional stationary is substituted into the functional, thereby, expressing the functional in terms of the unknown adjustable parameters. By differentiating the functional with respect to each parameter and setting the resulting equation equal to zero, a set of simultaneous equations is obtained where

is the number of parameters. This set of equations can be solved for the parameters, and thus, an approximate solution is obtained. The accuracy of the approximated solution depends on the choice of trial functions. Thus, as the number of trial functions and parameters increases the accuracy of the approximation improves.

When compared to the Ritz method the FEM differs in that the trial functions are not necessarily defined over the entire solution domain and do not have to satisfy the same boundary conditions. Rather, the trial functions only have to meet certain continuity requirements. Thus the Ritz method is limited to simple geometric solution domains, The FEM is restricted by the same geometric limitations, but they only apply to the individual element solution domain, and generally, the overall assembled solution domain is unaffected. Therefore approximate solutions of high accuracy can be attained for exceedingly complex geometric solution domains as long as the elements of the solution domain follow the geometric limitations of the method.

As was previously mentioned, the FEM consists of dividing up the continuum of solution domain into elements which are inter-connected at all nodal points and along the inter-elemental boundaries. The interpretation of the discretized solution domain is more a mathematical interpretation than a physical interpretation. In terms of solid mechanics and elasticity the elements of the solution domain do not deform. Instead, the nodes of the elements define points within the displacement field of

the domain where the displacement or its derivative is known or being sought. Thus, the mathematical interpretation of the finite element discretization is a spatial subdivision rather than a material subdivision.

The basis of the FEM consists of approximating the behavior of the unknown field variable over each element of the discretization with continuous functions defined in terms of the nodal values of the field variable within the solution domain. These continuous functions are referred to as interpolation functions and the summation of all interpolation functions over the entire solution domain provides the piecewise approximation to the unknown field variable of interest.

In order to represent the continuum of interest in the FEM analysis the continuum has to be discretized into a finite number of elements. There are many different element geometries and combinations of elements with both internal and external nodes. The optimal element geometry, element size and nodal density is dependent on the continuum geometry and the rate of change of the field variable of interest. Thus, the domain discretization involves more than simply constructing a uniform mesh of adequate geometric representation.

It is important that the finite element mesh consist of well proportioned elements. This requires that the individual elements ratio of height to width is nearly 1:1. This dictates that for triangular elements the optimal element shape would be that of an isosceles triangle. As elements become long and narrow they tend to

give directional bias to the FEM solution. This is due to the error in the solution being proportional to the inverse of the sine of the smallest angle of the element.

Assuming that the FEM solution converges on the exact solution, by increasing the mesh finess or nodal density, the accuracy of the finite element approximation improves. However, the increased number elements leads to greater computational cost, increased data input and data output. Thus, it is necessary to determine the number of elements which provides a satisfactory approximation to the solution while minimizing the cost and data input/output.

The other methods used in the formulation of the element properties include:

1. Direct approach, which utilizes the force-displacement characteristics of an individual element to determine the overall force-displacement relationship of the entire continuum.
2. Weighted Residuals, where the general functional behavior of the dependent field variable is assumed so as to satisfy a given differential equation and boundary condition with the error or residual vanishing.
3. Energy Balance approach where the equations are formulated from local or global energy balances.

#### APPLICATION TO ELASTICITY PROBLEMS

The finite element analysis of an elasticity problem usually involves the variational approach to element formation. When the potential energy of the system of interest is considered then the form of the displacement field within each element must be assumed. This type analysis is usually referred to as the displacement method of the finite element analysis.

The general form of the equation describing the potential energy of a two-dimensional elastic body experiencing surface and body forces and maintaining an equilibrium can be written as

$$\Pi(u, v) = \frac{1}{2} \iint_A [L\bar{\delta}] [B]^T [C] [B] \{\bar{\delta}\} - 2\{\bar{\delta}\} [B]^T [C] \{\varepsilon_0^*\} ] t dA \quad (24)$$

$$- \iint_A [L F^*] \{\bar{\delta}\} t dA - \int_{C_1} [T^*] \{\bar{\delta}\} dS$$

where

$t = t(x, y) =$  thickness of the body, considered constant for problems of plane strain

$\{\bar{\delta}\} = \begin{Bmatrix} u(x, y) \\ y(x, y) \end{Bmatrix} =$  column matrix of the components of the displacement field measured from some datum

$[B] = \begin{bmatrix} \partial/\partial x & 0 \\ 0 & \partial/\partial y \\ \partial/\partial y & \partial/\partial x \end{bmatrix} =$  matrix relating strains and displacements

$[C] =$  matrix stiffness matrix

$\{\varepsilon_0^*\} =$  column vector of initial strains due to temperature, connectors, shrinkage, etc.

$[L F^*] = \begin{bmatrix} * & * \\ X & Y \end{bmatrix} =$  body force components due to gravity, centrifugal action etc.

$[T^*] = \begin{bmatrix} * & * \\ T_x & T_y \end{bmatrix} =$  boundary traction components acting on the boundary

\* denotes known quantity

When the elastic body is at equilibrium the displacement field is such that the total potential energy of the body is a minimum.

When the interpolation functions are derived for the

displacement method it is necessary that they fulfill the compatibility and completeness requirements. These allow for a continuous displacement field across elemental boundaries and for rigid body displacements and constant strain states within elements. If this is done then the potential energy of the assemblage of elements is equal to the sum of the potential energies of all elements. Thus

$$\Pi(u, v) = \sum_{e=1}^m \Pi^e(u, v) \quad (25)$$

where  $M$  represents the number of elements in the discretized domain.

Considering one element of the discretized continuum the potential energy functional,  $\Pi^e(u, v)$ , can be expressed in terms of discrete values of the displacement components. Therefore, if the element has  $r$  nodes then the displacement field is approximated to its nodal values by  $r$  interpolating functions  $N_i(x, y)$ . The displacement field is thus expressed as

$$\begin{Bmatrix} u \\ v \end{Bmatrix}^{(e)} = \begin{Bmatrix} u(x, y) \\ v(x, y) \end{Bmatrix}^{(e)} = \begin{Bmatrix} \sum_{i=1}^r N_i(x, y) u_i \\ \sum_{i=1}^r N_i(x, y) v_i \end{Bmatrix} = \begin{Bmatrix} [N] \{u\} \\ [N] \{v\} \end{Bmatrix}^{(e)} = [N] \{\delta\} \quad (26)$$

where  $\{\delta\}^{(e)}$  is the element nodal displacements. For the finite element formulation for a two-dimensional elastic continuum the unknown field variable, displacement, is a vector composed of an  $x$  and  $y$  component. Therefore, at each node in the mesh there are two unknown nodal components of displacement.

The interpolation functions are determined by

considering a plane passing through the three nodal values of the displacement field variable for the given triangular element. Assuming that the displacements vary linearly across the element, the overall displacement of the element is expressed as

$$\phi^{(e)}(x, y) = \beta_1^{(e)} + \beta_2^{(e)}x + \beta_3^{(e)}y \quad (27)$$

The constants  $\beta_1^{(e)}$ ,  $\beta_2^{(e)}$ ,  $\beta_3^{(e)}$ , can be expressed in terms of the coordinates of the nodes defining the element and the corresponding nodal values of displacement. Thus

$$\begin{aligned} \phi_i &= \beta_1^{(e)} + \beta_2^{(e)}x_i + \beta_3^{(e)}y_i \\ \phi_j &= \beta_1^{(e)} + \beta_2^{(e)}x_j + \beta_3^{(e)}y_j \end{aligned} \quad (28)$$

$$\phi_m = \beta_1^{(e)} + \beta_2^{(e)}x_m + \beta_3^{(e)}y_m$$

This results in three simultaneous equations with three unknowns. Solving for the constants and substituting back into equation 27 yields

$$\begin{aligned} \phi^{(e)}(x, y) = \frac{1}{2\Delta} \left[ (a_i + b_i x + c_i y) \phi_i + (a_j + b_j x + c_j y) \phi_j \right. \\ \left. + (a_m + a_m x + a_m y) \phi_m \right] \end{aligned} \quad (29)$$

where

$$\begin{aligned} a_i &= x_j y_m - x_m y_j \\ b_i &= y_j - y_m \\ c_i &= x_m - x_j \end{aligned} \quad (30)$$

while the other coefficients are obtained by cyclic permutation of the subscripts  $i, j$ , and  $m$ . Also

$$2\Delta = \det \begin{vmatrix} 1 & x_i & y_i \\ 1 & x_j & y_j \\ 1 & x_m & y_m \end{vmatrix} = 2 \left( \begin{array}{l} \text{AREA OF TRIANGLE} \\ \text{WITH VERTICES } ijm \end{array} \right) \quad (31)$$

By defining

$$N_n^{(e)} = \frac{a_n + b_n x + c_n y}{2\Delta}, \quad n=i, j, m \quad (32)$$

and

$$\{\phi^{(e)}\} = \begin{Bmatrix} \phi_i \\ \phi_j \\ \phi_m \end{Bmatrix}, \quad [N^{(e)}] = [N_i^{(e)}, N_j^{(e)}, N_m^{(e)}] \quad (33)$$

equation 29 is reduced to

$$\phi^{(e)}(x, y) = [N^{(e)}] \{\phi^{(e)}\} = N_i^{(e)} \phi_i + N_j^{(e)} \phi_j + N_m^{(e)} \phi_m \quad (34)$$

Substituting equation 26 into the potential energy functional, equation 24, yields the potential energy of one element in terms of the nodal displacements. These nodal displacements are unknown while the interpolation functions are known. Thus, the functional can be expressed as

$$\Pi^{(e)}(\{\bar{\delta}\}^{(e)}) = \Pi(u_1, u_2, \dots, u_r, v_1, v_2, \dots, v_r) \quad (35)$$

or

$$\begin{aligned} \Pi^{(e)}(\{\delta\}^{(e)}) = & \frac{1}{2} \iint_{A^{(e)}} \left\{ \left[ \bar{L} \right]^{(e)} \left[ B \right]^{T(e)} \left[ C \right]^{(e)} \left[ B \right] \left\{ \delta \right\}^{(e)} - 2 \left[ \bar{L} \right]^{(e)} \left[ B \right] \left[ C \right]^{(e)} \left\{ \epsilon_0 \right\}^{(e)} \right\}^T dA \\ & - \iint_{A^{(e)}} \left[ F \right]^{(e)} \left\{ \delta \right\}^{(e)} dA - \int_{C_i^{(e)}} \left[ L \right]^{(e)} \left\{ \delta \right\}^{(e)} ds \end{aligned} \quad (36)$$

At equilibrium the potential energy functional is at a minimum. Because the functional for the continuum can be expressed as a summation of individual functionals for each element, the minimized functional for the continuum can be expressed as the summation of each element's minimized functional. Therefore, through the calculus of variations the potential energy of the discretized continuum is at a minimum when the first variation of the functional vanishes. This is expressed as

$$\delta \Pi(u, v) = \sum_{e=1}^m \delta \Pi^{(e)}(u, v) = 0 \quad (37)$$

where

$$\delta \Pi^{(e)}(u, v) = \sum_{i=1}^r \frac{\partial \Pi^{(e)}}{\partial u_i} \delta u_i + \sum_{i=1}^r \frac{\partial \Pi^{(e)}}{\partial v_i} \delta v_i = 0 \quad (38)$$

Because the  $u_i$  and  $v_i$  are independent variations then it is require that

$$\frac{\partial \Pi^{(e)}}{\partial u_i} = \frac{\partial \Pi^{(e)}}{\partial v_i} = 0, \quad i = 1, 2, \dots, r \quad (39)$$

for each element.

Equation 37 can be used to formulate the element equations. For a given node  $q$  in the discretized continuum the matrix equations consist of two equations

relating the displacements  $u$  and  $v$  to the two force components at node  $q$ . The submatrix form is

$$\left[ [k]^{q1} \quad [k]^{q2} \quad \dots \quad [k]^{qp} \quad \dots \quad [k]^{qr} \right] \begin{Bmatrix} \frac{u_1}{r_1} \\ \vdots \\ \frac{u_q}{r_q} \\ \vdots \\ \frac{u_r}{r_r} \end{Bmatrix} = \begin{Bmatrix} F \\ \vdots \\ F \\ \vdots \\ F \end{Bmatrix} \quad (40)$$

$q = 1, 2, \dots, r$

where  $p = 1, 2, \dots, r$  and  $r$  is the number of element nodes. The submatrix  $[k]^{qp}$  defines the stiffness relationship between nodes  $q$  and  $p$  and the resultant external load vector  $\{F\}^q$  at node  $q$ . Applying equation 39 to equation 24 to evaluate the matrices of equation 40 yields

$$\begin{Bmatrix} \frac{\partial \Pi^{(e)}}{\partial u_q} \\ \frac{\partial \Pi^{(e)}}{\partial v_q} \end{Bmatrix} = \{0\} = \iint_{A^{(e)}} \left[ [B]_q^{T(e)} [C]^{(e)} [B]_q \{ \delta \}_q^{(e)} - [B]_q^{T(e)} [C]^{(e)} \{ \epsilon \}_q^{(e)} \right] t \, dA^{(e)} \quad (41)$$

$$- \iint_{A^{(e)}} N_2 \{ F^* \}_q^{(e)} t \, dA^{(e)} - \int_{C_1^{(e)}} N_2 \{ T^* \}_q^{(e)} dS_2^{(e)}$$

for node  $q$  where

$$\{ \delta \}_q^2 = \begin{Bmatrix} u_q \\ v_q \end{Bmatrix} \quad (42)$$

$\{ \delta \}_q^2$  is the column vector of the two displacement components at node  $q$  and

$$[B]_q^{(e)} = \begin{bmatrix} \frac{\partial N_q}{\partial x} & 0 \\ 0 & \frac{\partial N_q}{\partial y} \\ \frac{\partial N_q}{\partial y} & \frac{\partial N_q}{\partial x} \end{bmatrix}, \quad q = 1, 2, \dots, p, \dots, r \quad (43)$$

represents the three non-zero strain components  $\epsilon_x^*$ ,  $\epsilon_y^*$  and  $\gamma_{xy}$ . The traction vector  $\{T\}^*$  in equation 41 only applies if the element lies on the boundary of the discretized continuum.

Expressing equation 41 in matrix notation, the force-displacement relationship of node q is

$$[k] \{s\} = \{F_0\} + \{F_B\} + \{F_T\} = \{F\} \quad (44)$$

where

$$[k] = \iint_{A^{(e)}} [B]_q^T [C] [B]_q t dA^{(e)} = \text{STIFFNESS MATRIX AT NODE } q$$

$$\{F_0\} = \iint_{A^{(e)}} [B]_q^T [C] \{\epsilon_0^*\}_q t dA^{(e)} = \text{INITIAL FORCE VECTOR AT NODE } q$$

$$\{F_B\} = \iint_{A^{(e)}} N_q(x,y) \{F^*\}_q t dA^{(e)} = \text{NODAL BODY FORCE VECTOR} \quad (45)$$

$$\{F_T\} = \iint_{C_i^{(e)}} N_q(x,y) \{T^*\}_q dS_q^{(e)} = \text{NODAL FORCE VECTOR DUE TO LOADING PRESENT FOR BOUNDARY ELEMENTS}$$

$$\{F\} = \text{RESULTANT EXTERNAL LOAD VECTOR AT NODE } q$$

The complete stiffness matrix for an element would be dimensioned  $2r \times 2r$  where  $r$  is the number of nodes defining the element. Expressed in matrix form

$$[K] = \begin{bmatrix} [k]^{11} & [k]^{12} & \dots & [k]^{1r} \\ [k]^{21} & [k]^{22} & \dots & [k]^{2r} \\ \vdots & \vdots & \ddots & \vdots \\ [k]^{r1} & [k]^{r2} & \dots & [k]^{rr} \end{bmatrix} \quad (46)$$

The column matrix for nodal displacements of the element is

$$\{\delta\}^{(e)} = \begin{Bmatrix} \{\delta\}^1 \\ \{\delta\}^2 \\ \vdots \\ \{\delta\}^r \end{Bmatrix} = \begin{Bmatrix} u_1 \\ v_1 \\ u_2 \\ v_2 \\ \vdots \\ u_r \\ v_r \end{Bmatrix} \quad (47)$$

Therefore, the force-displacement relationship of the element can be expressed in general as

$$[K]\{\delta\}^{(e)} = \{F\}^{(e)} \quad (48)$$

where

$$\{F\}^{(e)} = \begin{Bmatrix} \{F\}^1 \\ \{F\}^2 \\ \vdots \\ \{F\}^r \end{Bmatrix} \quad (49)$$

The force-displacement relationship for the entire continuum, known as the system equations, is an assembly of the element equations. Thus, the system equations describing the behavior of  $m$  nodes is written as

$$[K]\{\delta\} = \{F\} \quad (50)$$

where  $\{\delta\}$  is a column vector of nodal displacements for the entire system and  $\{F\}$  is the column vector of resultant forces.

Many times a three-dimensional elasticity problem can be reduced to an analysis in two dimensions if the geometry and loading criteria can be described by two independent coordinates. Plane strain problems involved

in the stress analysis of solids whose geometry and loading conditions are constant in the longest dimension. Therefore, stresses and displacements can be studied by considering a unit-thick slice of the solid in the x-y plane.

For a triangular element defined by three nodes, the linear variation of the displacement field within the element can be expressed in terms of horizontal and vertical displacements using natural coordinates as

$$\left\{ \tilde{\delta} \right\}^{(e)} = \left\{ \begin{matrix} u(x,y) \\ v(x,y) \end{matrix} \right\}^{(e)} = \left\{ \begin{matrix} N_1 u_1 + N_2 u_2 + N_3 u_3 \\ N_1 v_1 + N_2 v_2 + N_3 v_3 \end{matrix} \right\} \quad (51)$$

where  $N_i$  is the interpolation function.

To relate strain and displacement at each node the matrix is derived from equation 43 resulting in

$$[B]_i^{(e)} = \begin{bmatrix} \frac{\partial N_i}{\partial x} & 0 \\ 0 & \frac{\partial N_i}{\partial y} \\ \frac{\partial N_i}{\partial y} & \frac{\partial N_i}{\partial x} \end{bmatrix} = \frac{1}{2\Delta} \begin{bmatrix} b_i & 0 \\ 0 & c_i \\ c_i & b_i \end{bmatrix}, \quad i = 1, 2, 3 \quad (52)$$

$$[B]_i^T{}^{(e)} = \frac{1}{2\Delta} \begin{bmatrix} b_i & 0 & c_i \\ 0 & c_i & b_i \end{bmatrix}$$

If it is assumed that the material being modelled is homogeneous and isotropic then the plane strain stiffness matrix is expressed as

$$[C] = \frac{E}{(1+\nu)(1-2\nu)} \begin{bmatrix} 1-\nu & \nu & 0 \\ \nu & 1-\nu & 0 \\ 0 & 0 & \frac{1-2\nu}{2} \end{bmatrix} \quad (53)$$

where  $E$  is Young's modulus of elasticity and  $\nu$  is Poisson's ratio.

To determine the stiffness matrix at a specific node, equations 52 and 53 are substituted into equation 45 yielding

$$\begin{aligned}
 [k]_{ij} &= \frac{1}{4\Delta^2} \frac{E}{(1-\nu)(1-2\nu)} \iint_{A^{(e)}} \begin{bmatrix} b_i & 0 & c_i \\ 0 & c_i & b_i \end{bmatrix} \begin{bmatrix} 1-\nu & \nu & 0 \\ \nu & 1-\nu & 0 \\ 0 & 0 & \frac{1-2\nu}{2} \end{bmatrix} \begin{bmatrix} b_j & 0 \\ 0 & c_j \\ c_j & b_j \end{bmatrix} t dA^{(e)} \\
 &= \frac{1}{4\Delta^2} \frac{E}{(1-\nu)(1-2\nu)} \begin{bmatrix} b_i & 0 & c_i \\ 0 & c_i & b_i \end{bmatrix} \begin{bmatrix} 1-\nu & \nu & 0 \\ \nu & 1-\nu & 0 \\ 0 & 0 & \frac{1-2\nu}{2} \end{bmatrix} \begin{bmatrix} b_j & 0 \\ 0 & c_j \\ c_j & b_j \end{bmatrix} \iint_{A^{(e)}} E^{(e)} dA^{(e)} \quad (54)
 \end{aligned}$$

If the thickness  $t$  of the element is constant then equation 54 is reduced to

$$[k]_{ij} = \frac{1}{4\Delta} \frac{Et}{(1-\nu)(1-2\nu)} \begin{bmatrix} b_i & 0 & c_i \\ 0 & c_i & b_i \end{bmatrix} \begin{bmatrix} 1-\nu & \nu & 0 \\ \nu & 1-\nu & 0 \\ 0 & 0 & \frac{1-2\nu}{2} \end{bmatrix} \begin{bmatrix} b_j & 0 \\ 0 & c_j \\ c_j & b_j \end{bmatrix} \quad (55)$$

Carrying out the matrix multiplication of equation 55, the results are substituted into equation 46 to determine the element stiffness matrix.

The initial force vector for an element is determined by substituting the initial strain vector  $\{\epsilon_0^*\}$  into equation 45 and carrying out the integration over the element. Thus

$$\{F_0\}_i = \frac{1}{2\Delta} \frac{E}{(1-\nu)(1-2\nu)} \iint_{A^{(e)}} \begin{bmatrix} b_i & 0 & c_i \\ 0 & c_i & b_i \end{bmatrix} \begin{bmatrix} 1-\nu & \nu & 0 \\ \nu & 1-\nu & 0 \\ 0 & 0 & \frac{1-2\nu}{2} \end{bmatrix} \begin{Bmatrix} \epsilon_{x_0}^* \\ \epsilon_{y_0}^* \\ \gamma_{xy}^* \end{Bmatrix} t dA^{(e)} \quad (56)$$

The body force vector at node  $i$  is

$$\{F_B\}^i = \iint_{A^{(e)}} N_i \begin{Bmatrix} X_i^* \\ Y_i^* \end{Bmatrix} t^{(e)} dA^{(e)} = \frac{t^{(e)} \Delta}{3} \begin{Bmatrix} X_i^* \\ Y_i^* \end{Bmatrix} \quad (57)$$

where  $X^*$ ,  $Y^*$  are the body force components due to gravity, centrifugal action, etc.

To determine the nodal force vector due to loading consider the boundary element with the side of the element lying on the boundary being  $l_{ij}$  in length where  $i$  and  $j$  are nodes on the boundary. At node  $i$ , equation 45 is expressed as

$$\{F_T\}^i = \int_{C_i^{(e)}} N_i \begin{Bmatrix} X_i^* \\ Y_i^* \end{Bmatrix} dS = \int_0^{l_{ij}} N_i \begin{Bmatrix} X_i^* \\ Y_i^* \end{Bmatrix} dS \quad (58)$$

Assuming that the traction components  $X^*$  and  $Y^*$  are constant over the entire length  $l_{ij}$  of the element and that the interpolation function  $N_i$  varies linearly in the length coordinate along the boundary then

$$N_i(s) = 1 - \frac{s}{l_{ij}} \quad (59)$$

where  $S$  is the length coordinate from node  $i$  to node  $j$  and equation 58 can be expressed as

$$\begin{aligned} \{F_T\}^i &= \int_0^{l_{ij}} N_i \begin{Bmatrix} X_i^* \\ Y_i^* \end{Bmatrix} dS = \int_0^{l_{ij}} \left(1 - \frac{s}{l_{ij}}\right) dS \begin{Bmatrix} X_i^* \\ Y_i^* \end{Bmatrix} \\ &= \left( S - \frac{S^2}{2l_{ij}} \right) \Big|_0^{l_{ij}} \begin{Bmatrix} X_i^* \\ Y_i^* \end{Bmatrix} \\ &= \frac{l_{ij}}{2} \begin{Bmatrix} X_i^* \\ Y_i^* \end{Bmatrix} \end{aligned} \quad (60)$$

## 5.2 IF ECS-INTERACTIVE FINITE ELEMENT COMPUTING SYSTEM

With the development of the finite element method (FEM) software there has been corresponding increase in the difficulty of successfully applying the software to given problem. The increased sophistication of many of the FEM packages requires an enormous amount of data input to define the a given problem and the output generated tends to be overwhelming. The Interactive Finite Element Computing System (IFECS) allows the problem to be defined with minimal data input and output can be selected to provide only relevant and necessary information<sup>59-61</sup>. Also, IFECS can be implemented on very simple computing configurations as opposed to the sophisticated packages which require large main frame computer execution.

IFECS was developed to provide an interactive computing environment for the FEM application. This includes a mesh generation program, input data verification and an option to selectively view the results. A conversational mode of interaction allows for fast and easy access to modify or correct input variables and to make desired selections of output. The solution generation phase, however, is independent of user interaction.

The FEM can be divided into three phases, namely, data input, solution generation and results output. To simplify data input IFECS utilizes an automatic mesh generation routine. The user is required to define the nodes both on boundaries and within prescribed regions of the model. Having specified the nodal coordinates and which nodes lie on external boundaries, the material

types, corresponding material properties and internal boundaries are defined for the model. An optimal triangular mesh is generated using the prescribed nodes as vertices and sorting out the relevant material properties for each element. Any errors that occurred in defining the boundary are determined by the mesh generation procedure. Constraints of boundary nodes and load application (position and force) are defined in another input file.

The FEM solution routine is executed using the data files created by the automatic mesh generation routine. The nodes of the model are renumbered to minimize the profile of the stiffness matrix  $K$ . The storage scheme for the stiffness matrix is a variable bandwidth method. This allows only non-zero numbers to the diagonal number of each row of the matrix to be stored. These subvectors are kept consecutively in a one-dimensional array along with an integer array of pointers defining the position of each diagonal term. The solution to the linear set of equations is by Choleskii decomposition.

### 5.3 APPROACHES TO MODELLING

The FEM has gained ever increasing popularity in the field of applied stress analysis. This is primarily due to the adaptability of the FEM to the proposed problem. In the past this adaptability has been the limiting factor in the use of other numerical techniques and modelling schemes. However, for the FEM to be truly effective in terms of modelling a phenomena it is essential that

certain criterion are fulfilled in the formulation of the model.

Validity and accuracy of the model need to be established for the FEM to be effective. Model validity can be ascertained in a number of ways. One method of validating the model is through experimental verification. This method is difficult due to the inherent problems of experimental stress analysis. Not only are the problems being investigated complex but the experimental methodology tends to be insensitive to the overall strain distribution in the object being modelled. The accuracy of the model is assessed by using a convergency test. By refining the mesh density and repeating the calculations, the rate of convergence of the results can be determined. The degree of accuracy required is governed by the solution time necessary to run the model, the expense of the computing time and the complexity of the geometry of the model. Ideally, the grid should be refined up to a point such that any further refinement does not yield a significant change from the previously calculated results.

The first step in the formulation of a FEM model was to collect information on the physical properties of the materials comprising the tooth. Table 14 and 15 lists a review of the literature pertaining to the determination of the physical properties of enamel and dentin. It is evident that dentin can be treated as an isotropic solid while enamel is an orthotropic material. For the purpose of this study enamel will be treated as an isotropic

TABLE 14  
 REVIEW OF LITERATURE ON THE STUDY OF  
 THE PHYSICAL PROPERTIES OF DENTIN

Author	Experiment	Modulus of Elasticity 10 <sup>10</sup> N/m <sup>2</sup>
62 Peyton et al. 1952	Compressive test	1.15
63 Craig et al. 1958	Compressive test	1.65-1.86
64,65 Standford et al. 1959 and 1960	Compressive test	1.31-1.52
66 Tyldesley 1959	Four point bending test	1.23
67 Renson et al. 1975	Torsion test	1.59
68 Bowen et al. 1962	Tensile test	1.93
69 Renson 1970	Compressive test	1.31
	Cantilever test	1.17
70 Lehmann 1967	Tensile test	1.10
71 Renson et al. 1969	Indenter test	1.17

solid. The values of the modulus of elasticity and Poisson's ratio used in this study are listed below.

TABLE 15  
REVIEW OF LITERATURE ON THE STUDY OF  
THE PHYSICAL PROPERTIES OF ENAMEL

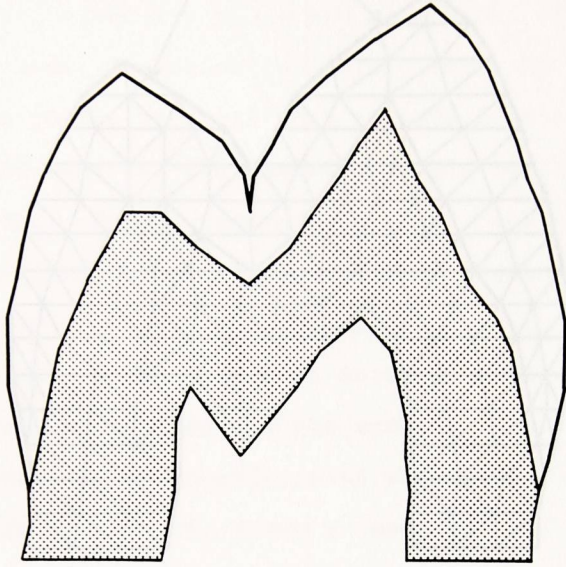
Author	Experiment	Modulus of Elasticity 10 <sup>10</sup> N/m <sup>2</sup>
64 Standford et al. 1958	Compressive test	cuspal 5.65 side 4.14 occlusal 1.24
65 Standford et al. 1960	Compressive test	cuspal 4.83 side 3.45 occlusal 1.24
66 Tyldesley 1959	Four point bending test	13.10
72 Craig et al. 1961	Compressive test	7.79-8.41
73 Haines 1968	Volumetric change theory	1.10

solid. The values of the modulus of elasticity and Poisson's ratio used in this study are listed below.

MATERIAL	YOUNG'S MODULUS	POISSON'S RATIO
ENAMEL	$4.69 \times 10^{10} \text{ N/m}^2$	0.30
DENTIN	$1.54 \times 10^{10} \text{ N/m}^2$	0.31

The model itself consisted of a buccolingual cross-sectional view of a maxillary first premolar, Fig. 10a. Initially, the root of the tooth was included in the model. However, it was found that the root experienced only minor stresses as compared to the coronal portion of the tooth. Thus, to minimize the model complexity and the size of the required computer storage, the model was truncated apical to the cemento-enamel junction. The dimensions of the model were such that it was representative of the average geometry of an actual tooth. The model of the sound tooth was defined by 185 nodes. This nodal density proved to be insensitive to any further grid refinement. Internal boundaries defining the dentino-enamel and pulpo-dentinal junctions were incorporated into the model. The pulp chamber was modelled as a void to minimize the number of nodes. The triangulation of the model resulted in 303 three-node triangular elements, Fig. 11a. The assumptions introduced into the modelling scheme were: (i) the materials comprising the model were homogenous and isotropic; (ii) the materials behave in an elastic manner throughout the

A



B

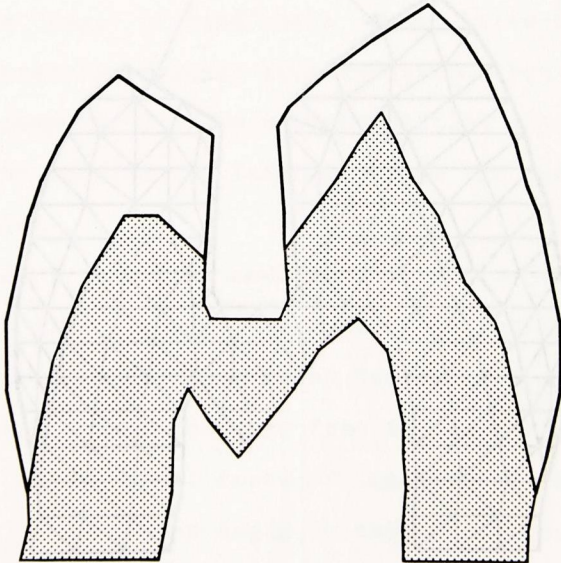
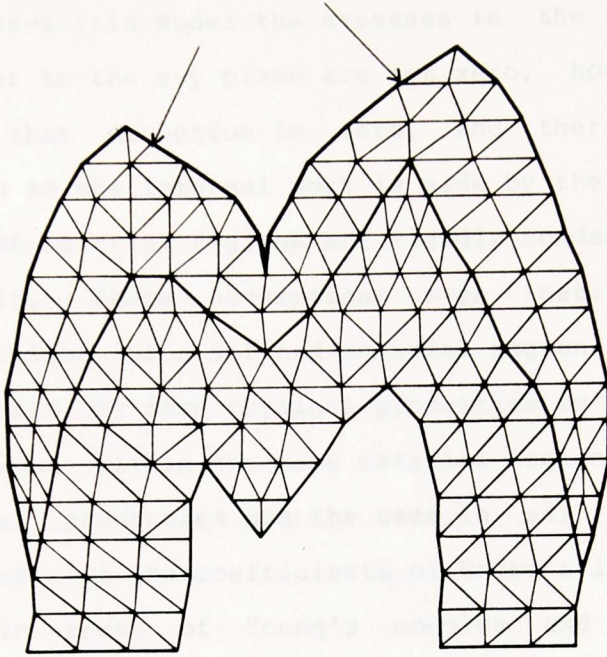


Figure 10. Cross-sectional view of a sound maxillary premolar, A, and cavity preparation #1, B.

A



B

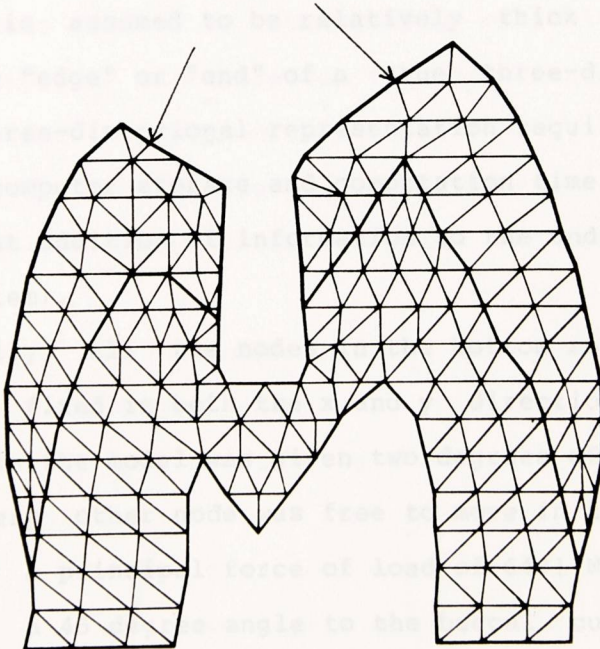


Figure 11. Triangulation of the sound tooth model, A, and A, and the cavity preparation #1 model, B.

entire deformation; (iii) only a cross-section of the tooth was considered under the constraint of plane-strain (in a plane-strain model the stresses in the direction perpendicular to the x-y plane are not zero, however, the strain in that direction is zero, and therefore, no contribution to the internal work is made by the stress); (iv) adjacent material regions are rigidly bonded allowing for no slip. These assumptions mean that: (i) any elemental volume of a defined material region within a body possesses the same physical properties as any other element volume within the same material region and that the physical properties are the same in all directions (this allows all the coefficients of Hooke's law to be expressed in terms of Young's modulus and Poisson's ratio); (ii) the effects of plasticity are ignored; (iii) the model is assumed to be relatively thick and thus ignores the "edge" or "end" of a true three-dimensional model (a three-dimensional representation requires a vast amount of computer storage and computation time yielding only a slight addition of information to the understanding of the problem).

Initially, all the nodes in the bottom row of the model were fixed in both the x and y direction. Every other node in the model was given two degrees of freedom, namely, every other node was free to move in the x and y direction. A principal force of load of 6491 N/meter was applied at a 45 degree angle to the buccal cusp and a principal force of 11746 N/meter at a 64.9 degree angle was applied to the lingual cusp, Fig. 11a. These forces

and angulations were determined by measuring the average occlusal angulation of four teeth and calculating the normal or principal force applied to each cusp. The points of nodes of load application modelled the experimental condition of loading with the 6.3 mm diameter sphere.

The boundary conditions of the model were varied until the surface strains in the model corresponded to those in the experiments. These boundary conditions consisted of fixing all nodes in the bottom row of the model as was initially done.

The existing sound tooth model was next modified so as to represent a tooth with a traditional conservative Class II cavity preparation, Fig. 10b. The cavity extended 0.61 mm past the dentino-enamel junction (DEJ) into the dentin and had an isthmus width of 1.03 mm. The cavity fraction, as calculated in the experiments, was 0.21. The model consisted of 191 nodes discretized into 303 triangular elements, Fig. 11b. The same loading scheme and boundary conditions were used as in the sound tooth model.

The model was further modified to represent two larger Class II cavity preparations, Fig. 12a, 12b. Both cavities extended 0.61 mm past the DEJ into the dentin and had isthmus widths of 1.77 mm and 2.57 mm. These represented cavity fractions of 0.35 and 0.51 respectively. These two models consisted of 183 nodes with 282 triangular elements and 172 nodes with 262 triangular elements respectively, Fig. 13a, 13b. The same

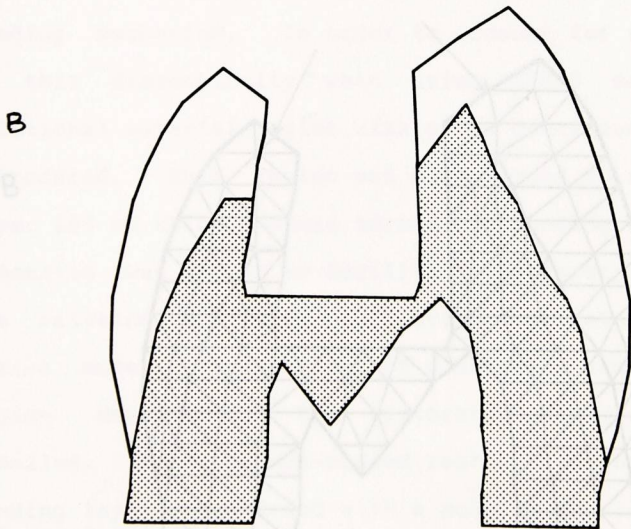
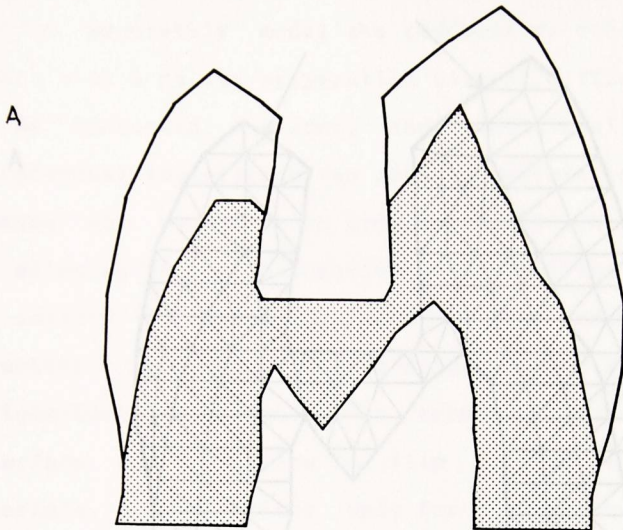
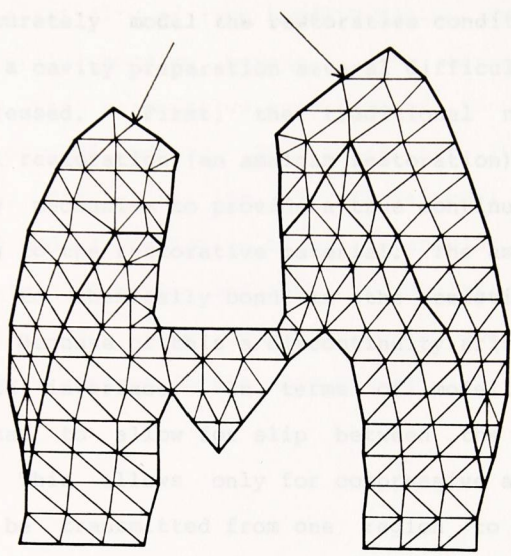


Figure 12. Cross-sectional views of the maxillary premolar cavity preparation #2, A, and cavity preparation #3, B.

loading scheme and boundary conditions were used as the previous model.

To accurately model the boundary conditions of a crack with a cavity preparation, the finite element model can be addressed. The finite element model does not possess any ability to model a crack. The finite element structure is a continuous mesh of elements. At the interface between two adjacent elements, the elements are bonded together. Tensile forces are not permitted due to the lack of any bonding mechanism. In order to model the behavior of this discontinuity when using finite element software, an additional element is added to the mesh. This element is a layer of elements that is added to the mesh. This dimension is the thickness of the bonding layer. The entire model is then modeled as a single entity. The bonding layer is modeled with a modulus of  $10^{-6}$  of the modulus of the surrounding material. For the bonding restoration

A



B

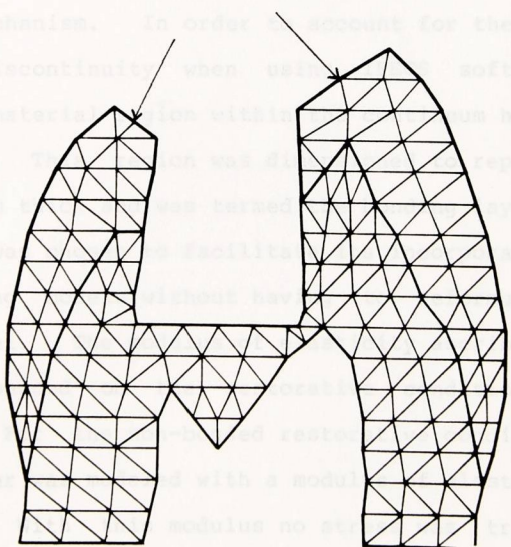


Figure 13. Triangulation for the cavity preparation #2 model, A, and the cavity preparation #3 model, B.



loading scheme and boundary conditions were used as the previous model.

To accurately model the restorative condition of a tooth with a cavity preparation several difficulties had to be addressed. First, the traditional non-bonded intracoronal restoration (an amalgam restoration) does not possess any mechanism to provide a true continuity from the existing tooth to the restorative material. The amalgam has no ability to chemically bond to the existing tooth structure. Because of this a discontinuity arises at the amalgam-tooth interface. In terms of modelling, the interface has to allow for slip between the adjacent materials. This allows only for compressive and shear forces to be transmitted from one region to another. Tensile forces are not permitted due to lack of any bonding mechanism. In order to account for the behavior of this discontinuity when using IF ECS software, an additional material region within the continuum had to be introduced. This region was dimensioned to represent a layer 285  $\mu\text{m}$  thick and was termed the bonding layer. This dimension was chosen to facilitate its incorporation into the existing models without having to reformulate the entire model. The modulus of elasticity ascribed to the region depended on the restorative condition being modelled. For the non-bonded restorative condition the bonding layer was modeled with a modulus of elasticity of  $10^5 \text{ N/m}^2$ . With this modulus no stress was transmitted through the bonding layer. For the bonding restorative material the bonded layer was divided into three regions,

a dentinal bonding region, an etched enamel bonding region and an enamel non-bonding region, Fig. 14a, 14b, 15. The modulus of elasticity of each bonding region contributed to the overall bonding scheme. The three models representing the restorative condition of the cavities consisted of 206 nodes, 209 nodes and 206 nodes respectively, Fig. 16a, 16b, 17. These nodal densities resulted in models consisting of 345 triangular elements, 351 triangular elements and 346 triangular elements respectively. The same loading scheme and boundary conditions were used as in previous models.



Figure 14. Cross-sectional view of restored cavity #1, A, and restored cavity #2, B.

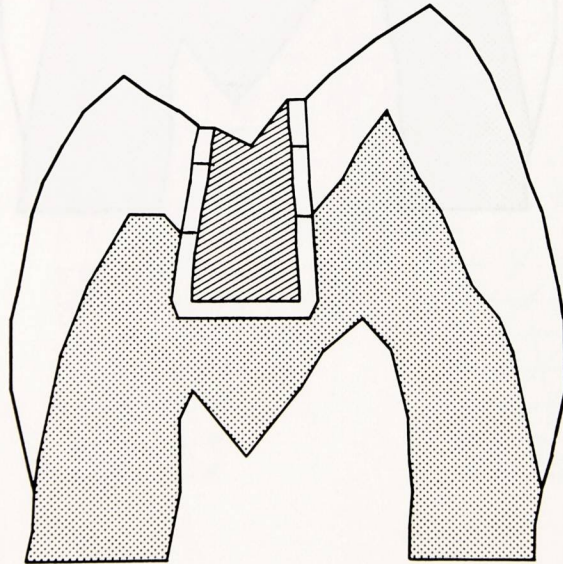
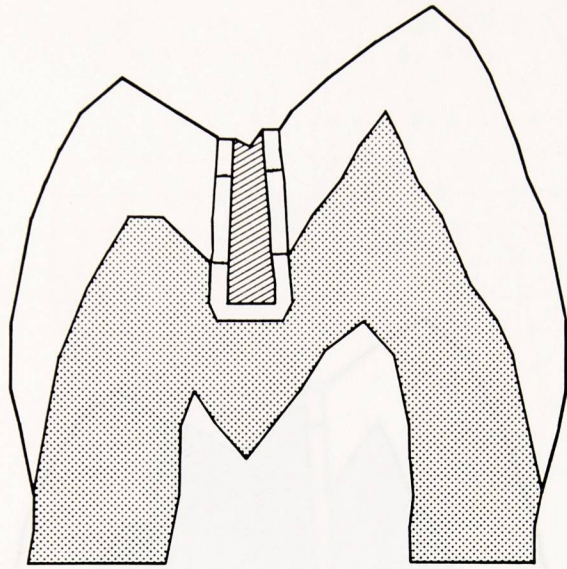


Figure 14. Cross-sectional view of restored cavity #1, A, and restored cavity #2, B.

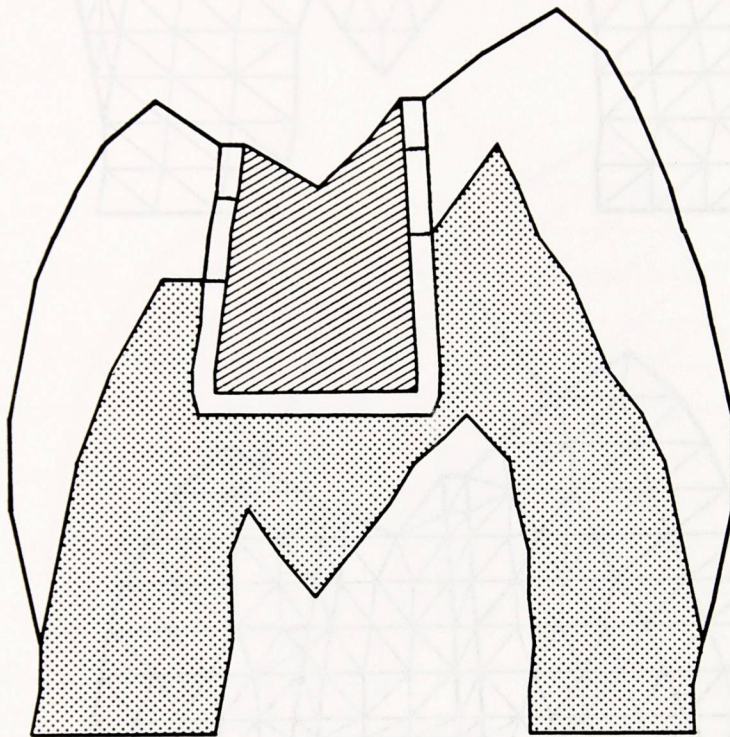


Figure 15. Cross-sectional view of restored cavity #3.

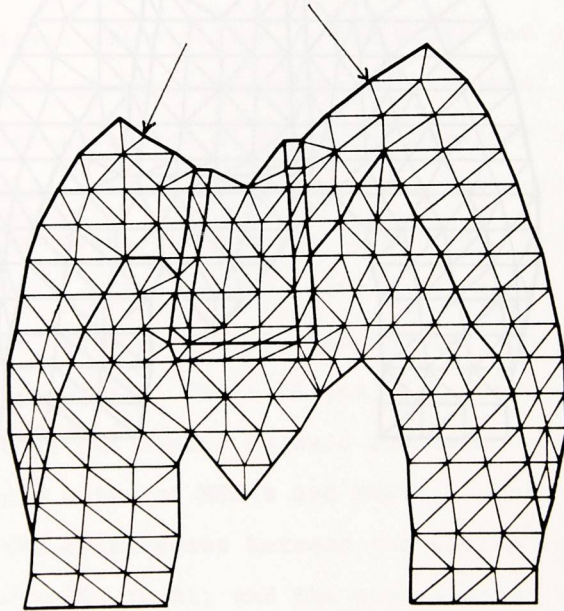
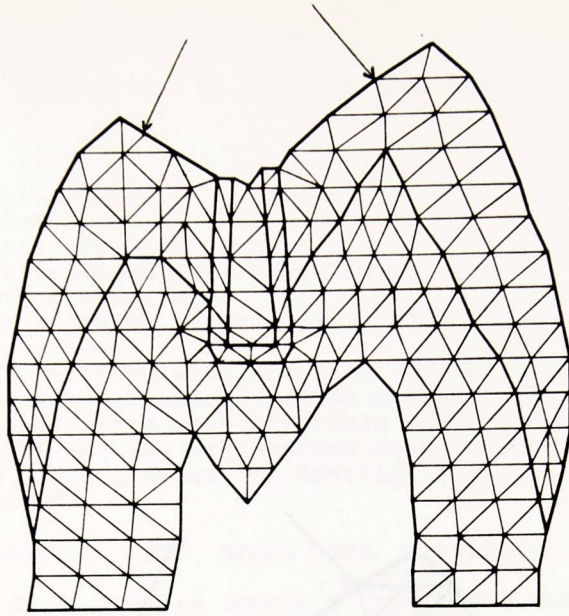


Figure 16. Triangulation of the restored cavity #1 model, A, and the restored cavity #2 model, B.

## 6. FINITE ELEMENT MODELING

The FEM models were developed into seven categories.

They are:

1. Model validation
2. Strain gauge
3. Cavity preparation
4. Cavity preparation with restorative material
5. Cavity preparation with bonding agent
6. Cavity preparation with restorative material and bonding agent
7. Cavity preparation with restorative material and bonding agent with a bonding layer

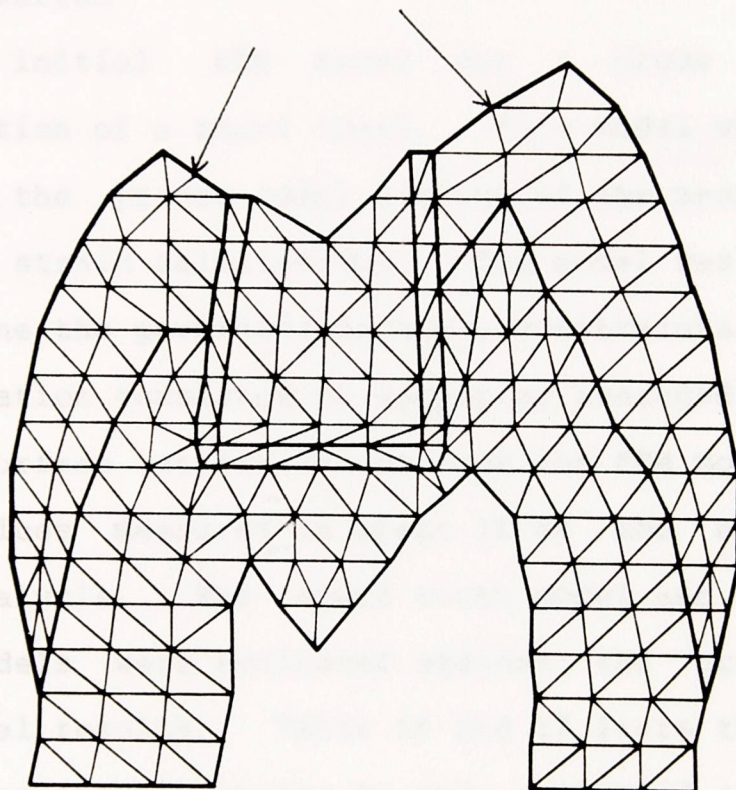


Figure 17. Triangulation of the restored cavity #3 model.

## 6. FINITE ELEMENT METHOD RESULTS

The FEM results can be divided into seven categories.

They are:

1. Model validation
2. Sound tooth
3. Cavity preparations
4. Cavities restored with traditional, non-bonded restorative materials
5. Cavities restored using bonding to acid-etched enamel
6. Cavities restored with materials bonded to both the dentin and the acid-etched enamel
7. Cavities restored with materials bonded to both the dentin and the acid-etched enamel were the bonding properties of the dentinal bonding layer were varied

The initial FEM model was a crude geometric representation of a sound tooth. This model was used to establish the proper nodal density of the mesh to yield convergent strain calculations. The model was also used to determine the governing boundary constraints.

Validation consisted of comparing averaged buccal and lingual surface strain values from the FEM model to the strain values measured in phase II of the experimental stress analysis. The sound tooth model and the three cavity models were evaluated against the corresponding experimental results. Table 16 and 17 lists the results. The FEM results for cavity #3 were evaluated against the averaged strain value of MOD-3 and MOD-4. This was done because of the differences between the cavity ratios for the FEM cavity #3 (0.51) and the experimental MOD-3 and MOD-4 (0.47 and 0.56). Table 17 demonstrates that the FEM results corresponded with the experimental strain measurements and are well within the experimental error. Figures 18 and 19 demonstrate the resulting strain

TABLE 16  
 COMPARISONS USED IN THE FEM VALIDATION

Finite Element Method Condition	Experimental Conditions
Sound tooth	Sound tooth
Cavity #1	MOD-1
Cavity #2	MOD-2
Cavity #3	Average of (MOD-3 + MOD-4)

TABLE 17  
 VALIDATION OF FEM STRAIN VALUES AGAINST  
 EXPERIMENTAL STRAIN MEASUREMENTS

Condition	Lingual		Buccal	
	FEM	EXP	FEM	EXP
	(microstrain)		(microstrain)	
Sound tooth	123	147	49	52
Cavity #1 MOD-1	243	263	157	135
Cavity #2 MOD-2	282	266	171	141
Cavity #3 Average of MOD-3 + MOD-4	416	332	201	212

Legend

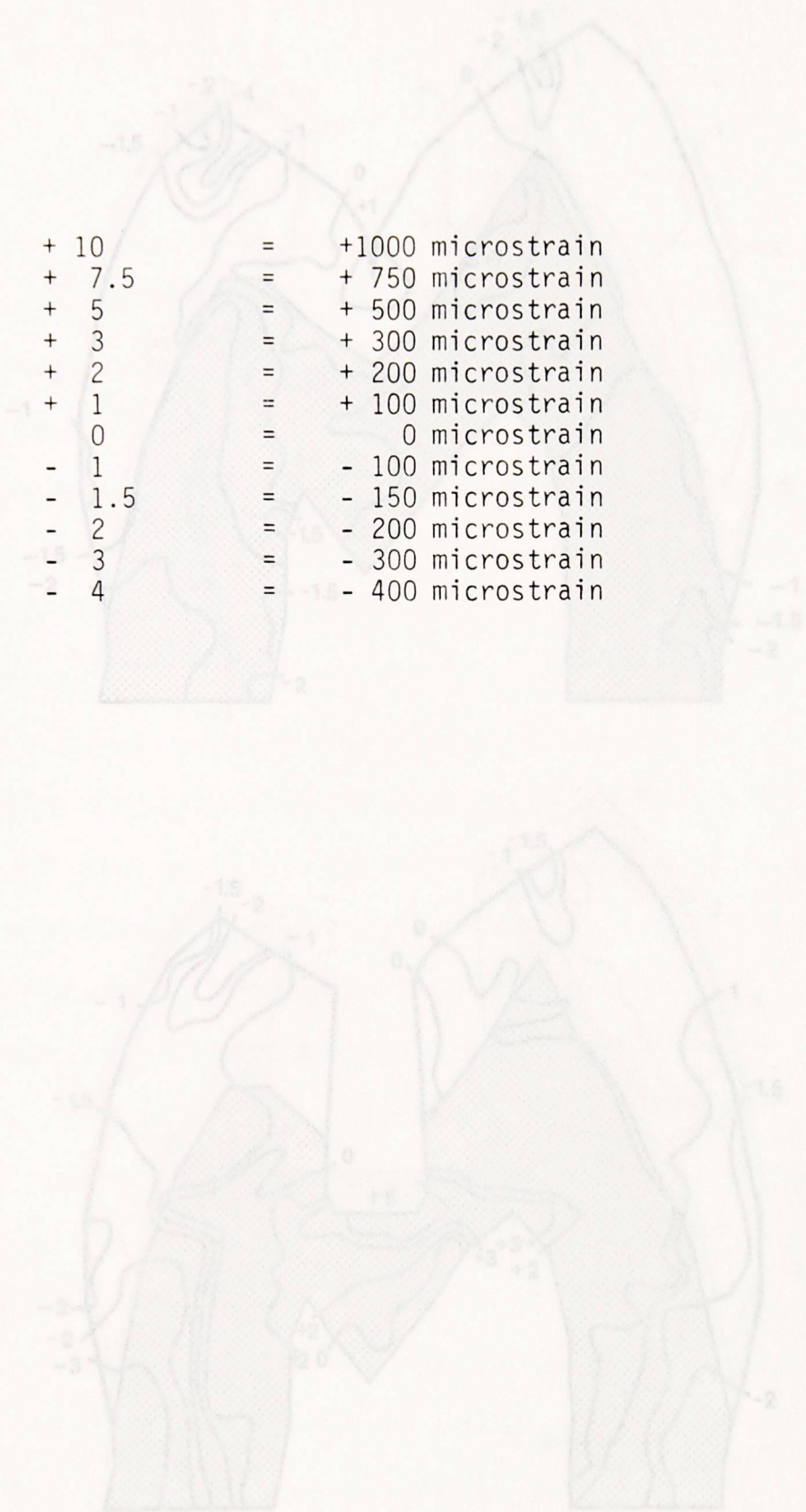


Figure 18. Resulting strain contours in the sound tooth model, A, and the cavity preparation #1 model, B.

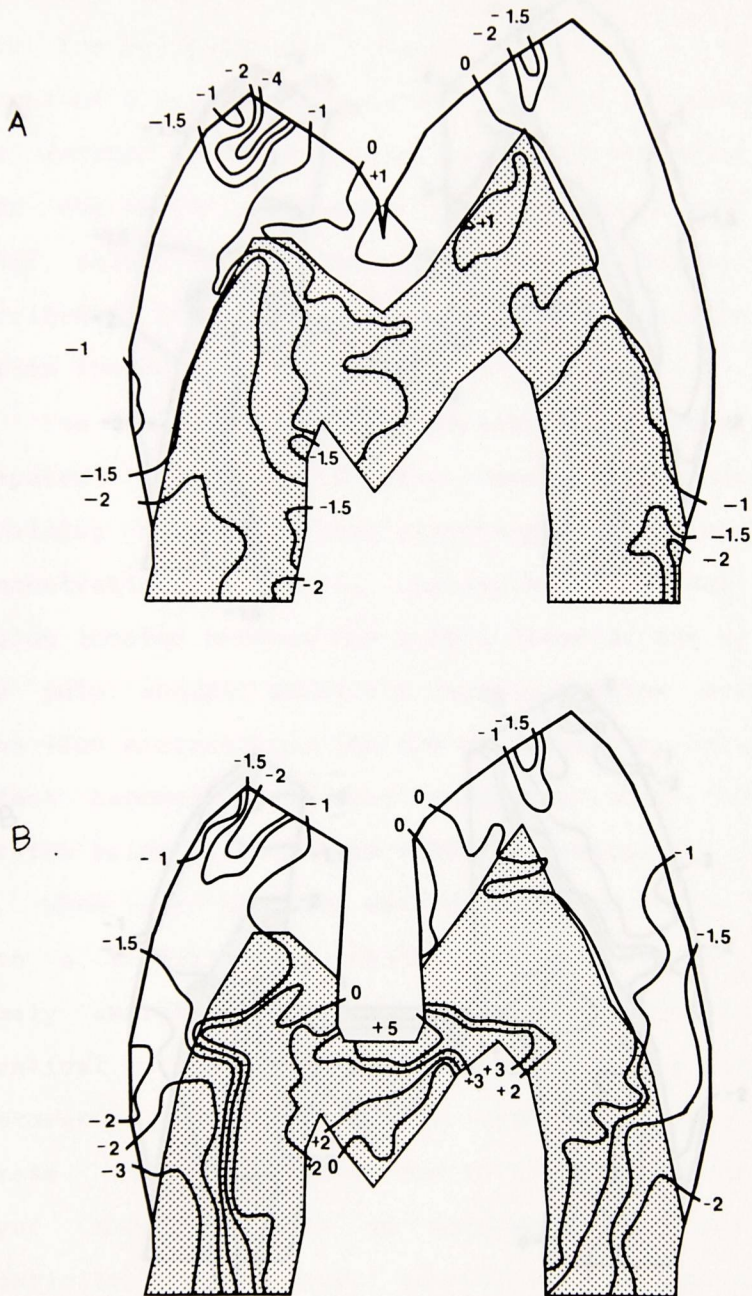


Figure 18. Resulting strain contours in the sound tooth model, A, and the cavity preparation #1 model, B.



contours for the sound tooth and the three cavity models. The sound tooth model shows that the resulting strains are uniformly distributed throughout the crown of the tooth with the majority of the tooth experiencing compressive forces of 0 to -150 microstrain. An area of tensile strain was located in the center of the model extending through both the dentin and enamel. Localized areas within the model showed higher compressive strains but this can be attributed to the load application and fixation of the bottom row of nodes.

The cavity models demonstrated that when a tooth is prepared with even a very conservative cavity the remaining tooth structure experiences significant strain concentration. This is particularly evident in the region located between the pulpal floor of the cavity and the pulp chamber where the tensile strains are greater than +500 microstrain. As the cavities were enlarged this effect becomes even more prominent with the tensile strains being greater than +1000 microstrain.

When the cavities were modelled as being restored with a traditional, non-bonded restorative material, namely amalgam, the resulting strain distribution was identical to that of the corresponding cavity model. The restorative material itself, did not experience any stress. This was expected due to the intermediary bonding layer modelled with an extremely low modulus of elasticity. This layer essentially represented a void which allowed for the simulation of non-bonding material. In phase I of the experimental stress analysis, the

treatment condition of restoring with amalgam did not show any difference from the MOD cavity preparation.

The FEM cavity models restored with materials that bond to a portion of the enamel were examined. In this simulation bonding to acid-etched enamel was modelled with a modulus of elasticity of  $3 \times 10^9 \text{ N/m}^2$ . There was no bonding to the dentin and this region was modelled as a void. Comparisons of the surface strain values from the FEM models to the experimental results in phase II were made. It was found that the the FEM model of the restored teeth using only bonding to acid-etched enamel corresponded with the the experimental condition of the the tooth restored with both dentinal bonding and bonding to acid-etched enamel. Table 18 show the buccal surface strain from the model approximating that of the experimental measurements. However, the lingual surface strains from the model predicted a greater strain reduction as compared to the experiments. The models predicted the same surface strain values as the sound tooth model. Inspection of the strain contours in figures 20 and 21 show the strain distribution resembling that of the sound tooth model except in the immediate area surrounding the restorative material. For the three restorative conditions in figures 20 and 21, exceedingly large strains with steep gradients were produced in the region of the bonding of the restorative material to the acid-etched enamel. Also, the restorative material itself was not being uniformly stressed.

When the restorative conditions were modelled with

TABLE 18

VALIDATION OF FEM STRAIN VALUES FOR THE RESTORATIVE  
 MODELS AGAINST EXPERIMENTAL STRAIN MEASUREMENTS

Condition	Lingual		Buccal	
	FEM	EXP	FEM	EXP
	(microstrain)		(microstrain)	
Sound tooth	123	147	49	52
Cavity #1 Restored	128	174	48	54
Cavity #2 Restored	124	207	52	53
Cavity #3 Restored	124	242	57	68

Figure 18. Resulting strain contours for the restored cavity #1 model with bonding to enamel only, A, and restored cavity #2 model with bonding to enamel only, B.



with the acid-etched enamel bond the surface strains will correspond with the bond layer bond. Again the bonding layer was modeled with a modulus of elasticity of 10 X 10<sup>9</sup> N/m<sup>2</sup>. The significant effect of this restorative model was in the distribution of the resulting strain. The strain throughout each of the model conditions was much more uniform than the other restorative conditions with the only stress gradient occurring in the region of the acid-etched enamel bond (Fig. 21 and 22).

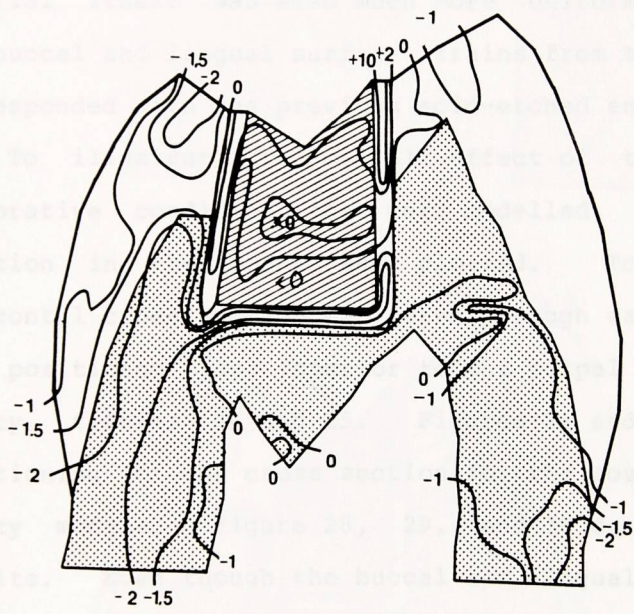


Figure 21. Resulting strain contours for the restored cavity #3 model with bonding to enamel only.

with the acid-etched enamel bond the surface strains still corresponded with the sound tooth model. Again the bonding layer was modelled with a modulus of elasticity of  $3 \times 10^9$  N/m<sup>2</sup>. The significant effect of this restorative model was in the distribution of the resulting strain. The strain throughout each of the modelled conditions was much more uniform than the other restorative conditions with the only steep gradients occurring in the region of the acid-etched enamel bond, Figs, 22 and 23. The restorative material itself was also much more uniformly strained. The buccal and lingual surface strains from the FEM models corresponded with the previous acid-etched enamel model.

To illustrate the overall effect of the different restorative conditions that were modelled, strain verses position in the model was plotted. To do this a horizontal cross section was taken through each model and was positioned just inferior to the pulpal floor of the cavity, figures 24 and 25. Figures 26 and 27 show the positioning of the cross section for the sound tooth and cavity models. Figure 28, 29, and 30 demonstrate the results. Even though the buccal and lingual strains for both restorative conditions coincide with the sound tooth strain, it is the model of dentinal bonding in conjunction with bonding to acid-etched enamel that restores the overall integrity of the tooth to that of the sound tooth.

To determine the contribution that the dentinal bonding layer had on the overall strain distribution the modulus of elasticity of the bonding region was varied while maintaining a constant modulus for the acid-etched

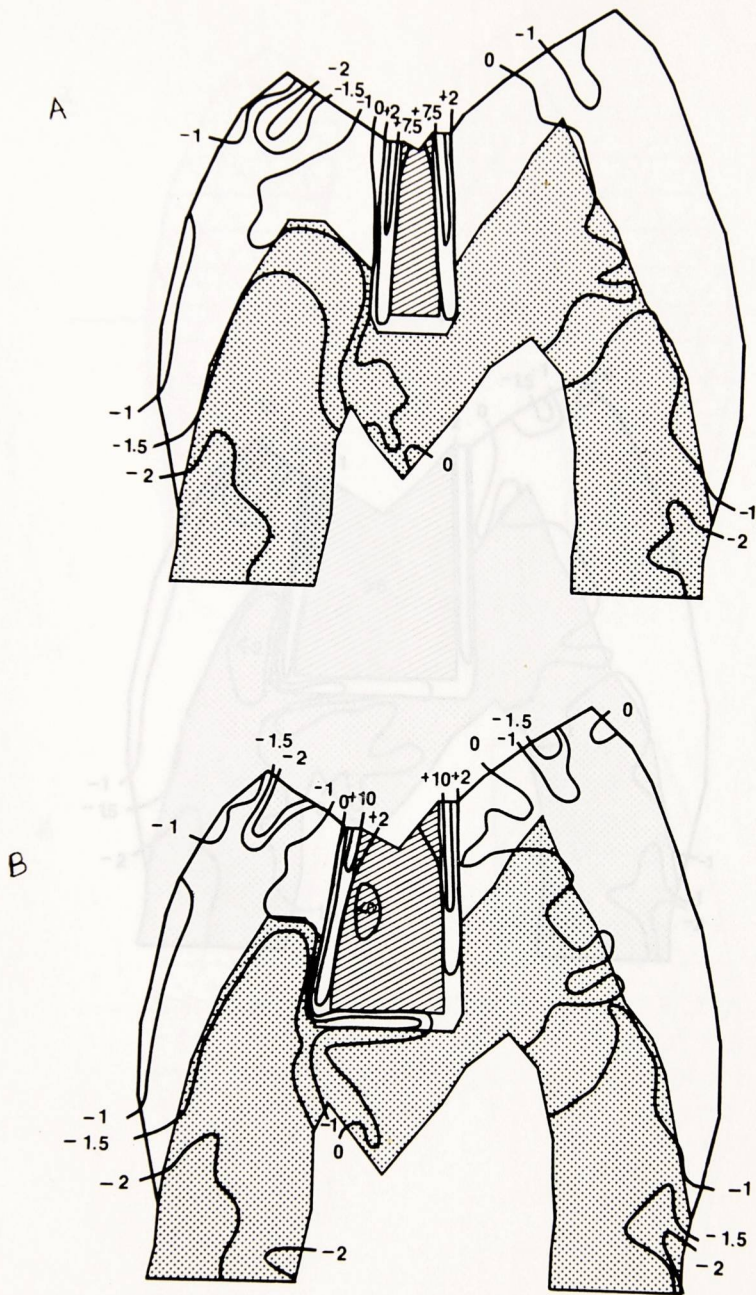


Figure 22. Resulting strain contours for the restored cavity #1 model with bonding to both enamel and dentin, A, and restored cavity #2 model with bonding to both enamel and dentin, B.

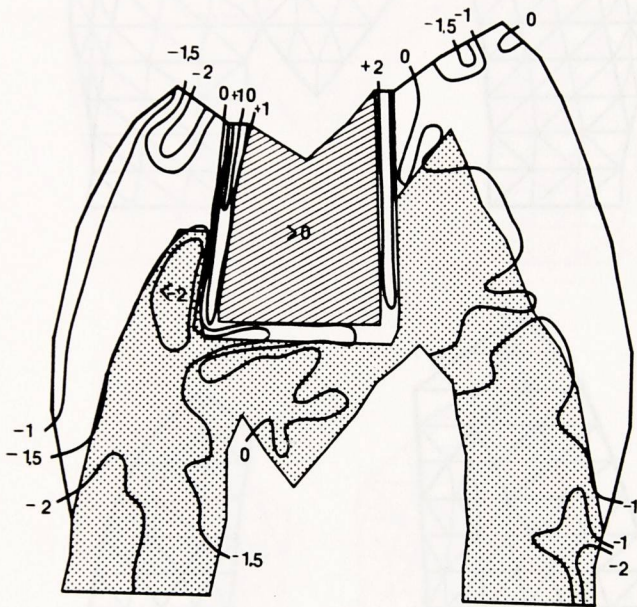


Figure 23. Resulting strain contours for the restored cavity #3 model with bonding to both enamel and dentin.

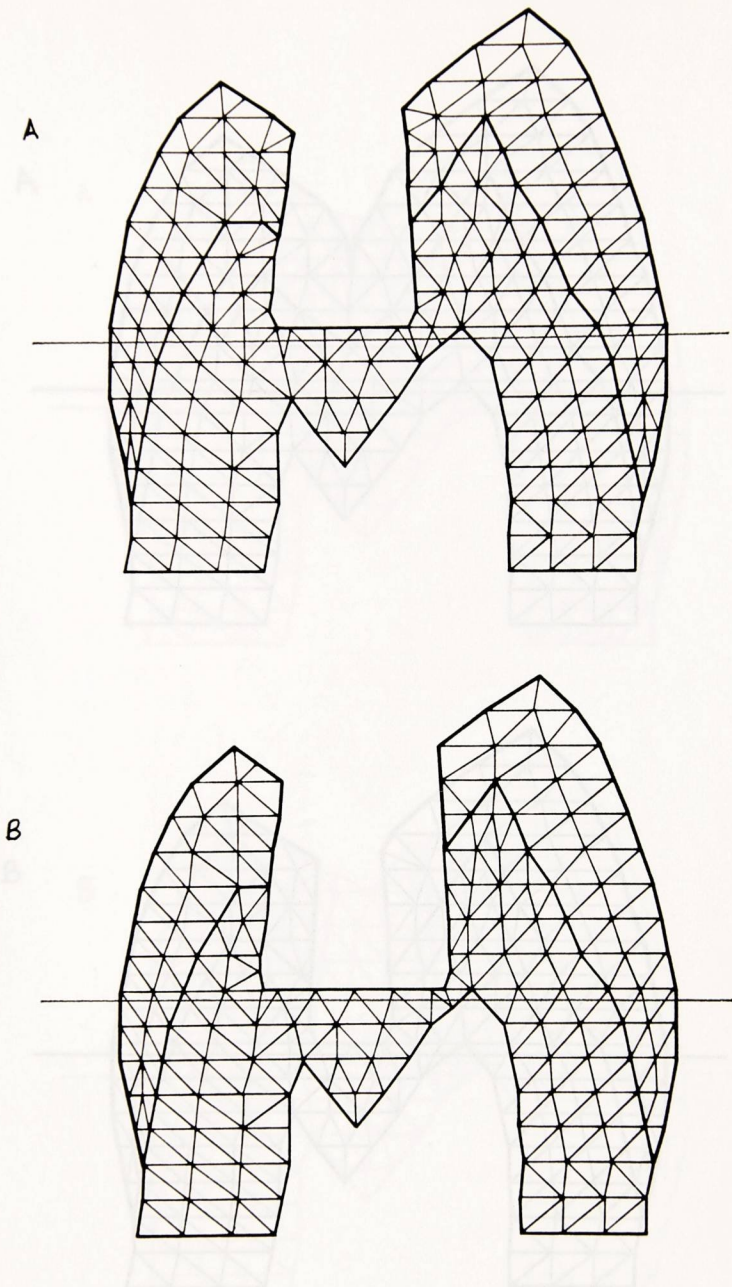


Figure 24. The horizontal location of the elements used to plot strain versus position in the cavity preparation #2 model, A, and the cavity preparation #3 model, B.

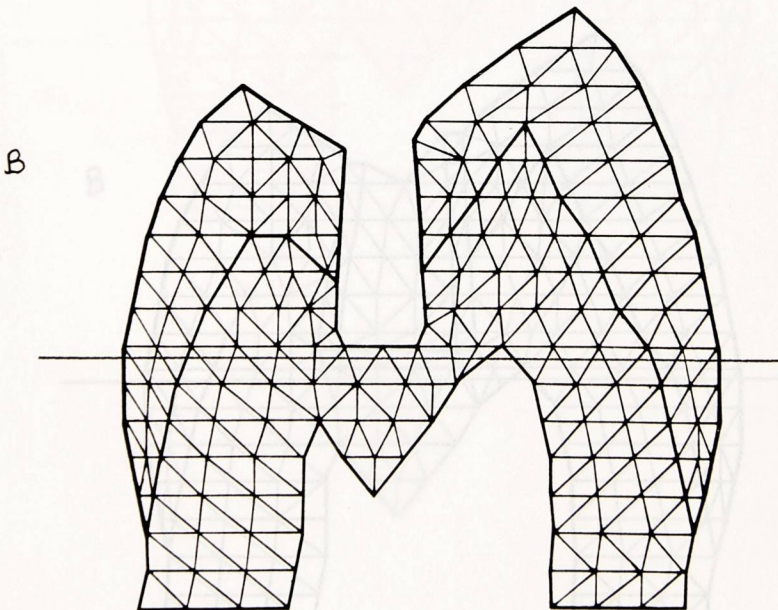
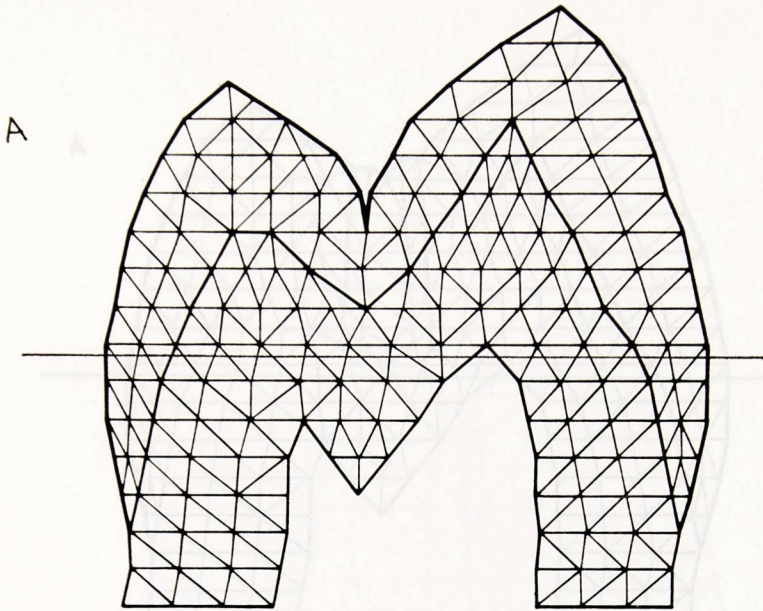


Figure 25. The horizontal location of the elements used to plot strain verses position in the sound tooth model, A, and the cavity preparation #1 model, B.

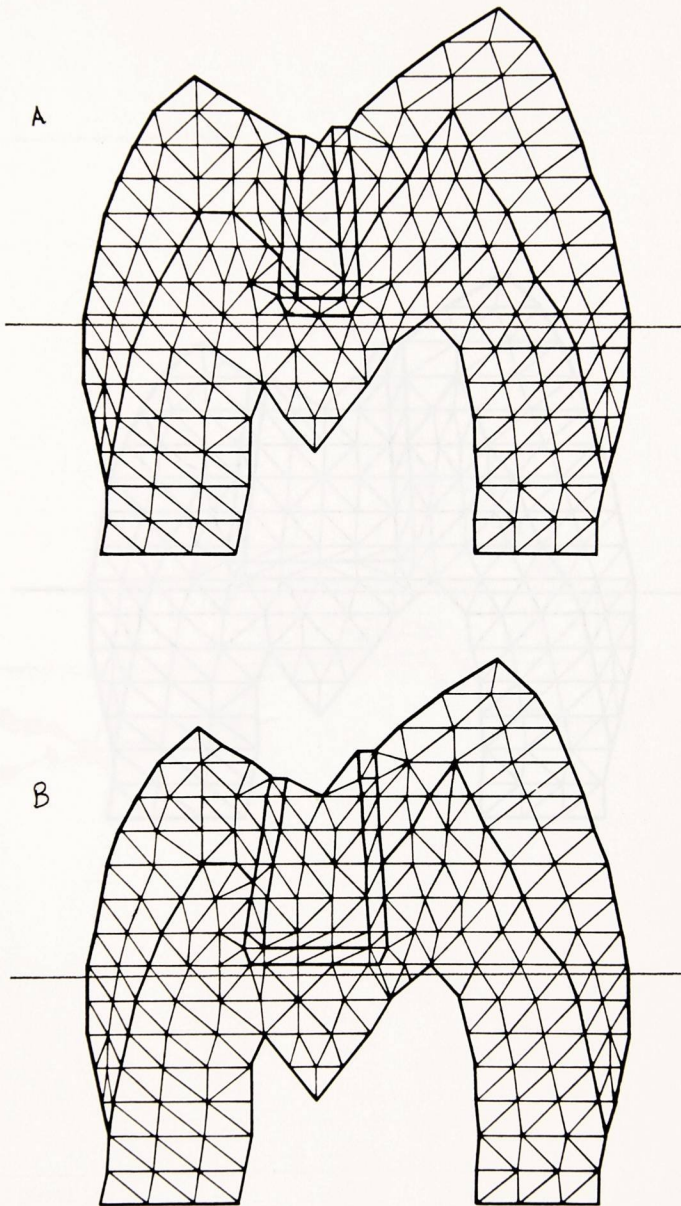


Figure 26. The horizontal level of the elements used to plot strain versus position in the restored cavity #1 model, A, and the restored cavity #2 model, B.

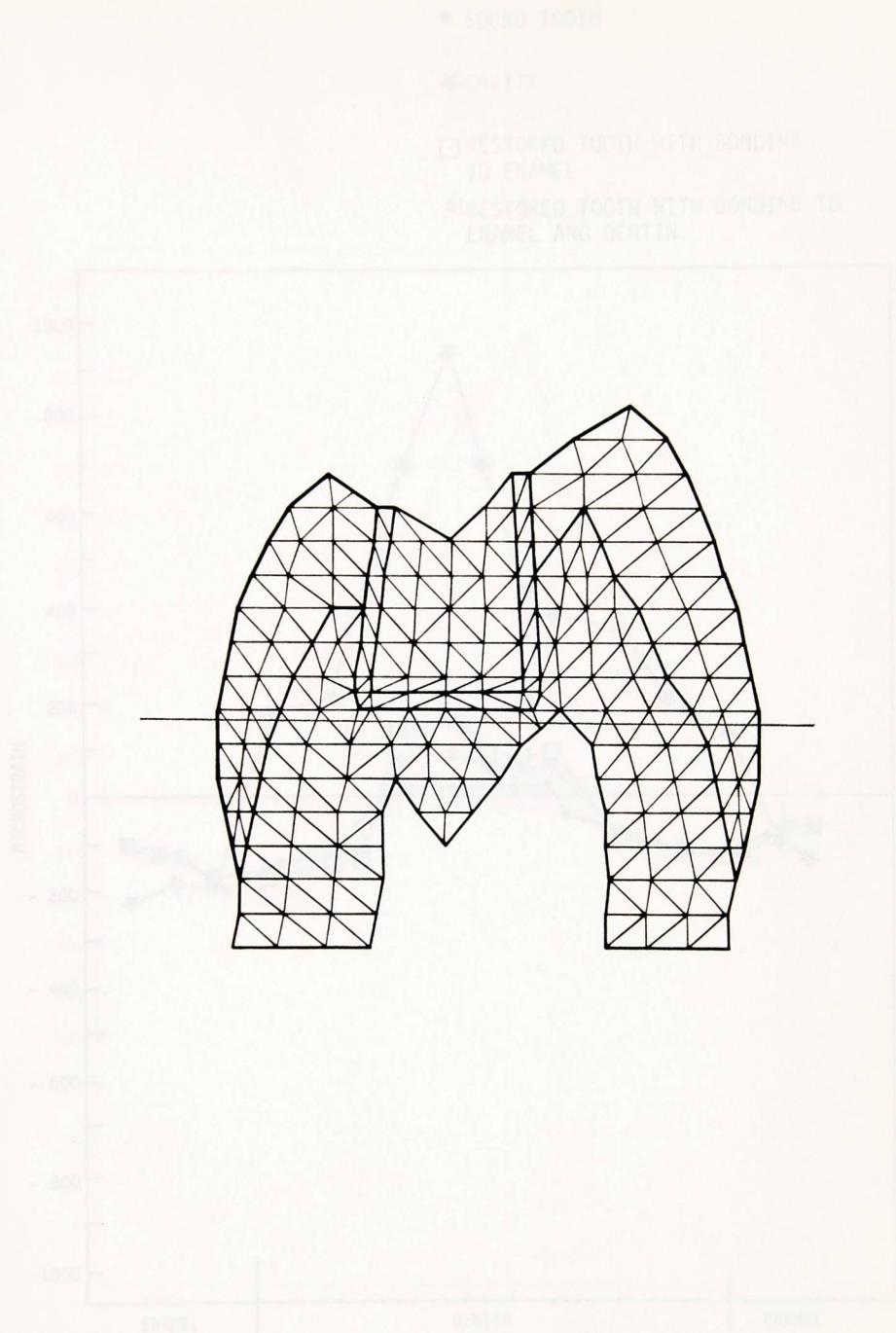


Figure 27. The horizontal level of the elements used to plot strain versus position in the restored cavity #3 model.

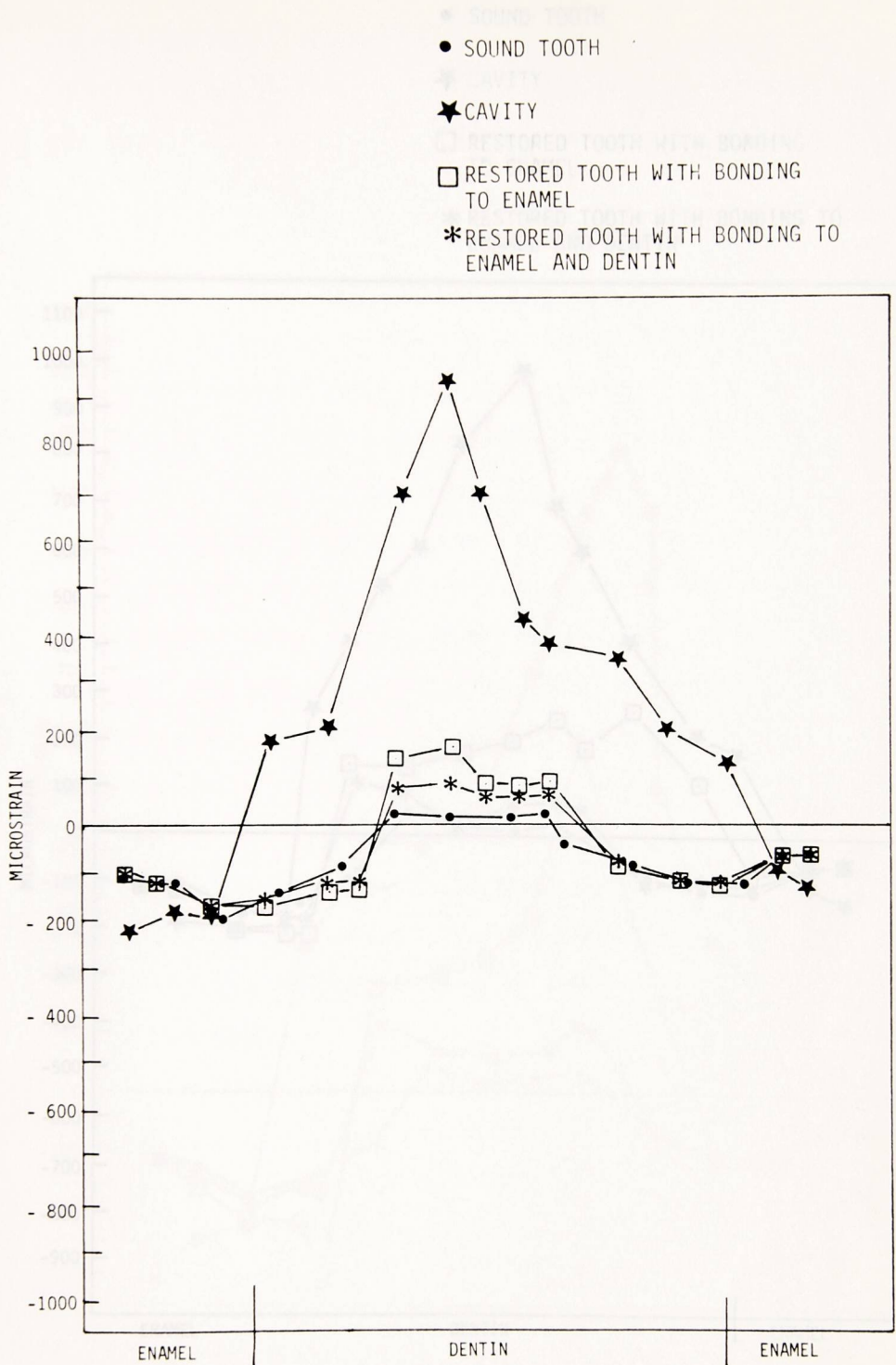


Figure 28. Plot of strain verses position within the tooth for the sound tooth, cavity #1 model, restored cavity #1 model with bonding to enamel, and restored cavity #1 model with bonding to enamel and dentin.



enamel bonding region. Increasing the modulus of the  
 dentinal bonding region by a factor of 100 did not yield  
 any significant change in

- SOUND TOOTH
- ★ CAVITY
- RESTORED TOOTH WITH BONDING TO ENAMEL
- \* RESTORED TOOTH WITH BONDING TO ENAMEL AND DENTIN

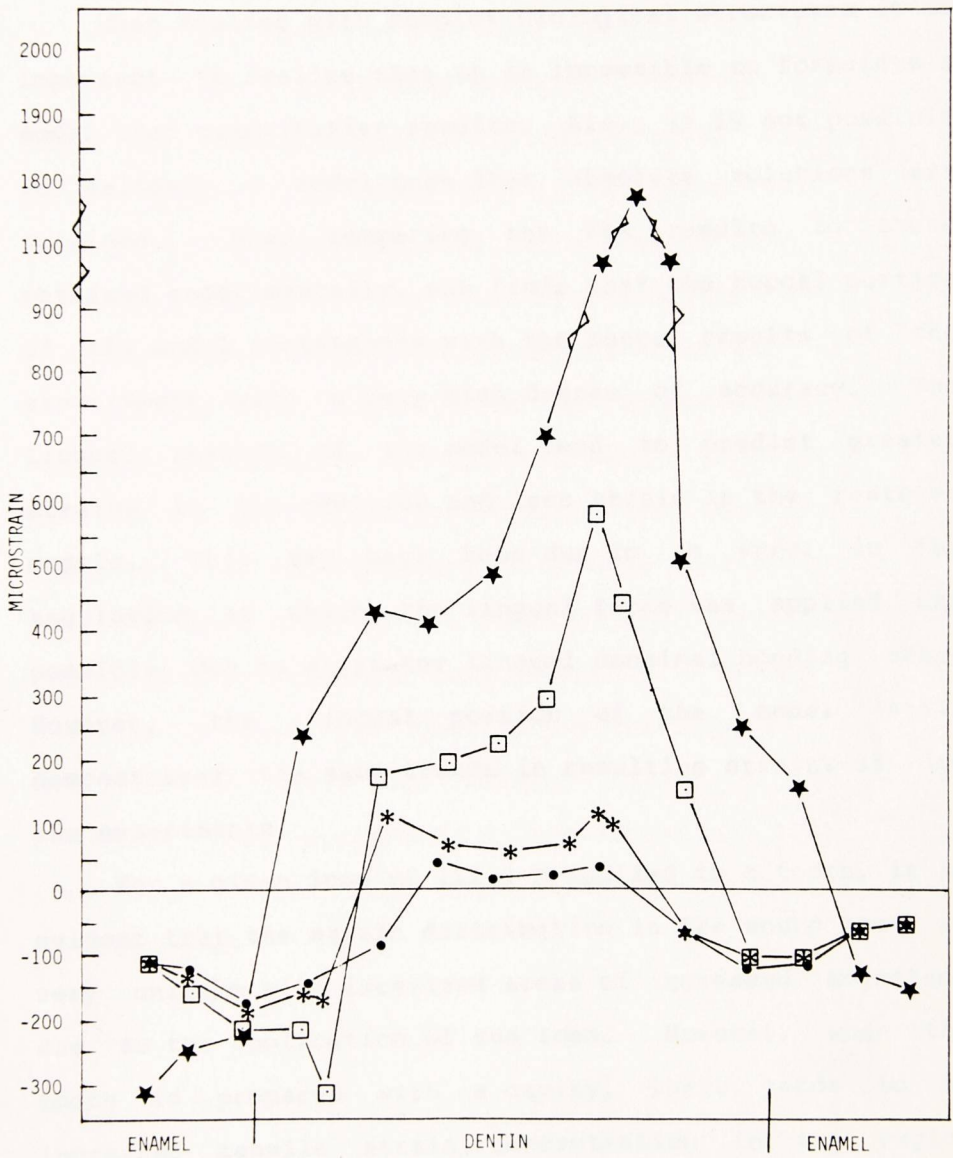


Figure 30. Plot of strain verses position within the tooth for the sound tooth model, cavity preparation #3 model, restored cavity #3 model with bonding to enamel, and restored cavity #3 model with bonding to enamel and dentin.

enamel bonding region. Increasing the modulus of the dentinal bonding region by a factor of 100 did not yield any significant change in the resulting strain. This provided a method by which the overall strain distribution within a tooth could easily be examined.

When dealing with complex biological structures it is important to realize that it is impossible to formulate a model that quantitative results. Also, it is not possible to validate a model such that absolute solutions are obtained. When comparing the FEM results to those obtained experimentally, one finds that the buccal portion of the model corresponds with the buccal results of the experiments with a very high degree of accuracy. The lingual results of the model tend to predict greater strains in the cavities and less strain in the restored models. This may have been due to an error in the angulation at which the lingual force was applied and possibly due to a greater lingual dentinal bonding area. However, the lingual portion of the model still demonstrated the same trends in resulting strains as did the experiments.

For a given load of 111.2 N applied to a tooth, it is evident that the strain distribution in the sound tooth is very uniform with localized areas of increased magnitude due to the application of the load. However, when the tooth is prepared with a cavity, there tends to be increased tensile strain concentration in the region bounded by the pulpal floor and the pulp chamber. Also, the internal line angles of the cavities produce areas of

## 7. DISCUSSION OF FEM RESULTS

The modelling results demonstrated the use of the FEM in conjunction with experimental validation. This provided a method by which the overall strain distribution within a tooth could easily be examined.

When dealing with complex biological structures it is important to realize that it is impossible to formulate a model that quantitative results. Also, it is not possible to validate a model such that absolute solutions are obtained. When comparing the FEM results to those obtained experimentally, one finds that the buccal portion of the model corresponds with the buccal results of the experiments with a very high degree of accuracy. The lingual results of the model tend to predict greater strains in the cavities and less strain in the restored models. This may have been due to an error in the angulation at which the lingual force was applied and possibly due to a greater lingual dentinal bonding area. However, the lingual portion of the model still demonstrated the same trends in resulting strains as did the experiments.

For a given load of 111.2 N applied to a tooth, it is evident that the strain distribution in the sound tooth is very uniform with localized areas of increased magnitude due to the application of the load. However, when the tooth is prepared with a cavity, there tends to be increased tensile strain concentration in the region bounded by the pulpal floor and the pulp chamber. Also, the internal line angles of the cavities produce areas of

increased strain concentration. When these cavities were restored with the traditional non-bonded restoration there was no change in the strain distribution from that of the cavity models have been presented. The correlation of the

The bonding of the restorative material to a portion of enamel provided a significant reduction of strain on the buccal and lingual cusp surface. However, the region below the pulpal floor of the cavity still demonstrated strains greater than those seen in the sound tooth model. When the restorative material was bonded to both a portion of enamel and to the dentinal surface of the cavity, the greatest overall strain reduction was achieved.

Because the objective of the FEM modelling was to simulate the behavior of the tooth when a force is applied to it, an exact quantitative model was not formulated. Thus, it was not necessary to produce mesh that resulted in a triangulation with a bonding layer dimensioned to provide a true geometric representation. However, it was possible to use the qualitative results of the FEM modelling to scale the bonding layer to its actual thickness and determine a corresponding modulus of elasticity. This was done using the proportionality expression of

$$k_1 d_1 = k_2 d_2 \quad (61)$$

where  $k$  is the modulus of elasticity and  $d$  is the thickness of the region of interest. Thus, the scaled value for the dentinal bonding layer equaled  $8.4 \times 10^{10}$  N/m<sup>2</sup>.

## 8. CONCLUSION

The details relating to the development, experimental verification and analysis of a 2-D plane strain finite element model have been presented. The correlation of the FEM model predictions with the experimental test results indicate that the model represents a very reasonable simulation of an in vitro human tooth.

The stress analysis data from the experimental phase of the study indicates that cavity preparation causes a substantial decrease in stiffness of the remaining cuspal tooth structure. When the cavity is restored with traditional, non-bonding, restorative materials no stiffness integrity is restored to the weakened cusps. However, when the cavity is restored with materials that bond to the enamel, a significant recovery of cuspal stiffness is obtained. In addition to this, if the restorative material is bonded to both the enamel and dentin, the stiffness recovery approaches that of an intact, sound tooth. The shape of the relaxation curve also shows a dependence on the restorative material. For traditional, non-bonding, restorative materials, the relaxation curve displays a wide divergence or hysteresis indicating a possible gap formation at the interface of the restorative material and the remaining tooth structure. For the bonded restoration, the relaxation curve was essentially identical to the relaxation curve for the sound tooth indicating minimal hysteresis.

The results from the FEM modelling demonstrated that it is possible to formulate a model of moderated nodal

density, using the plane strain assumption, that is verifiable with experimental data. The model of a sound tooth indicated that under a given load the strain distribution is very uniform throughout the tooth. However, when a cavity preparation is introduced into the tooth model there is significant strain concentration in the region bounded by the pulpal floor and the pulp chamber. When the cavity model is restored with the traditional, non-bonding, restoration, the strain distribution does not change from that of the cavity model. Bonding the restoration to enamel plays a major role in the overall strain dissipation, approximating the strain distribution in the enamel portion of the sound tooth model. However, in the region of the pulpal floor, the strain concentration is not reduced to the same degree. When bonding to both dentin and enamel are utilized in the restoration there is a significant strain reduction in the overall model approximating that of the sound tooth model.

10. Granath, L. E. A Technique of Photoelasticity Employed in Comparative Dental Investigations, *Odontologisk Revy* 14:136-144 (1963).
11. Granath, L. E. Photoelastic Studies on Certain Factors Influencing the Relation Between Cavity and Restoration, *Odontologisk Revy* 14:278-293 (1963).
12. Granath, L. E. Photoelastic Studies on Occluso-proximal Sections of Class II Restorations, *Odontologisk Revy* 15:169-183 (1964).
13. Granath, L. E. Further Photoelastic Studies on the Relations Between the Cavity and the Occlusal Portion of Class II Restorations, *Odontologisk Revy* 15:290-298 (1964).
14. Granath, L. E. Photoelastic Model Experiments on Class II Cavity Restorations of Dental Amalgam, *Odontologisk Revy* 16:Supplement 9 (1965).

## 9. REFERENCES

1. Bronner, F. J. Engineering Principles Applied to Class II Cavities, *J. Dent. Res.* 10:115-119 (1930).
2. Gabel, A. B. The Amalgam Proximocclusal Restoration in Deciduous Molars, *J. Dent. for Children* 11:52-55 (1944).
3. Brown, W. B. A Mechanical Basis for the Preparation of Class II Cavities for Amalgam Fillings in Deciduous Molars, *JADA* 38:417-423 (1949).
4. Noonan, M. A. The Use of Photoelasticity in a Study of Cavity Preparations, *J. Dent. for Children* 16:24-28 (1949).
5. Weiland, W. F. An Engineer's Evaluation of Class II Cavity Preparation for Silver Amalgam Restorations in Primary Teeth, *J. Dent. for Children* 18:29-32 (1951).
6. Haskins, R. C., Haack, D. C., Ireland, R. L. A Study of Stress Pattern Variations in Class II Cavity Restorations as a Result of Different Cavity Design, *J. Dent. Res.* 33:757-766 (1954).
7. Guard, W. F., Haack, D. C., Ireland, R. L. Photoelastic Stress Analysis of Buccolingual Sections of Class II Cavity Restorations, *J. Dent. Res.* 37:63-635 (1958).
8. Mahler, D. B., Peyton, F. A. Photoelasticity as a Research Technique for Analyzing Stresses in Dental Structures, *J. Dent. Res.* 34:831-838 (1955).
9. Mahler, D. B. An Analysis of Stresses in Dental Amalgam Restoration, *J. Dent. Res.* 37:516-526 (1958).
10. Granath, L. E. A Technique of Photoelasticity Employed in Comparative Dental Investigations, *Odontologisk Revy* 14:136-144 (1963).
11. Granath, L. E. Photoelastic Studies on Certain Factors Influencing the Relation Between Cavity and Restoration, *Odontologisk Revy* 14:278-293 (1963).
12. Granath, L. E. Photoelastic Studies on Occluso-proximal Sections of Class II Restorations, *Odontologisk Revy* 15:169-185 (1964).
13. Granath, L. E. Further Photoelastic Studies on the Relations Between the Cavity and the Occlusal Portion of Class II Restorations, *Odontologisk Revy* 15:290-298 (1964).
14. Granath, L. E. Photoelastic Model Experiments on Class II Cavity Restorations of Dental Amalgam, *Odontologisk Revy* 16:Supplement 9 (1965).

15. Craig, R. G., El-Ebrashi, M. K., LePeak, P. J., Peyton, F. A. Experimental Stress Analysis of Dental Restorations, Part I. Two-dimensional Photoelastic Stress Analysis of Inlays, *J. Pros. Dent.* 17:277-291 (1967).
16. Granath, L. E., Edlund, J. The Role of the Pulpoaxial Line Angle in the Origin of Isthmus Fracture, *Odontologisk Revy* 19:317-334 (1968).
17. Davidson, G. B. A Method for Three-Dimensional Photoelastic Stress Analysis of the Remaining Tooth Structure Associated with Various Cavity Preparations, *J. Dent. Res.* 43:912, M4a (1964).
18. Johnson, E. W., Castaldi, C. R., Gau, D. J., Wysocki, G. P. Stress Pattern Variations in Operatively Prepared Human Teeth, Studied by Three-Dimensional Photoelasticity, *J. Dent. Res.* 47:548-558 (1968).
19. Granath, L. E., Hiltcher, R. Strength of Edge of Class II Cavity Restorations in Relation to Buccolingual Shape of Cavity, *Odontologisk Revy* 21:189-197 (1970).
20. Tanner, A. N. Factors Affecting the Design of Photoelastic Models for Two-dimensional Analysis, *J. Pros. Dent.* 27:48-62 (1972).
21. Fisher, D. W., Caputo, A. A., Shillingburger, H. T., Duncanson, M. G. Photoelastic Analysis of Inlay and Onlay Preparations, *J. Pros. Dent.* 33:47-53 (1975).
22. Craig, R. G., Farah, J. W. Stress Analysis and Design of Single Restorations and Fixed Bridges, *Oral Sciences Review, The Scientific Basis of Reconstructive Dentistry* 10:45-74 (1977).
23. Brekelmans, W. A. M., Poort, H. W., Sloof, T. J. J. H. A New Method to Analyze the Mechanical Behavior of Skeletal Parts, *Acta Orthop. Scand.* 43:301-317 (1972).
24. Thresher, R. W., Saito, G. E. The Stress Analysis of Human Teeth, *J. Biomechanics* 6:443-449 (1973).
25. Farah, J. W., Craig, R. G., Sikarski, D. L. Photoelastic and Finite Element Stress Analysis of a Restored Axisymmetric First Molar, *J. Biomechanics* 6:551-520 (1973).
26. Farah, J. W., Hood, J. A. A., Craig, R. G. Stresses and Deflections in the Floor of Model Cavity Preparations, *J. Oral Rehabilitation* 1:207-215 (1974).

27. Farah, J. W., Hood, J. A. A., Craig, R. G. Effects of Cement Bases on the Stresses in Amalgam Restorations, *J. Dent. Res.* 54:10-15 (1975).
28. Selna, L. G., Shillingburg, Jr., H. T., Kerr, P. A. Finite Element Analysis of Dental Structures - Axisymmetric and Plane Stress Idealizations, *J. Biomedical Materials Res.* 9:237-252 (1975).
29. Yettram, A. L., Wright, K. W. J., Pickard, H. M. Finite Element Stress Analysis of the Crowns of Normal and Restored Teeth, *J. Dent. Res.* 55:1004-1011 (1976).
30. Lehmann, M. L., Meyer, M. L. Relationship of Dental Caries and Stress: Concentration in Teeth as Revealed by Photoelastic Tests, *J. Dent. Res.* 45:1706-1714 (1966).
31. Wright, K. W. J., Yettram, A. L. Finite Element Stress Analysis of a Class I Amalgam Restoration Subjected to Setting and Thermal Expansion, *J. Dent. Res.* 57:715-723 (1978).
32. Takahashi, N., Kitagami, T., Komori, T. Behavior of Teeth Under Various Loading Conditions with Finite Element Method, *J. Oral Rehabilitation* 7:453-461 (1980).
33. Atmaram, G. H., Mohammed, H. Estimation of Physiologic Stresses with a Natural Tooth Considering Fibrous PDL Structure, *J. Dent. Res.* 60:873-877 (1981).
34. Bell, J. G., Smith, M. C., dePont, J. J. Cuspal Failures of MOD Restored Teeth, *Aust. Dent. J.* 27:283-287 (1982).
35. Peters, M. C. R. B., Poort, H. W. Biomechanical Stress Analysis of the Amalgam-Tooth Interface, *J. Dent. Res.* 62:358-362 (1983).
36. Rubin, C., Krishnamurthy, N., Capilouto, E., Yi, H. Stress Analysis of the Human Tooth Using a Three-dimensional Finite Element Model, *J. Dent. Res.* 62:82-86 (1983).
37. Davy, D. T., Dilley, G. L., Krejci, R. F. Determination of Stress Patterns in Root Filled Teeth Incorporating Various Dowel Designs, *J. Dent. Res.* 60:1301-1310 (1981).
38. Reinhardt, R. A., Krejci, R. F., Pao, Y. C., Stannard, J. G. Dentin Stresses in Post-reconstructed Teeth with Diminishing Bone Support, *J. Dent. Res.* 62:1002-1008 (1983).
39. Cook, S. D., Weinstein, A. M., Klawitter, J. J. A

- Three- Dimensional Finite Element Analysis of a Porous Rooted Co-Cr- Mo Alloy Dental Implant, J. Dent. Res. 61:25-29 (1982).
40. Buch, J. D., Crose, J. G., Bechtol, C. D. Biomechanical and Biomaterials Considerations of Natural Teeth, Tooth Replacements and Skeletal Fixation, J. Biomaterial Med. Devices, Artificial Organs 2:171-186 (1974).
  41. Gupta, K. K., Knoell, A. C., Grenoble, D. E. Mathematical Modeling and Structural Analysis of the Mandible, J. Biomaterial Med. Devices, Artificial Organs 1:469-479 (1973).
  42. Knoell, A. C. A Mathematical Model of an In Vitro Human Mandible, J. Biomechanics 10:159-166 (1977).
  43. Vale, W. A. Cavity Preparation, Irish Dental Review 2:33-41 (1956).
  44. Vale, W. A. Cavity Preparation and Further Thoughts on High Speed, British Dental J. 107:333-346 (1959).
  45. Rasmussen, S. T., Patchin, R. E., Scott, D. B., Heuer, A. H. Fracture Properties of Human Enamel and Dentin, J. Dent. Res. 55:154-164 (1976).
  46. Mondelli, J., Steagall, L., Ishikrirama, A., deLima Navarro, M. F., Soares, F. B. Fracture Strength of Human Teeth with Cavity Preparations, J. Pros. Dent. 43:419-422 (1980).
  47. Holman, J. P. Experimental Methods for Engineers, Second Edition, McGraw Hill (1971).
  48. Budynas, R. G. Advance Strength and Applied Stress Analysis, McGraw Hill (1977).
  49. Micro-Measurements Tech Notes: TN-501, 502, TN-127-3, TN-132-2, TN-137, TN-139-2.
  50. Delong, R., Douglas, W. H. Development of an Artificial Oral Environment for the Testing of Dental Restoratives: Bi-axial Force and Movement Control, J. Dent. Res. 62(1):32-36 (1983).
  51. Huiskes, R., Chao, E. Y. S. A Survey of Finite Element Analysis in Orthopedic Biomechanics: The First Decade, J. Biomechanics 16:385-409 (1983).
  52. Zienkiewicz, O. C. Finite Element in Engineering Science, McGraw Hill, London (1971).
  53. Huebner, K. H., Thornton, E. A. The Finite Element Method for Engineers, John Wiley and Sons (1982).
  54. Irons, B., Ahmad, S. Techniques of Finite Elements,

Ellis Horwood Limited, London (1981).

55. Dally, J. W., Riley, W. F. Experimental Stress Analysis, Second Edition, McGraw Hill (1978).
56. Van Vlack, L. H. Materials Science for Engineers, Addison-Wesley (1970).
57. Lewis, B. A., Robinson, J. S. Triangulation of Planar Regions with Application, Comp. J. 21:324-332 (1977).
58. Lewis, B. A., Cross, M. IF ECS - An Interactive Finite Element Computing System, Appl. Math. Modelling 2:165-175 (1978).
59. Lewis, B. A. IF ECS - Software for Modelling Thermal Stress Problems, in Modelling and Simulation in Practice. M. Cross, R. D. Gibson, M. J. O'Carroll, and T. S. Wilkinson, Eds., Pentech Press (1979).
60. Cross, M., Lewis, B. A., Forster, J. K. Strain Generation During Firing of Dense Silica Shapes, Refract. J. 1:10-22 (1978).
61. Voller, V. R., Cross, M. A Model of Thermally Induced Strain Development in Coke Oven Walls During Carbonization, Math. Modelling 3:279-291 (1982).
62. Peyton, F. A., Mahler, D. B., Hershenov, B. Physical Properties of Dentin, J. Dent. Res. 31:366-370 (1952).
63. Craig, R. G., Peyton, F. A. Elastic and Mechanical Properties of Human Dentin, J. Dent. Res. 37:710-718 (1958).
64. Stanford, J. W., Paffenberger, G. L., Kampula, J. W., Sweeney, W. T. Determination of Some Compressive Properties of Human Enamel and Dentin, JADA 57:487-495 (1958).
65. Stanford, J. W., Weigel, K. V., Paffenberger, G. L., Sweeney, W. T. Compressive Properties of Hard Tooth Structure and Some Restorative Materials, JADA 60:746-756 (1960).
66. Tyldesley, W. R. The Mechanical Properties of Human Enamel and Dentin, British Dental Journal 106:269-278 (1959).
67. Renson, C. E., Braden, M. Experimental Determination of the Rigidity Modulus, Poisson's Ratio and Elastic Limit in Shear of Human Dentin, Archives of Oral Biology 20:43-47 (1975).
68. Bowen, R. L., Rodriguez, M. S. Tensile Strength and modulus of Elasticity of Tooth Structure and Several

- Restorative Materials, JADA 64:378-387 (1962).
69. Renson, C. E. An Experimental Study of the Physical Properties of Human Dentin, Ph.D. Thesis, University of London, 105, 107, 149-170 (1970).
  70. Lehmann, M. L. Tensile Strength of Human Dentin, J. Dent. Res. 46:197-201 (1967).
  71. Renson, C. E., Braden, M. The Mechanical Properties of Human Dentin in Shear, J. Dent. Res. 48:1123 (Abstract) (1969).
  72. Craig, G. G., Peyton, F. A., Johnson D. W. Compressive Properties of Enamel, Dentin, Cements and Gold, J. Dent. Res. 40:936-945 (1961).
  73. Haines, D. J. Physical Properties of Human Tooth Enamel and Enamel Sheath Material Under Load, J. of Biomechanics 1:117-125 (1968).

## 9.1 GLOSSARY

- Alveolar bone -- The bone which supports the teeth.
- Apical -- Pertaining to the apex or end of the root of a tooth.
- Axial wall -- The walls of the cavity preparation parallel to the long axis of the tooth.
- Axiopulpal line angle -- The junction of the axial and pulpal surfaces of a cavity preparation.
- Buccal -- Pertaining to the cheek.
- Buccogingival line angle -- The junction of the buccal and gingival portion of the tooth.
- Buccolingual -- A dimension from the cheeks towards the tongue.
- Cavosurface -- That portion of the cavity preparation that meets with the external surface of the tooth.
- Cement base -- A material used to line the pulpal floor in a cavity preparation.
- Central groove -- The groove located midway buccolingually on the occlusal surface of the tooth.
- Cervical -- Pertaining to the neck of cervix of a tooth.
- Class I -- A cavity design which includes only the occlusal surface of a tooth.

Class II -- A cavity design which includes the occlusal surface and either one of both of the proximal surfaces of the tooth.

Condensor -- Instrument used to place an amalgam restoration.

Developmental groove -- A groove on the tooth formed during appositional growth of enamel.

Fissure -- A long narrow fault at the base of a groove on the surface of a tooth.

Gingival -- Pertaining to the gums.

Inlay -- A intracoronal restoration.

Internal line angle -- The junction of internal surfaces in a cavity preparation.

Isthmus -- The long narrow occlusal portion of the cavity preparation.

Lingual -- Pertaining to the tongue.

Linguogingival line angle -- The junction of the lingual and gingival portion of the tooth.

Marginal design -- Pertaining to the manner in which a restoration meets the tooth.

Marginal ridge -- The ridges on the margin of the occlusal surface of a tooth.

Midsagittal -- Pertaining to or situated in the antero-posterior median plane of the body.

MOD restoration -- Mesio-occluso-distal restoration which is analogous to a Class II restoration.

Occlusal -- Pertaining to closure, shuttering or the occlusion of teeth.

PDL -- Analogous to the peridontal membrane.

Periodontal membrane -- The formative, supportive and sensory connective tissue between the root of a tooth and its alveolous.

Pulpal -- Pertaining to the pulp.

Pulpal floor -- The floor of a cavity preparation.

Pulpal wall -- Analogous to axial wall.

Resistive form -- The design of a restoration such that rotational forces do not displace the restoration.

Retention points -- Points made in a cavity preparation to provide retention to the restorative material.

Retentive form -- The design of a restoration such that axial displacement is prevented.



THAMES POLYTECHNIC

M E M O R A N D U M

From: Dr. A.F.C. Sherratt

Date: 7th November 1985

To: Mr. D. Heathcote

Ref: AFCS/MPH

Re: Daniel MORIN

I enclose the MPhil thesis in respect of the above candidate and should be grateful if you would lodge this in the Library.



Dr. A. F. C. Sherratt